Monographic Series TU Graz

Computation in Engineering and Science

Michael Meßner

A Fast Multipole Galerkin Boundary Element Method for the Heat Equation

Graz, September 2013

Version 1.0

Acknowledgment

The author is gratefully indebted to the *Marshallplan–Jubiläumsstiftung* for their financial support and to the *Southern Methodist University* for their hospitality during the visiting scholar position from January until May 2013.

Abstract

Transient heat transfer plays a major role in many physical and chemical processes, which implies the need for efficient numerical simulation tools in a wide range of engineering fields, such as mechanical, chemical and process engineering. Our aim is to develop a stable, robust and efficient Boundary Element algorithm to solve problems arising from applications in those disciplines. It is a well known fact that uniqueness, solvability and quasi-optimality of space-time Galerkin Boundary Element Methods follows from the boundedness and ellipticity of the thermal single layer- and hyper-singular operator. To handle the arising dense matrix problems we accelerate our solver via the parabolic Fast Multipole Method and thus obtain almost optimal complexity in the number of unknowns. Since the heat kernel is smooth for positive time and exponentially decaying in space, we approximate the kernel by a multivariate Lagrange-Chebyshev interpolation for well separated space-time clusters, which allows us to efficiently evaluate their contributions to the thermal layer potentials. Finally, we investigate some benchmark problems to show that the error induced by the Fast Multipole method can be controlled and does not destroy the convergence rates of the Galerkin scheme. Furthermore, we simulate some problems from industrial applications to show the fitness of the proposed method for realistic application-size problems.

Zusammenfassung

Die instationäre Wärmeleitung spielt eine wichtige Rolle in vielen physikalischen und chemischen Prozessen, was die Notwendigkeit von effizienten numerischen Methoden zur Folge hat. Unser Ziel ist es einen stabilen, robusten und effizienten Randelemente Algorithmus zu entwickeln um Probleme aus diesen Anwendungsbereichen zu simulieren. Es ist allgemein bekannt, dass die eindeutige Lösbarkeit und Stabilität sowie die Quasi-Optimalität von Galerkin Randelemente Methoden aus der Beschränktheit und Elliptizität des Einfachschicht- und Hypersinglären Operators folgt. Um die resultierenden voll besetzten Matrizen effizient handhaben zu können, beschleunigen wir unsere Randelemente Formulierung mittels der parabolischen Fast Multipole Methode, welche einen beinahe optimalen Algorithmus in der Anzahl der Unbekannten ermöglicht. Da der Kern für positive Zeit glatt und im Raum exponentiell abklingend ist, verwenden wir eine Raum-Zeit Entwicklung in Chebysev und Lagrange Polynomen um die Faltung der Vergangenheit effizient zu berechnen. An einigen Referenz Beispielen wollen wir zeigen, dass die parabolische Fast Multipole Method das theoretischen Konvergenzverhalten der Galerkin Methode nicht zerstört. Danach werden wir noch Industrie Anwendungen modellieren um die Eignung der Methode zur Simulation industrieller Probleme zu zeigen.

CONTENTS

1 INTRODUCTION

1.1 Overview

The physical problem of transient heat transport and storage in solid media, coined by the term heat conduction, has caught the interest of scientific society from the early 18^{th} century on. It was people like Gabriel Daniel Fahrenheit ($1686-1736$) with the invention of the *mercury thermometer*, Joseph Black ($1728-1799$) with the observation of *specific heat*, Pierre Simon Laplace ($1749-1827$) with its experimental determination, and many more, who lead to Jean Baptiste Joseph Fourier's ($1768-1830$) masterpiece *Théorie de la Propagation de la Chaleur dans les Solids* [33], submitted to the French Academy in 1807. However, due to lack of approval by his colleagues this paper got never published and it was not until 1822, when Fourier decided to publish *Théorie Analytique de la Chaleur* [33] by himself that his theory became accessible to a broader audience. Soon, this latter contribution got widely accepted by the scientific community, even more so as analogies to other fields had been recognized. Among others, some of the fields inspired by Fourier's theory were *chemistry* with molecular diffusion, *electrodynamics* although there the analogy was misleading, *probability theory* with random walks and stochastic differential equations. While each of those individual fields offers its fascination, we refer the reader for a more profound survey to [33] and steer our attention towards the heat equation and its application in the original intention.

Already Fourier himself offered a powerful way of solving initial boundary value problems of the heat equation – following the approach of his predecessors Daniel Bernoulli ($1700-1782$), Jean D'Alembert ($1717-1783$), and Leonhard Euler ($1707-1783$) he applied the method of separation of variables yielding solutions in form of trigonometric series [33]. However, it was not until the second half of the 20^{th} century when the integral equation approach from classical potential [24] theory was extended to the heat equation [28, 37], which proved to be a powerful tool for showing existence and uniqueness of solutions to the heat equation in terms of layer potentials. While in general a closed form solution for neither of these approaches can be found, they still provide the basics for approximation schemes to solve heat conduction problems in more general settings. In this context one should mention Finite Difference- and Finite Element Methods, which are PDE based approximation techniques. Of course these techniques are not limited to the heat equation, nonetheless we would like to refer the reader to [12, 15] for some groundbreaking developments made in the context of the heat equation and [48] for the apparently first application of the FEM to heat conduction problems. While these

PDE based methods are domain based as well, the second category of approximations schemes is boundary based and may be summarized by the term Boundary Integral Equation (BIE) Methods with the corresponding counterparts being Nyström- and Boundary Element Methods (BEM) – in the same way as in the Finite Difference scheme the derivatives are replaced by finite difference quotients instead of taking the variational approach, the Nyström method replaces the integrals by quadrature rules. It appears that the former method was first applied to the heat equation in [44] while the latter seems to have a longer history and appearing first with a detour via an inverse Laplace transformation [38], then directly in time domain with a space-time Galerkin discretization [10, 35], and finally with a convolution quadrature method (CQM) based approach [30]. For a more complete review we refer to [11].

Besides the distinction between PDE (or domain) and BIE (or boundary) based approaches these two categories of solvers feature other opposing properties, too. The most evident probably being that the resulting linear system in the former case turns out to be sparsely, while in the latter case it is densely populated. Even though the reduction to the boundary leads to $N_\Gamma = \mathcal{O}(h_\Gamma^{-2})$ instead of $N_\Omega = \mathcal{O}(h_\Omega^{-3})$ in the case of a domain based method, where N_Ω/N_Γ are the numbers of degrees of freedom and h_Ω/h_Γ the discretization parameters. The quadratic complexity of solving for a dense system matrix destroys this advantage due to $\mathcal{O}(N_\Gamma^{-2}) = \mathcal{O}(h_\Gamma^{-4})$ instead of $\mathcal{O}(N_\Omega) = \mathcal{O}(h_\Omega^{-3})$ for a sparsely populated system. At first sight this drawback seems to completely rule out BIE based methods for large scale problems, however, there are fast algorithms available [19, 26, 43, 45] to reduce the cost to almost $\mathcal{O}(N_\Gamma) = \mathcal{O}(h_\Gamma^{-2})$ and thus gain competitiveness again. Together, with the boundary reduction this is the motivation for us to improve upon such approaches for the efficient solution of heat conduction problems.

Most industrial processes are strongly linked to and driven by heat transfer. Therefore, it is a crucial task for the design engineer to be able to accurately and efficiently perform thermal simulations, e.g. the simulation of press hardening tools within the thermo-mechanical simulation of the press hardening process, which serves as the main motivation for our efforts. The conceptual idea of this process is to heat the raw metal sheet above crystallization temperature, bring it into the final shape and cool it down at a high, predefined rate. This can be achieved by an arbitrarily complicated grid of cooling channels penetrating the press hardening tool. With the aid of some agent flowing through these channels such a layout allows to withdraw energy from the hot metal sheet. Roughly speaking, the influence of elastic/plastic stresses onto the thermal behavior of such tools can be neglected and, therefore, the thermal simulation can be isolated from the thermo-mechanical simulation. The design engineer knows which cooling rate leads to the desired crystal structure and computes the energy to be withdrawn by the tools. This information can be translated into a set of mixed boundary conditions for a homogeneous initial boundary value problem describing the heat diffusion through the tools. We decide to work with fast Boundary Element Methods for two major reasons. First, the geometry of the press hardening tools is extremely complicated and, therefore, a reduction of the problem to the boundary leads to a

significantly reduced meshing effort. Second, since only the surface temperature distribution of the press hardening tool is required for the coupled thermo-mechanical simulation of the press hardening process a direct Boundary Element Method seems a rather natural approach.

1.2 State of the Art

Boundary integral equations related to the heat equation have been studied in [3, 7, 10, 35, 37]. For classically used second kind integral equations, e.g. a double layer potential approach for the Dirichlet problem and an adjoint double layer potential ansatz for the Neumann problem, the compactness of these integral operators on smooth domains provided by Pogorzelski et al. [37] guarantees well posedness of the problem and the analysis of numerical methods. However, in the case of non smooth domains and first kind integral equations the situation is more complicated. Brown [7] gave some first results on Lipschitz domains before almost contemporaneously Arnold and Noon [3] and Costabel [10] showed the boundedness and coercivity of the thermal single layer operator. Furthermore, Costabel [10] showed the coercivity of the hyper-singular operator and the boundedness of all thermal boundary integral operators in the appropriate anisotropic Sobolev space setting on Lipschitz domains. With these results the analysis follows the well known pattern of the elliptic theory, i.e. the lemma of Lax Milgram guarantees uniqueness and solvability of corresponding operator equations and their Galerkin variational formulation. Using conforming finite dimensional sub-spaces of the natural energy spaces, uniqueness and solvability translates directly to the discrete system, where Cea's Lemma guarantees quasi-optimality. Using the approximation property of the finite dimensional ansatz spaces, the regularity of the boundary integral operators, and assuming certain regularity of the discretization one can derive explicit error estimates in various norms around the energy norm. Despite the beauty of this theory, the problem with the high computational complexity has yet to be solved.

The first attempt to solve heat conduction problems by thermal layer potential representations in almost optimal complexity was presented by Greengard and Strain [19]. However, their method is limited to bounded domains, where they split the temporal range of the heat kernel into a local (recent) and history (distant) part. For the history part they use a Fourier series expansion with periodic boundary conditions, which converges exponentially due to the smoothness of the heat kernel with sufficient temporal separation. For the local part, on the other hand, a representation via the method of images is used. In this case the short temporal range results in a sharply peaked heat kernel where Taylor expansion is very well suited. One year later, the same authors presented the Fast Gauss Transform (FGT) [20], which can be used to efficiently represent the solution of pure initial value problems of the heat equation via an initial potential in form of a Gauss transform (heat kernel with fixed variance is a Gaussian). Their approach is based on a hierarchical subdivision of the

computational domain and expansion of the Gaussian kernel in a Hermite series around the center of source boxes. Such an expansion allows to efficiently evaluate the collective influence of all sources contained in that box onto a collection of target points located in some target box. Later on Strain [41] extended this idea to two-dimensional free-space heat conduction by interpreting the representation of the initial value solution by an initial potential as an evolution equation and thus finding the solution by repeated application of the FGT. Duhamel's principle is used to find solutions of the inhomogeneous problems and an analogy between the forcing term and surface densities in the thermal layer potential representation of initial boundary value problems is used to sketch the solution of heat conduction problems in domains with boundaries. Unfortunately this paper only presents some preliminary results and refers to forthcoming papers that seem to never have appeared. In an attempt to overcome the limitations of the earlier presented spectral approach Greengard and Lin [16] presented a spectral approximation of the free-space heat kernel, where the difficulties of dealing with the approximation of the now continuous spectrum are elaborated. Instead of sampling a finite number of Fourier modes a finite range of the Fourier integral needs to be approximated, which is done via dyadic splitting and a composite quadrature rule. Note that this makes an application of the Fast Fourier Transform (FFT) impossible and requires some nonuniform FFT instead. From there it appears that it took a few years until Li and Greengard [26] incorporated this approach into a method for the evaluation of thermal layer potentials. They propose to combine the spectral approximation of the free-space heat kernel for the history part with a full product integration scheme for the evaluation of the local part to overcome the 'geometrically induced stiffness' proper to asymptotic expansions and partial product integration schemes [26] and fed the readers hope with the presentation of some numerical examples in a future paper. To the authors knowledge this has been the last contribution in the field of spectral methods, while in the meantime Tausch [43] introduced the parabolic Fast Multipole Method (pFMM). A Lagrange interpolation of the heat kernel in time together with a hierarchical clustering and incorporation of causality leads to a causal FMM structure in time. What remains is a family of Gauss transforms, which are efficiently evaluated by means of the FGT concept based on a Chebyshev expansion of the time interpolated heat kernel and a spatial clustering. Thus, using the causal Fast Multipole Method (cFMM) structure in time to collect spatial contributions via an adapted FGT scheme in space according to some spatio-temporal admissibility condition dictated by the time scaling of the heat kernel one ends up with the parabolic FMM. The asymptotic smoothness of the heat kernel in time and the exponential decay in space together with the exponential convergence of the Chebyshev-Lagrange expansion guarantees an application of the pFMM accelerated farfield or smooth part of the thermal layer potential in optimal time. Furthermore, the nearfield or singular part of the potential can be evaluated directly in optimal complexity because the exponential decay in space allows a truncation of distant potential contributions.

What are the advantages of a pFMM accelerated Space-Time Galerkin BEM? We opted for a Galerkin approach due to the fact that it can deal with Lipschitz domains compared to the higher regularity requirements by product integration and Nyström methods. Moreover, due to the complications encountered by the spectral approximation of the free-space heat kernel, we resort to the parabolic Fast Multipole Method based on a hierarchical space-time clustering and a Lagrange-Chebyshev expansion of the free-space heat kernel. We would like to remark that such an approach seems to rule out the combination of the CQM in combination with a fast algorithm in space because the Laplace transform destroys the Gaussian structure of the heat kernel, hence the spatial variables do not separate into individual directions and, therefore, was not further pursued.

1.3 Outline

Chapter 2 is concerned with a derivation of the heat equation and related initial boundary value problems. Subsequently, we derive related boundary integral equations and use them to present boundary integral formulations of these initial boundary value problems and their Galerkin variational formulations.

In Chapter 3 we introduce a rather standard space-time discretization on which we define finite dimensional tensor product ansatz and test spaces. With these ingredients we define Galerkin Boundary Element Methods for the approximate solution of the previously defined initial boundary value problems related to the heat equation. Additionally, we provide some error estimates, which promise optimal convergence of these methods.

These Boundary Element Methods lead to densely populated system matrices, which imply $\mathcal{O}(N_x^2 N_t^2)$ work in the number of spatial N_x and temporal unknowns N_t in terms of storage and computation. Therefore, we devote Chapter 4 to reduce both storage and work to almost $\mathcal{O}(N_x N_t)$. The strategy that we pursue is a variant of the Fast Multipole Method, which itself is based on the idea that one can cluster the influence of degrees of freedom in a hierarchic way.

Finally, in Chapter 5 we test our method on some benchmark problems to verify that the stated goals were achieved, namely a stable and robust algorithm with optimal complexity in the number of unknowns. This is not enough though, we use our fast method to efficiently solve some industrial applications involving heat diffusion, which without the fast algorithm were not conceivable.

2 HEAT TRANSFER

2.1 Heat Diffusion

In this thesis, we deal with the solution of initial boundary value problems related to the heat equation in open domains $\Omega \subset \mathbb{R}^3$ with Lipschitz boundary Γ. We are interested in the solution throughout a time interval $\Upsilon := (0,T)$ with $\mathbb{R} \ni T > 0$ and assume once and for all that Ω does not change over time. Furthermore, we restrict ourselves to problems with homogeneous, isotropic, and incompressible material behavior.

2.1.1 Heat Equation

The heat equation describes heat diffusion through solids and static fluids or gases[4, 23]. It is derived from Fourier's law and conservation of energy. The former is obtained from phenomenological observations and links the heat flux $\mathbf{q}[\mathrm{W}/\mathrm{m}^2]$ to the negative gradient of the temperature $u[^\circ\mathrm{C}]$ via the thermal conduction coefficient $\lambda\,[\mathrm{W}/^\circ\mathrm{Cm}]$

$$\mathbf{q}(\tilde{\mathbf{x}},t) = -\lambda \nabla_{\tilde{\mathbf{x}}} u(\tilde{\mathbf{x}},t) \quad (\tilde{\mathbf{x}},t) \in \Omega \times \Upsilon\,. \tag{2.1}$$

Observe that the homogeneous and isotropic material behavior leads to a constant thermal conduction coefficient. Furthermore, conservation of energy is required by the first law of thermodynamics, which states that the rate of internal energy change $\frac{\partial U}{\partial t} := \partial_t U[\mathrm{W}]$ must balance the heat flux $Q[\mathrm{W}]$ through the boundary Γ and the internal energy generation $P[\mathrm{W}]$ at all times

$$\partial_t U(t) = Q(t) + P(t) \quad t \in \Upsilon\,. \tag{2.2}$$

Due to the assumption of homogeneous and incompressible material behavior we have a constant density $\rho[\mathrm{kg}/\mathrm{m}^3]$ and a constant specific heat capacity $c_p[\mathrm{Wsec}/^\circ\mathrm{Ckg}]$, hence the rate of internal energy change is given by

$$\partial_t U(t) := \int_\Omega \rho c_p \partial_t u(\tilde{\mathbf{x}},t)\mathrm{d}\tilde{\mathbf{x}} \quad t \in \Upsilon\,. \tag{2.3}$$

An application of the Divergence Theorem to the heat flux through the boundary Γ together with Fourier's law (2.1) yields

$$Q(t) := -\int_\Gamma \mathbf{n}_{\mathbf{x}}{}^\top \mathbf{q}(\mathbf{x},t)\mathrm{d}s_{\mathbf{x}} = -\int_\Omega \nabla_{\tilde{\mathbf{x}}}^\top \mathbf{q}(\tilde{\mathbf{x}},t)\mathrm{d}\tilde{\mathbf{x}} = \int_\Omega \lambda \Delta u(\tilde{\mathbf{x}},t)\mathrm{d}\tilde{\mathbf{x}} \quad t \in \Upsilon\,, \tag{2.4}$$

where $\mathbf{n}_\mathbf{x}$ denotes the unit outer normal vector at $\mathbf{x} \in \Gamma$ and the minus sign guarantees that an outward heat flux is positive. Last but not least, the internal energy generation is given by the volume integral over the energy density function $f[\mathrm{W/m^3}]$

$$P(t) := \int_\Omega f(\tilde{\mathbf{x}},t)\mathrm{d}\tilde{\mathbf{x}} \quad t \in \Upsilon\,. \tag{2.5}$$

Finally, since Ω is arbitrary, (2.2) with (2.3), (2.4) and (2.5) leads to the heat equation

$$\rho c_p \partial_t u(\tilde{\mathbf{x}},t) = \lambda \Delta u(\tilde{\mathbf{x}},t) + f(\tilde{\mathbf{x}},t) \quad (\tilde{\mathbf{x}},t) \in \Omega \times \Upsilon\,. \tag{2.6}$$

2.1.2 Initial Boundary Value Problems

In order to give proper statements of heat diffusion problems in form of initial boundary value problems according to our original aim, we need to supplement the heat equation (2.6) with a combination of initial- and boundary values. Therefore, we prescribe an initial condition throughout the entire domain

$$u(\tilde{\mathbf{x}},0) = u_0(\tilde{\mathbf{x}}) \quad \tilde{\mathbf{x}} \in \Omega$$

and boundary conditions on some subsets of the space–time cylinder's lateral boundary. To this end we split the boundary into disjoint parts $\Gamma_D, \Gamma_N, \Gamma_R$ such that $\Gamma_D \cap \Gamma_N = \Gamma_D \cap \Gamma_R = \Gamma_N \cap \Gamma_R = \emptyset$ and $\Gamma_D \cup \Gamma_N \cup \Gamma_R = \Gamma$. Imposing a temperature field $u[^\circ\mathrm{C}]$ is classically referred to as Dirichlet boundary condition

$$u(\mathbf{x},t) = g_D(\mathbf{x},t) \quad (\mathbf{x},t) \in \Gamma_D \times \Upsilon\,,$$

whereas prescribing a surface heat flux $q[\mathrm{W/m}]$ is called a Neumann boundary condition

$$q(\mathbf{x},t) := \lambda\, \partial_{n_\mathbf{x}} u(\mathbf{x},t) = g_N(\mathbf{x},t) \quad (\mathbf{x},t) \in \Gamma_N \times \Upsilon\,,$$

with $\partial_{n_\mathbf{x}} := \mathbf{n}_\mathbf{x}{}^\top \nabla_\mathbf{x}$. Finally, a linear combination of Dirichlet and Neumann boundary conditions is denoted a Robin type or convective boundary condition with the heat transfer coefficient $\kappa[\mathrm{W/^\circ Cm^2}]$

$$\lambda\, \partial_{n_\mathbf{x}} u(\mathbf{x},t) + \kappa(\mathbf{x},t) u(\mathbf{x},t) = g_R(\mathbf{x},t) \quad (\mathbf{x},t) \in \Gamma_R \times \Upsilon\,.$$

Remark 2.1. *The latter type of boundary condition is the most physical one for heat transfer problems, where it is referred to as Newton's law of cooling*

$$\lambda\, \partial_{n_\mathbf{x}} u(\mathbf{x},t) = -\kappa(\mathbf{x},t)\,(u(\mathbf{x},t) - u_\infty(\mathbf{x},t)) \quad (\mathbf{x},t) \in \Gamma_R \times \Upsilon\,.$$

It states that the surface heat flux $q(\mathbf{x},t)$ is proportional to the temperature difference between the surface of the domain and the surrounding environment $u(\mathbf{x},t) - u_\infty(\mathbf{x},t)$ with the proportionality factor being the heat transfer coefficient κ. In general $\kappa = \kappa(\mathbf{x},t,u(\mathbf{x},t))$, however, for our purpose $\kappa = \kappa(\mathbf{x},t)$ with $0 \le \kappa(\mathbf{x},t) \le \kappa_0 \in \mathbb{R}$ will be sufficient.

For the remainder of this work we assume a vanishing energy density function $f(\tilde{\mathbf{x}},t) \equiv 0$ and vanishing initial conditions $u(\tilde{\mathbf{x}},0) \equiv 0$. Then we may state a homogeneous initial boundary value problem of the homogeneous heat equation involving all three types of boundary condition by

$$\alpha \Delta u(\tilde{\mathbf{x}},t) = \partial_t u(\tilde{\mathbf{x}},t) \qquad (\tilde{\mathbf{x}},t) \in \Omega \times \Upsilon\,, \tag{2.7a}$$

$$u(\tilde{\mathbf{x}},0) = 0 \qquad \tilde{\mathbf{x}} \quad \in \Omega\,, \tag{2.7b}$$

$$u(\mathbf{x},t) = g_D(\mathbf{x},t) \qquad (\mathbf{x},t) \in \Gamma_D \times \Upsilon\,, \tag{2.7c}$$

$$\lambda \partial_{n_\mathbf{x}} u(\mathbf{x},t) = g_N(\mathbf{x},t) \qquad (\mathbf{x},t) \in \Gamma_N \times \Upsilon\,, \tag{2.7d}$$

$$\lambda \partial_{n_\mathbf{x}} u(\mathbf{x},t) + \kappa(\mathbf{x},t) u(\mathbf{x},t) = g_R(\mathbf{x},t) \qquad (\mathbf{x},t) \in \Gamma_R \times \Upsilon\,, \tag{2.7e}$$

with the heat diffusion coefficient $\alpha[\mathrm{m}^2/\mathrm{sec}] = \lambda/\rho c_p$. Eliminating appropriate boundary parts $\Gamma_i \subset \Gamma$ with $i \in \{D,N,R\}$ one obtains homogeneous initial boundary value problems of different type. However, since we intend to work with boundary integral equations we refer to the respective boundary integral formulations in Section 2.4.

2.2 Boundary Integral Equations of the Heat Equation

2.2.1 Representation Formula

We know that the solution of the homogeneous heat equation with homogeneous initial conditions is given by the representation formula [10, Theorem 2.20]

$$u(\tilde{\mathbf{x}},t) = \int_0^t \int_\Gamma G(\tilde{\mathbf{x}}-\mathbf{y},t-\tau)\frac{q(\mathbf{y},\tau)}{\rho c_p}\mathrm{d}s_\mathbf{y}\mathrm{d}\tau - \int_0^t \int_\Gamma \alpha \partial_{n_\mathbf{y}} G(\tilde{\mathbf{x}}-\mathbf{y},t-\tau)u(\mathbf{y},\tau)\mathrm{d}s_\mathbf{y}\mathrm{d}\tau$$
$$(\tilde{\mathbf{x}},t) \in \Omega \times \Upsilon\,, \tag{2.8}$$

provided that the Dirichlet- and Neumann trace of the solution are known and the heat equation's fundamental solution [37] is given by

$$G(\mathbf{x}-\mathbf{y},t-\tau) = \begin{cases} (4\pi\alpha(t-\tau))^{-3/2}\exp\left(-\frac{|\mathbf{x}-\mathbf{y}|^2}{4\alpha(t-\tau)}\right) & \mathbf{x}-\mathbf{y} \in \mathbb{R}^3, t-\tau \geq 0 \\ 0 & \mathbf{x}-\mathbf{y} \in \mathbb{R}^3, t-\tau < 0\,. \end{cases} \tag{2.9}$$

Observe that in the classical terminology [37] the first expression on the left hand side of (2.8) is called the single layer potential and the second term the double layer potential.

It is a well known fact that one way of solving homogeneous initial boundary value problems of the homogeneous heat equation (2.7a) – (2.7e) boils down to computing the complete set of Dirichlet- and Neumann traces. This is achieved by taking the Dirichlet- and

Neumann traces of the representation formula (2.8), which leads to the first- and second boundary integral equation, respectively. Then one can use this set of equations, incorporate appropriate boundary conditions and solve for the yet unknown trace data, which together with the representation formula (2.8) defines the solution of the respective initial boundary value problem. Such a strategy is commonly referred to as direct boundary integral approach.

Remark 2.2. *While we focus on the direct approach, there are other possible techniques based on the observation that both potentials in* (2.8) *satisfy the homogeneous heat equation with homogeneous initial conditions. Thus one can find solutions of related initial boundary value problems by solving a single- or double layer ansatz for unknown densities $q(\mathbf{x},t)$ or $u(\mathbf{x},t)$, respectively, which satisfy the boundary data. Those potentials are then solutions $u(\tilde{\mathbf{x}},t)$ of the initial boundary value problems. Such strategies are called indirect boundary integral approaches.*

2.2.2 Boundary Integral Equations

As mentioned before, we take the Dirichlet trace of the representation formula (2.8), i.e. $\Omega \ni \tilde{\mathbf{x}} \to \mathbf{x} \in \Gamma$, to obtain the first boundary integral equation

$$\mathcal{V}q(\mathbf{x},t) - (\mathcal{I} - \mathcal{J} + \mathcal{K})\, u(\mathbf{x},t) = 0\,, \tag{2.10}$$

with the thermal single- and double layer operator

$$\mathcal{V}q(\mathbf{x},t) := \int_0^t \int_\Gamma G(\mathbf{x}-\mathbf{y},t-\tau)\frac{q(\mathbf{y},\tau)}{\rho c_p}\mathrm{d}s_\mathbf{y}\mathrm{d}\tau\,, \tag{2.11}$$

$$\mathcal{K}u(\mathbf{x},t) := \int_0^t \int_\Gamma \alpha\frac{\partial}{\partial n_\mathbf{y}}G(\mathbf{x}-\mathbf{y},t-\tau)u(\mathbf{y},\tau)\mathrm{d}s_\mathbf{y}\mathrm{d}\tau\,. \tag{2.12}$$

Observe that the jump term is given by $\mathcal{J}(\mathbf{x}) = \pm\mathcal{I}(\mathbf{x})/2$ almost everywhere on Γ, with the plus sign applying for the interior and the minus sign for the exterior problem. Next we take the Neumann trace of the representation formula (2.8), i.e. the gradient with $\tilde{\mathbf{x}} \ni \Omega \to \mathbf{x} \in \Gamma$ in the inner product with the outer normal vector $\mathbf{n}_\mathbf{x}$, which yields the second boundary integral equation

$$\left(\mathcal{J} - \mathcal{I} + \mathcal{K}'\right) q(\mathbf{x},t) + \mathcal{D}u(\mathbf{x},t) = 0\,, \tag{2.13}$$

with the adjoint double layer- and the hyper-singular operator

$$\mathcal{K}'q(\mathbf{x},t) := \alpha\frac{\partial}{\partial n_{\mathbf{x}}}\int_0^t\int_\Gamma G(\mathbf{x}-\mathbf{y},t-\tau)\frac{q(\mathbf{y},\tau)}{\rho c_p}\mathrm{d}s_{\mathbf{y}}\mathrm{d}\tau\,, \tag{2.14}$$

$$\mathcal{D}u(\mathbf{x},t) := -\alpha\frac{\partial}{\partial n_{\mathbf{x}}}\int_0^t\int_\Gamma \alpha\frac{\partial}{\partial n_{\mathbf{y}}}G(\mathbf{x}-\mathbf{y},t-\tau)u(\mathbf{y},\tau)\mathrm{d}s_{\mathbf{y}}\mathrm{d}\tau\,. \tag{2.15}$$

2.3 Properties of Boundary Integral Operators

Even though the heat equation is the prototypical parabolic partial differential equation, it turns out that the related boundary integral operators have similar properties as in the elliptic case. However, the setting is slightly different [10, 35], the correct function spaces are not the rather well known classical Sobolev spaces $H^r(\Gamma)$ [2, 27] but their anisotropic counterparts $H^{r,s}(\Gamma\times\Upsilon)$ [27, 28]. Since it is not the aim of this thesis to elaborate their theory in full detail, we only provide a short exposition of some basic concepts in Appendix A. That is just enough details to understand the basic properties of thermal boundary integral operators (remainder of this section), Galerkin variational formulations of boundary integral formulations of initial boundary value problems (Section 2.4) and error estimates for their approximate solutions (Section 3.2).

2.3.1 The Calderon Projector in the Energy Norm

The Calderon projector of the heat equation [10] $\mathcal{C} : H^{\frac{1}{2},\frac{1}{4}}(\Gamma\times\Upsilon)\times H^{-\frac{1}{2},-\frac{1}{4}}(\Gamma\times\Upsilon)\to H^{\frac{1}{2},\frac{1}{4}}(\Gamma\times\Upsilon)\times H^{-\frac{1}{2},-\frac{1}{4}}(\Gamma\times\Upsilon)$ is defined by the boundary integral equations (2.10) and (2.13)

$$\begin{pmatrix} u \\ q \end{pmatrix} = \begin{pmatrix} \frac{\mathcal{I}}{2}-\mathcal{K} & \mathcal{V} \\ \mathcal{D} & \frac{\mathcal{I}}{2}+\mathcal{K}' \end{pmatrix}\begin{pmatrix} u \\ q \end{pmatrix} := \mathcal{C}\begin{pmatrix} u \\ q \end{pmatrix}\,.$$

Interchanging its columns we get the isomorphism $\mathcal{A} : H^{-\frac{1}{2},-\frac{1}{4}}(\Gamma\times\Upsilon)\times H^{\frac{1}{2},\frac{1}{4}}(\Gamma\times\Upsilon)\to H^{\frac{1}{2},\frac{1}{4}}(\Gamma\times\Upsilon)\times H^{-\frac{1}{2},-\frac{1}{4}}(\Gamma\times\Upsilon)$

$$\mathcal{A} := \begin{pmatrix} \mathcal{V} & \frac{\mathcal{I}}{2}-\mathcal{K} \\ \frac{\mathcal{I}}{2}+\mathcal{K}' & \mathcal{D} \end{pmatrix}\,.$$

Theorem 2.1. *$\mathcal{A}$ is bounded and $H^{-\frac{1}{2},-\frac{1}{4}}(\Gamma\times\Upsilon)\times H^{\frac{1}{2},\frac{1}{4}}(\Gamma\times\Upsilon)$ elliptic [10, Theorem 3.11], which implies the boundedness of all boundary integral operators, the $H^{-\frac{1}{2},-\frac{1}{4}}(\Gamma\times\Upsilon)$ ellipticity of the single layer operator [3, 35] [10, Corollary 3.13] and the $H^{\frac{1}{2},\frac{1}{4}}(\Gamma\times\Upsilon)$ ellipticity of hyper-singular operator [10, Corollary 3.13].*

Corollary 2.1. *The single layer operator is invertible due to Theorem 2.1, hence we get a Dirichlet to Neumann map* $\mathcal{S} : H^{\frac{1}{2},\frac{1}{4}}(\Gamma\times\Upsilon) \to H^{-\frac{1}{2},-\frac{1}{4}}(\Gamma\times\Upsilon)$ *through the symmetric Steklov-Poincaré operator* $\mathcal{S} := \mathcal{D} + (\frac{\mathcal{I}}{2} + \mathcal{K}')\mathcal{V}^{-1}(\frac{\mathcal{I}}{2} + \mathcal{K})$ *whose* $H^{\frac{1}{2},\frac{1}{4}}(\Gamma\times\Upsilon)$ *boundedness and ellipticity is a direct consequence of Theorem 2.1.*

Remark 2.3. *Due to the definition of the spaces* $\widetilde{H}^{r,s}(\Gamma_i\times\Upsilon)$ *with* $\Gamma_i \subset \Gamma$ *and* $i \in \{D,N,R\}$ *in Appendix A, it is clear that the properties of all operators in Theorem 2.1 and Lemma 3.3 hold for them, too.*

2.3.2 Mapping Properties of Boundary Integral Operators

Theorem 2.2. *On Lipschitz boundaries* Γ *and for* $s \in \left(-\frac{1}{2},\frac{1}{2}\right)$ *the boundary integral operators of the heat equation*

$$\begin{aligned}
\mathcal{V} &: H^{-\frac{1}{2}+s,(-\frac{1}{2}+s)/2}(\Gamma\times\Upsilon) \to H^{\frac{1}{2}+s,(\frac{1}{2}+s)/2}(\Gamma\times\Upsilon)\\
\tfrac{\mathcal{I}}{2} - \mathcal{K} &: H^{\frac{1}{2}+s,(\frac{1}{2}+s)/2}(\Gamma\times\Upsilon) \to H^{\frac{1}{2}+s,(\frac{1}{2}+s)/2}(\Gamma\times\Upsilon)\\
\tfrac{\mathcal{I}}{2} + \mathcal{K}' &: H^{-\frac{1}{2}+s,(-\frac{1}{2}+s)/2}(\Gamma\times\Upsilon) \to H^{-\frac{1}{2}+s,(-\frac{1}{2}+s)/2}(\Gamma\times\Upsilon)\\
\mathcal{D} &: H^{\frac{1}{2}+s,(\frac{1}{2}+s)/2}(\Gamma\times\Upsilon) \to H^{-\frac{1}{2}+s,(-\frac{1}{2}+s)/2}(\Gamma\times\Upsilon)
\end{aligned}$$

are isomorphisms [10, Theorem 4.8 and 4.16].

2.4 Galerkin Variational Boundary Integral Formulations

Now, we are in the position to provide boundary integral formulations of homogeneous initial boundary value problems related to the homogeneous heat equation, i.e. (2.7a) through (2.7e). As mentioned before, we limit ourselves to direct formulations based on the Calderon projector and its restrictions in Theorem 2.1 and focus purely on formulations which we use in Chapter 5 at the end of this thesis.

2.4.1 Initial Dirichlet Boundary Value Problem

Using the first boundary integral equation (2.10) we state the initial Dirichlet boundary value problem, i.e. (2.7a), (2.7b), (2.7c) with given $g_D \in H^{\frac{1}{2},\frac{1}{4}}(\Gamma\times\Upsilon)$ and $\Gamma := \Gamma_D$

$$\mathcal{V}q(\mathbf{x},t) = \left(\tfrac{\mathcal{I}}{2} + \mathcal{K}\right) g_D(\mathbf{x},t) \quad (\mathbf{x},t) \in \Gamma\times\Upsilon\,,$$

which in $H^{-\frac{1}{2},-\frac{1}{4}}(\Gamma\times\Upsilon)$ is equivalent to solving the Galerkin variational form

$$\langle \mathcal{V}q, w\rangle_{\Gamma\times\Upsilon} = \langle \left(\tfrac{\mathcal{I}}{2} + \mathcal{K}\right) g_D, w\rangle_{\Gamma\times\Upsilon} \quad \forall w \in H^{-\frac{1}{2},-\frac{1}{4}}(\Gamma\times\Upsilon)\,. \tag{2.16}$$

Uniqueness and quasi optimality for the solution $q \in H^{-\frac{1}{2},-\frac{1}{4}}(\Gamma \times \Upsilon)$ of (2.16) follow from the boundedness and $H^{-\frac{1}{2},-\frac{1}{4}}(\Gamma \times \Upsilon)$ ellipticity of the single layer operator provided by Theorem 2.1.

2.4.2 Initial Neumann Boundary Value Problem

We use the second boundary integral equation (2.13) to give a boundary integral formulation of the initial Neumann boundary value problem, i.e. (2.7a), (2.7b), (2.7d) with given $g_N \in H^{-\frac{1}{2},-\frac{1}{4}}(\Gamma \times \Upsilon)$ and $\Gamma := \Gamma_N$

$$\mathcal{D}u(\mathbf{x},t) = \left(\tfrac{\mathcal{I}}{2} - \mathcal{K}'\right) g_N \quad (\mathbf{x},t) \in \Gamma \times \Upsilon \,,$$

which in $H^{\frac{1}{2},\frac{1}{4}}(\Gamma \times \Upsilon)$ is equivalent to solving the Galerkin variational form

$$\langle Du, v\rangle_{\Gamma\times\Upsilon} = \langle \left(\tfrac{\mathcal{I}}{2} - \mathcal{K}'\right) g_N, v\rangle_{\Gamma\times\Upsilon} \quad \forall v \in H^{\frac{1}{2},\frac{1}{4}}(\Gamma \times \Upsilon) \,. \tag{2.17}$$

Uniqueness and quasi-optimality for the solution $u \in H^{\frac{1}{2},\frac{1}{4}}(\Gamma \times \Upsilon)$ of (2.17) follow from the boundedness and $H^{\frac{1}{2},\frac{1}{4}}(\Gamma \times \Upsilon)$ ellipticity of the hyper-singular operator ensured by Theorem 2.1.

2.4.3 Initial Robin Boundary Value Problem

Similar to [40, page 181] we use the symmetric approximation of the Steklov-Poincaré operator (3.24) as a Dirichlet to Neumann map and state a boundary integral formulation for the homogeneous initial Robin boundary value problem, i.e. (2.7a), (2.7b), (2.7e) with given $g_R \in H^{-\frac{1}{2},-\frac{1}{4}}(\Gamma \times \Upsilon)$, $0 \leq \kappa \leq \kappa_0 \in \mathbb{R}$ and $\Gamma := \Gamma_R$

$$(\mathcal{S} + \kappa)u(\mathbf{x},t) = g_R(\mathbf{x},t) \quad (\mathbf{x},t) \in (\Gamma \times \Upsilon) \,.$$

In $H^{\frac{1}{2},\frac{1}{4}}(\Gamma \times \Upsilon)$ this is equivalent to solving the Galerkin variational form

$$\langle (\mathcal{S} + \kappa)\, u, v\rangle_{\Gamma\times\Upsilon} = \langle g_R, v\rangle_{\Gamma\times\Upsilon} \quad \forall v \in H^{\frac{1}{2},\frac{1}{4}}(\Gamma \times \Upsilon) \,. \tag{2.18}$$

Uniqueness and quasi-optimality for the solution $u \in H^{\frac{1}{2},\frac{1}{4}}(\Gamma \times \Upsilon)$ of (2.18) follow from the $H^{\frac{1}{2},\frac{1}{4}}(\Gamma \times \Upsilon)$ boundedness and ellipticity of the Steklov-Poincareé operator (3.24) given in Corollary 2.1 and the properties of the heat transfer coefficient κ.

2.4.4 Mixed Initial Boundary Value Problems

In what follows now we present a boundary integral formulation similar to [40, page 180] for a mixed initial boundary value problem, i.e. (2.7a), (2.7b), (2.7c), (2.7d) and (2.7e) with $\Gamma := \Gamma_D \cup \Gamma_N \cup \Gamma_R$ and $0 \leq \kappa \leq \kappa_0 \in \mathbb{R}$. For this purpose we define

$$g_{NR}(\mathbf{x},t) := \begin{cases} g_N(\mathbf{x},t) & (\mathbf{x},t) \in \Gamma_N \times \Upsilon \\ g_R(\mathbf{x},t) & (\mathbf{x},t) \in \Gamma_R \times \Upsilon \end{cases}, \quad \kappa_{NR}(\mathbf{x},t) := \begin{cases} 0 & (\mathbf{x},t) \in \Gamma_N \times \Upsilon \\ \kappa(\mathbf{x},t) & (\mathbf{x},t) \in \Gamma_R \times \Upsilon \end{cases},$$

$\Gamma_{NR} := \Gamma_N \cup \Gamma_R$ and assume an appropriate extension of the given Dirichlet data

$$u(\mathbf{x},t) = \tilde{g}_D(\mathbf{x},t) + \tilde{u}(\mathbf{x},t) \quad (\mathbf{x},t) \in \Gamma \times \Upsilon \,,$$

such that $H^{\frac{1}{2},\frac{1}{4}}(\Gamma \times \Upsilon) \ni \tilde{g}_D(\mathbf{x},t) = g_D(\mathbf{x},t)$ for $(\mathbf{x},t) \in \Gamma_D \times \Upsilon$ and $\tilde{u} \in \widetilde{H}^{\frac{1}{2},\frac{1}{4}}(\Gamma_{NR} \times \Upsilon)$. We choose a boundary integral formulation based on the symmetric Steklov-Poincaré operator defined in Corollary 2.1 as a Dirichlet to Neumann map

$$(\mathcal{S} + \kappa_{NR})\,\tilde{u}(\mathbf{x},t) = g_{NR}(\mathbf{x},t) - (\mathcal{S} + \kappa_{NR})\,\tilde{g}_D(\mathbf{x},t) \quad (\mathbf{x},t) \in \Gamma_{NR} \times \Upsilon \,,$$

which in $\widetilde{H}^{\frac{1}{2},\frac{1}{4}}(\Gamma_{NR} \times \Upsilon)$ is equivalent to solving

$$\langle (\mathcal{S} + \kappa_{NR})\,\tilde{u}, v \rangle_{\Gamma_{NR} \times \Upsilon} = \langle g_{NR} - (\mathcal{S} + \kappa_{NR})\,\tilde{g}_D, v \rangle_{\Gamma_{NR} \times \Upsilon} \quad \forall v \in \widetilde{H}^{\frac{1}{2},\frac{1}{4}}(\Gamma_{NR} \times \Upsilon)\,. \tag{2.19}$$

Uniqueness and quasi-optimality for the solution $\tilde{u} \in \widetilde{H}^{\frac{1}{2},\frac{1}{4}}(\Gamma_{NR} \times \Upsilon)$ of (2.19) follow from the $\widetilde{H}^{\frac{1}{2},\frac{1}{4}}(\Gamma_{NR} \times \Upsilon)$ boundedness and ellipticity of the Steklov-Poincareé operator provided by Corollary 2.1, Remark 2.3 and the properties of the heat transfer coefficient κ.

Remark 2.4. *Assume the absence of some boundary parts $\Gamma_i \subset \Gamma$ with $i \in \{D,N,R\}$ in the exposition of Subsection 2.4.4, then we obtain the following initial boundary value problems:*

- $\Gamma_R := \emptyset$ *initial Dirichlet-Neumann boundary value problem.*
- $\Gamma_N := \emptyset$ *initial Dirichlet-Robin boundary value problem.*
- $\Gamma_D := \emptyset$ *initial Neumann-Robin boundary value problem.*

3 SPACE-TIME GALERKIN BOUNDARY ELEMENT METHODS

Due to the properties of the Calderon projector in Theorem 2.1 a space-time Galerkin discretization with conforming sub-spaces in Section 3.1 is straight forward [5, 6, 40, 42] and inherits the unique solvability and quasi-optimality of the continuous Galerkin variational formulations presented in Section 2.4. Furthermore, these properties allow us to derive error estimates in close analogy to the elliptic theory [39, 40] (see Section 3.2).

3.1 Space-Time Discretization

3.1.1 Triangulation

All of the Galerkin variational forms stated in Section 2.4 are discretized by using piecewise polynomial space-time tensor product spaces. In order to do so we need a triangulation of our computational domain $\Gamma \times \Upsilon$ on which we define those spaces.

Spatial Triangulation We only work with flat triangular boundary elements and, therefore, restrict our exposition explicitly to that case. Thus let us assume we have an interpolation approximation of the boundary Γ of our Lipschitz domain Ω by Q triangular and linear elements χ_q such that

$$\Gamma \approx \Gamma_{h_x} = \bigcup_{q=1}^{Q-1} \overline{\chi}_q \tag{3.1}$$

with $\chi_i \cap \chi_j = \emptyset$ for $i \neq j$. If $\overline{\chi}_i$ and $\overline{\chi}_j$ share one common edge or point, they are said to be neighboring elements. For such a triangulation we introduce local parametrizations, which consist of mappings $\vartheta_q(\hat{\mathbf{x}}) : \hat{\chi} \to \chi_q$ between the reference element $\hat{\chi} \subset \mathbb{R}^2$ in parameter domain and a physical element $\chi_q \subset \mathbb{R}^3$ such that

$$\Gamma_{h_x} = \bigcup_{q=1}^{Q-1} \vartheta_q(\overline{\hat{\chi}}) \, .$$

We observe that each boundary element χ_q is uniquely defined by its vertices $\{\mathbf{x}_q^j\}_{j=1}^3 \subset \Gamma$ and linear interpolation in between. The reference element on the other hand is defined by

$$\hat{\chi} := \{\hat{x}_1, \hat{x}_2 : 0 < \hat{x}_1 < 1, 0 < \hat{x}_2 < \hat{x}_1\}$$

with vertices $\{\hat{\mathbf{x}}^j\}_{j=1}^3$. Hence together with a set of linear functions $\{\hat{\eta}_j : \hat{\chi} \to [0,1]\}_{j=1}^3$ with

$$\eta_j(\hat{\mathbf{x}}) = \begin{cases} 1 & \hat{\mathbf{x}} = \hat{\mathbf{x}}^k \quad k = j\,, \\ 0 & \hat{\mathbf{x}} = \hat{\mathbf{x}}^k \quad k \neq j \end{cases}$$

we can then define the above mentioned mappings by

$$\vartheta_q(\hat{\mathbf{x}}) = \sum_{j=1}^{3} \eta_j(\hat{\mathbf{x}}) \mathbf{x}_q^j\,.$$

Finally, in order to provide error bounds of the Galerkin boundary element methods afterwards, we need the boundary triangulation to be globally quasi-uniform, i.e. there is a constant $C > 0$ independent of Q such that

$$\min_{\chi \in \{\chi_q\}_{q=0}^{Q-1}} (\operatorname{diam}(\chi)) \leq C \max_{\chi \in \{\chi_q\}_{q=0}^{Q-1}} (\operatorname{diam}(\chi))\,.$$

Temporal Triangulation Contrary to the more general assumptions on the spatial aspects of the computational domain, time is one-dimensional linear and directional. Therefore, we restrict ourselves to an equidistant partition of the time interval Υ with continuously indexed time steps $\nu_p = (ph_t, (p+1)h_t)$ of step size h_t

$$\overline{\Upsilon} = \overline{\Upsilon}_{h_t} = \bigcup_{p=0}^{P-1} \overline{\nu}_p\,. \tag{3.2}$$

With the definition of the reference element $\hat{\nu} := (0,1)$ and the mappings $\theta_p : \hat{\nu} \to \nu_p$

$$\theta_p(\hat{t}) = (p + \hat{t})h_t\,,$$

this leads to the local parametrization of the time interval

$$\overline{\Upsilon} = \bigcup_{p=0}^{P-1} \theta_p(\overline{\hat{\nu}})\,.$$

3.1.2 Tensor Product Test- and Trial Spaces

On these triangulations, i.e. (3.1) and (3.2), we define piece-wise polynomial ansatz spaces of polynomial degree d_x in space and d_t in time. The spatial ansatz space can either consist of globally continuous c_{d_x} or discontinuous d_{d_x} functions (see [25, 32])

$$\begin{aligned} X_{h_x}^{c_{d_x}}(\Gamma) &:= \operatorname{span}\{\psi_\ell^{d_x}(\mathbf{x})\}_{\ell=0}^{N_x-1}\,, \\ X_{h_x}^{d_{d_x}}(\Gamma) &:= \operatorname{span}\{\varphi_\ell^{d_x}(\mathbf{x})\}_{\ell=0}^{N_x-1}\,. \end{aligned} \tag{3.3}$$

In principle the same holds true for the temporal ansatz space, however, in order not to destroy the Toeplitz structure of the system [35], we restrict ourselves to globally discontinuous test and trial spaces. Nevertheless, for consistency sake we have chosen the same notation as in the spatial case, hence

$$T_{h_t}^{d_{d_t}}(\Upsilon) := \operatorname{span}\{\phi_j^{d_t}(t)\}_{j=0}^{N_t-1} . \tag{3.4}$$

Finally, we use (3.3) and (3.4) to construct piece-wise polynomial space-time tensor product spaces

$$\begin{aligned} S_{h_x,h_t}^{c_{d_x},d_{d_t}}(\Gamma\times\Upsilon) :=& X_{h_x}^{c_{d_x}}(\Gamma)\otimes T_{h_t}^{d_{d_t}}(\Upsilon) , \\ S_{h_x,h_t}^{d_{d_x},d_{d_t}}(\Gamma\times\Upsilon) :=& X_{h_x}^{d_{d_x}}(\Gamma)\otimes T_{h_t}^{d_{d_t}}(\Upsilon) \end{aligned}$$

for the discretization of all Galerkin discretized thermal layer potentials in Section 2.4.

3.1.3 Galerkin Discretization of Thermal Layer Potentials

The Galerkin variational forms of the thermal single–, double– and adjoint double layer operators appearing in Section 2.4 are defined as the weakly singular bilinear forms listed below

$$\langle \mathcal{V}q, v\rangle_{\Gamma\times\Upsilon} = \int_{t=0}^{T}\int_{\Gamma} v(\mathbf{x},t)\int_{\tau=0}^{t}\int_{\Gamma} G(\mathbf{x}-\mathbf{y},t-\tau)\frac{q(\mathbf{y},\tau)}{\rho c_p}\,\mathrm{d}s_{\mathbf{y}}\mathrm{d}\tau\,\mathrm{d}s_{\mathbf{x}}\mathrm{d}t , \tag{3.5}$$

$$\langle \mathcal{K}u, v\rangle_{\Gamma\times\Upsilon} = \int_{t=0}^{T}\int_{\Gamma} v(\mathbf{x},t)\int_{\tau=0}^{t}\int_{\Gamma} \alpha\frac{\partial}{\partial n_{\mathbf{y}}}G(\mathbf{x}-\mathbf{y},t-\tau)u(\mathbf{y},\tau)\,\mathrm{d}s_{\mathbf{y}}\mathrm{d}\tau\,\mathrm{d}s_{\mathbf{x}}\mathrm{d}t , \tag{3.6}$$

$$\langle \mathcal{K}'q, w\rangle_{\Gamma\times\Upsilon} = \int_{t=0}^{T}\int_{\Gamma} w(\mathbf{x},t)\alpha\frac{\partial}{\partial n_{\mathbf{x}}}\int_{\tau=0}^{t}\int_{\Gamma} G(\mathbf{x}-\mathbf{y},t-\tau)\frac{q(\mathbf{y},\tau)}{\rho c_p}\,\mathrm{d}s_{\mathbf{y}}\mathrm{d}\tau\,\mathrm{d}s_{\mathbf{x}}\mathrm{d}t , \tag{3.7}$$

while for the hyper-singular operator we need to perform integration by parts to obtain the following weakly singular representation

$$\begin{aligned} \langle \mathcal{D}u, w\rangle_{\Gamma\times\Upsilon} =& \int_{t=0}^{T}\int_{\Gamma} \mathbf{curl}_{\mathbf{x}}^{\top} w(\mathbf{x},t)\int_{\tau=0}^{t}\int_{\Gamma} \alpha^2 G(\mathbf{x}-\mathbf{y},t-\tau)\mathbf{curl}_{\mathbf{y}}u(\mathbf{y},\tau)\,\mathrm{d}s_{\mathbf{y}}\mathrm{d}\tau\,\mathrm{d}s_{\mathbf{x}}\mathrm{d}t - \\ & \int_{t=0}^{T}\int_{\Gamma} \mathbf{n}_{\mathbf{x}}{}^{\top} w(\mathbf{x},t)\int_{\tau=0}^{t}\int_{\Gamma} \alpha^2\frac{\partial}{\partial\tau}G(\mathbf{x}-\mathbf{y},t-\tau)\mathbf{n}_{\mathbf{y}}u(\mathbf{y},\tau)\,\mathrm{d}s_{\mathbf{y}}\mathrm{d}\tau\,\mathrm{d}s_{\mathbf{x}}\mathrm{d}t \end{aligned} \tag{3.8}$$

with $\mathbf{curl}_{\mathbf{x}} := \mathbf{n}_{\mathbf{x}}\times\nabla_{\mathbf{x}}$. This result is due to some unpublished notes of G. Of, which follow along the lines of [40, Theorem 6.17] but can already be found in [10, Theorem 6.1].

We observe that piece-wise constant ansatz functions in time are an appropriate choice for the Galerkin discretization of all boundary integral operators in Theorem 2.2 since $T^{d_0}_{h_t}(\Upsilon)$ is a conforming sub-space of $H^s(\mathbb{R})$ with $s < 1/2$. Therefore, and due to the fact that all Galerkin variational forms (3.5), (3.5), (3.5) and (3.8) are defined in a weakly singular sense, the space-time discretization for all of them looks the same as long as we use conforming spatial sub-spaces as well. Hence we will exemplary perform the discretization for the single layer operator (3.5), where we write for notational convenience φ_k and φ_ℓ instead of $\varphi_k^{d_x}$ and $\varphi_\ell^{d_x}$. We exchange the order of integration to end up with

$$
\begin{aligned}
\langle \mathcal{V}q, v\rangle_{\Gamma\times\Upsilon} \approx & \langle \mathcal{V}q_h, \varphi_k\phi_i^0\rangle_{\Gamma\times\Upsilon} \\
&= \int_{t=0}^{T}\int_{\Gamma} \varphi_k(\mathbf{x})\phi_i^0(t) \int_{\tau=0}^{t}\int_{\Gamma} G(\mathbf{x}-\mathbf{y},t-\tau) \sum_{j=0}^{i}\sum_{\ell=0}^{N_x-1} \varphi_\ell(\mathbf{y})\phi_j^0(\tau)\frac{q_{j,\ell}}{\rho c_p}\,\mathrm{d}s_{\mathbf{y}}\mathrm{d}\tau\,\mathrm{d}s_{\mathbf{x}}\mathrm{d}t \\
&= \sum_{j=0}^{i}{}'\sum_{\ell=0}^{N_x-1} \int_{\mathrm{supp}(\varphi_k)}\int_{\mathrm{supp}(\varphi_\ell)} \varphi_k(\mathbf{x})\varphi_\ell(\mathbf{y}) \int_{t=ih_t}^{(i+1)h_t}\int_{\tau=jh_t}^{(j+1)h_t} G(\mathbf{x}-\mathbf{y},t-\tau)\,\mathrm{d}\tau\mathrm{d}t\,\mathrm{d}s_{\mathbf{y}}\mathrm{d}s_{\mathbf{x}}\,\frac{q_{j,\ell}}{\rho c_p} \\
&= \sum_{j=0}^{i}{}'\sum_{\ell=0}^{N_x-1} \int_{\mathrm{supp}(\varphi_k)}\int_{\mathrm{supp}(\varphi_\ell)} \varphi_k(\mathbf{x})\varphi_\ell(\mathbf{y})V_{ij}(\mathbf{x}-\mathbf{y})\,\mathrm{d}s_{\mathbf{y}}\mathrm{d}s_{\mathbf{x}}\,\frac{q_{j,\ell}}{\rho c_p} \qquad \forall k,i\,,
\end{aligned}
$$

where we use $\sum'$ to point out the special case where $j = i$, in which the upper limit of the inner time integral is changed to

$$
V_{ii}(\mathbf{x}-\mathbf{y}) = \int_{t=ih_t}^{(i+1)h_t}\int_{\tau=ih_t}^{t} G(\mathbf{x}-\mathbf{y},t-\tau)\,\mathrm{d}\tau\mathrm{d}t
$$

Due to the translational invariance of the kernel $G(\mathbf{x}-\mathbf{y},t-\tau)$ and the equidistant time discretization, the time integrated kernel $V_{ij}(\mathbf{x}-\mathbf{y})$ does not depend on the absolute value of the indices i and j but only on their difference $d := i-j$. Due to this fact and causality we end up with a lower triangular Toeplitz structure

$$
\sum_{j=0}^{i}{}'\mathbf{V}_{ij}\mathbf{q}_j = \sum_{d=0}^{i}{}'\mathbf{V}_d\mathbf{q}_{i-d} = \frac{1}{\rho c_p}\begin{pmatrix} \mathbf{V}_0 & 0 & \dots & 0 \\ \mathbf{V}_1 & \ddots & \ddots & \vdots \\ \vdots & \ddots & \ddots & 0 \\ \mathbf{V}_i & \dots & \mathbf{V}_1 & \mathbf{V}_0 \end{pmatrix}\begin{pmatrix} \mathbf{q}_0 \\ \mathbf{q}_1 \\ \vdots \\ \mathbf{q}_i \end{pmatrix}, \tag{3.9}
$$

where we have replaced the spatial sum by matrix notation. It is easily seen that solving for such an operator

$$
\sum_{d=0}^{i}{}'\mathbf{V}_d\mathbf{q}_{i-d} = \mathbf{f}_i \quad \forall i = 0,\dots N_t-1
$$

can be done explicitly in each time step

$$\mathbf{q}_i = (\mathbf{V}_0)^{-1} \left(\mathbf{f}_i - \sum_{d=1}^{i} \mathbf{V}_d \mathbf{q}_{i-d} \right) .$$

However, it involves the convolution over the complete history on the right hand side, which is computationally very expensive. How to deal with this problem effectively is the main topic of this thesis and elaborated in Chapter 4.

3.1.4 Computation of Matrix Entries

Since all Galerkin bilinear forms (3.5) through (3.8) are defined in a weakly singular form, we can exchange the order of integration. Then the previously defined tensor product trial and test spaces allow us to perform spatial and temporal integration completely independent from each other. Since we limit ourselves to equidistant time discretization, it is rather straightforward to perform time integration analytically. For the single layer operator this has been done in [35] and is extended to the remaining operators here.

Analytic Integration in Time. Introducing local time variables $t = (i+\hat{t})h_t$ and $\tau = (j+\hat{\tau})h_t$ with $0 \leq \hat{t}, \hat{\tau} \leq 1$ we obtain

$$V_d(\mathbf{r}) = \begin{cases} \sqrt{h_t} \int_0^1 \int_0^{\hat{t}} G\left(\frac{\mathbf{r}}{\sqrt{h_t}}, d+\hat{t}-\hat{\tau}\right) \mathrm{d}\hat{\tau}\mathrm{d}\hat{t} & d = 0 , \\ \sqrt{h_t} \int_0^1 \int_0^1 G\left(\frac{\mathbf{r}}{\sqrt{h_t}}, d+\hat{t}-\hat{\tau}\right) \mathrm{d}\hat{\tau}\mathrm{d}\hat{t} & d \geq 1 , \end{cases} \tag{3.10}$$

which results in

$$V_d(\mathbf{r}) = \sqrt{h_t} \left[G^{(-2)}\left(\tfrac{\mathbf{r}}{\sqrt{h_t}}, d+1\right) - 2G^{(-2)}\left(\tfrac{\mathbf{r}}{\sqrt{h_t}}, d\right) + G^{(-2)}\left(\tfrac{\mathbf{r}}{\sqrt{h_t}}, d-1\right) \right] \tag{3.11}$$

with

$$G^{(-2)}(\boldsymbol{r}, \mathfrak{d}) = \begin{cases} 0 & \mathfrak{d} \leq 0 , \\ \frac{\sqrt{\mathfrak{d}}}{4\pi} \left[\operatorname{erfc}\left(\frac{|\boldsymbol{r}|}{\sqrt{4\mathfrak{d}}}\right) \left(\frac{|\boldsymbol{r}|}{\sqrt{4\mathfrak{d}}} + \frac{\sqrt{\mathfrak{d}}}{|\boldsymbol{r}|}\right) - \exp\left(-\frac{|\boldsymbol{r}|^2}{4\mathfrak{d}}\right) \left(\frac{1}{\sqrt{\pi}}\right) \right] & \mathfrak{d} > 0 . \end{cases}$$

Since all the integrals in (3.5) – (3.8) are well defined, we are allowed to exchange the order of integration and differentiation to obtain the time integrated kernels for the double-

and the adjoint double layer potential

$$\begin{aligned}
K_d(\mathbf{r}) =& \frac{\partial}{\partial \mathbf{n_y}} V_d(\mathbf{r}) = \mathbf{n_y}^\top \nabla_{\mathbf{y}} V_d(\mathbf{r}) \\
=& \mathbf{n_y}^\top \sqrt{h_t} \left[\nabla_{\mathbf{y}} G^{(-2)} \left(\tfrac{\mathbf{r}}{\sqrt{h_t}}, d+1 \right) - 2\nabla_{\mathbf{y}} G^{(-2)} \left(\tfrac{\mathbf{r}}{\sqrt{h_t}}, d \right) + \nabla_{\mathbf{y}} G^{(-2)} \left(\tfrac{\mathbf{r}}{\sqrt{h_t}}, d-1 \right) \right] , \\
K'_d(\mathbf{r}) =& \frac{\partial}{\partial \mathbf{n_x}} V_d(\mathbf{r}) = \mathbf{n_x}^\top \nabla_{\mathbf{x}} V_d(\mathbf{r}) = -\mathbf{n_x}^\top \nabla_{\mathbf{y}} V_d(\mathbf{r}) \\
=& -\mathbf{n_x}^\top \sqrt{h_t} \left[\nabla_{\mathbf{y}} G^{(-2)} \left(\tfrac{\mathbf{r}}{\sqrt{h_t}}, d+1 \right) - 2\nabla_{\mathbf{y}} G^{(-2)} \left(\tfrac{\mathbf{r}}{\sqrt{h_t}}, d \right) + \nabla_{\mathbf{y}} G^{(-2)} \left(\tfrac{\mathbf{r}}{\sqrt{h_t}}, d-1 \right) \right]
\end{aligned}$$

with

$$\nabla_{\mathbf{y}} G^{(-2)}(\boldsymbol{r}, \mathfrak{d}) = \begin{cases} 0 & \mathfrak{d} \le 0 \\ -\frac{\boldsymbol{r}\sqrt{\mathfrak{d}}}{4\pi|\boldsymbol{r}|^2} \left[\operatorname{erfc}\left(\frac{|\boldsymbol{r}|}{\sqrt{4\mathfrak{d}}} \right) \left(\frac{|\boldsymbol{r}|}{\sqrt{4\mathfrak{d}}} - \frac{\sqrt{\mathfrak{d}}}{|\boldsymbol{r}|} \right) - \exp\left(-\frac{|\boldsymbol{r}|^2}{4\mathfrak{d}} \right) \left(\frac{1}{\sqrt{\pi}} \right) \right] & \mathfrak{d} > 0 \end{cases} .$$

Finally, we still have to perform the time integration for the hyper-singular operator. For the first part of (3.8) the time integration coincides with the results obtained in (3.11) and we can recycle $V_d(\mathbf{r})$ while the time integrated kernel for the second part is given by

$$D_d(\mathbf{r}) = \sqrt{h_t} \left[G^{(-1)} \left(\tfrac{\mathbf{r}}{\sqrt{h_t}}, d+1 \right) - 2G^{(-1)} \left(\tfrac{\mathbf{r}}{\sqrt{h_t}}, d \right) + G^{(-1)} \left(\tfrac{\mathbf{r}}{\sqrt{h_t}}, d-1 \right) \right] \tag{3.12}$$

with

$$G^{(-1)}(\boldsymbol{r}, \mathfrak{d}) = \begin{cases} 0 & \mathfrak{d} \le 0 , \\ -\frac{1}{4\pi|\boldsymbol{r}|} \operatorname{erfc}\left(\frac{|\boldsymbol{r}|}{\sqrt{4\mathfrak{d}}} \right) & \mathfrak{d} > 0 . \end{cases}$$

Numerical Integration in Space. The spatial integration for general unstructured domains can in general not be performed analytically, hence we resort to numerical schemes. For $d > 1$ the time integrated kernels (3.11) – (3.12) are $C^\infty(\mathbb{R}^3)$ and one can use standard Gauss quadrature. However, for $d \in \{0, 1\}$ they behave like

$$\begin{aligned}
\lim_{\mathbf{r}\to\mathbf{0}} V_0(\mathbf{r}) &= \mathcal{O}\left(\tfrac{1}{|\mathbf{r}|} \right) , & \lim_{\mathbf{r}\to\mathbf{0}} V_1(\mathbf{r}) &= \mathcal{O}(|\mathbf{r}|) , \\
\lim_{\mathbf{r}\to\mathbf{0}} K_0(\mathbf{r}) &= \mathcal{O}\left(\tfrac{\mathbf{n_y}^\top \mathbf{r}}{|\mathbf{r}|^3} \right) , & \lim_{\mathbf{r}\to\mathbf{0}} K_1(\mathbf{r}) &= \mathcal{O}\left(\tfrac{\mathbf{n_y}^\top \mathbf{r}}{|\mathbf{r}|} \right) , \\
\lim_{\mathbf{r}\to\mathbf{0}} K'_0(\mathbf{r}) &= \mathcal{O}\left(\tfrac{\mathbf{n_x}^\top \mathbf{r}}{|\mathbf{r}|^3} \right) , & \lim_{\mathbf{r}\to\mathbf{0}} K'_1(\mathbf{r}) &= \mathcal{O}\left(\tfrac{\mathbf{n_x}^\top \mathbf{r}}{|\mathbf{r}|} \right) , \\
\lim_{\mathbf{r}\to\mathbf{0}} D_0(\mathbf{r}) &= \mathcal{O}\left(\tfrac{1}{|\mathbf{r}|} \right) , & \lim_{\mathbf{r}\to\mathbf{0}} D_1(\mathbf{r}) &= \mathcal{O}(|\mathbf{r}|) ,
\end{aligned}$$

thus we use the formulas of Erichsen and Sauter [14].

3.2 Error Estimates for Galerkin Boundary Element Methods

In this section, we provide error estimates for boundary element formulations based on the Galerkin variational formulations given in Section 2.4. In the following, we recall the approximation properties of piece-wise polynomial tensor product spaces $S^{d_x,d_t}_{h_x,h_t}(\Gamma\times\Upsilon)\subset H^{p,q}(\Gamma\times\Upsilon)$, where $d_t = d_{d_t}$ and d_x can either mean c_{d_x} or d_{d_x} according to (3.3) if not specified any further.

Theorem 3.1. *[10, Proposition 5.3] Assume $0\le r\le d_x+1$, $0\le s\le d_t+1$ and $p\le r$, $q\le s$ with $pq\ge 0$. Moreover, let $\mathcal{Q}_{h_x}\mathcal{Q}_{h_t}: H^{p,q}(\Gamma\times\Upsilon)\to S^{d_x,d_t}_{h_x,h_t}(\Gamma\times\Upsilon)$ be the $L_2(\Gamma\times\Upsilon)$ projection*

$$\langle u-\mathcal{Q}_{h_x}\mathcal{Q}_{h_t}u, v_h\rangle_{H^{p,q}(\Gamma\times\Upsilon)} = 0 \quad \forall v_h\in S^{d_x,d_t}_{h_x,h_t}(\Gamma\times\Upsilon)\,,$$

then we have for all $u\in H^{r,s}(\Gamma\times\Upsilon)$

$$\inf_{v\in S^{d_x,d_t}_{h_x,h_t}(\Gamma\times\Upsilon)}\|u-v\|_{H^{p,q}(\Gamma\times\Upsilon)}\le\|u-\mathcal{Q}_{h_x}\mathcal{Q}_{h_t}u\|_{H^{p,q}(\Gamma\times\Upsilon)}\le C(h_x^\alpha+h_t^\beta)\|u\|_{H^{r,s}(\Gamma\times\Upsilon)}\,,$$

where

$$\alpha=\min\left\{r-p, r-\frac{qr}{s}\right\}\quad \beta=\min\left\{s-q, s-\frac{ps}{r}\right\}\,.$$

We will always have $q=p/2$ in this paper, hence the most meaningful choice for s and r is $s=r/2$, which leads to the full convergence rates in space and time of $\alpha=r-p$ and $\beta=s-q$, respectively. Due to $\beta=\alpha/2$ it is obvious that choosing $h_x=\mathcal{O}(\sqrt{h_t})$ leads to the optimal combined convergence rate.

Theorem 3.1 will be useful for error estimates in the energy norm, however, it is more practical to work with the L_2 error. In order to provide such estimates in the case of the energy space being a negative indexed Sobolev space, we need the following inverse inequality.

Theorem 3.2. *[35, Lemma 7.4] Assume a globally quasi-uniform triangulation. Then for $0\le p\le d_x$ and $0\le q\le d_t$ there is a constant C independent of $S^{d_x,d_t}_{h_x,h_t}(\Gamma\times\Upsilon)$ such that*

$$\|u\|_{L_2(\Gamma\times\Upsilon)}\le C(h_x^{-p}+h_t^{-q})\|u\|_{H^{-p,-q}(\Gamma\times\Upsilon)}\quad\forall u\in S^{d_x,d_t}_{h_x,h_t}(\Gamma\times\Upsilon)\,.$$

Whenever the energy space is a positive Sobolev space we will use a duality argument called Aubin-Nitsche trick [40] to estimate the L_2 error.

3.2.1 Initial Dirichlet Boundary Value Problem

If we solve the variational form (2.16) for the approximate solution $q_h \in S^{d_1,d_0}_{h_x,h_t}(\Gamma\times\Upsilon)$

$$\langle \mathcal{V} q_h, v_h\rangle_{\Gamma\times\Upsilon} = \langle \left(\tfrac{\mathcal{I}}{2}+\mathcal{K}\right) g_D, v_h\rangle_{\Gamma\times\Upsilon} \quad \forall v_h \in S^{d_1,d_0}_{h_x,h_t}(\Gamma\times\Upsilon)\,, \tag{3.13}$$

all assumptions of Cea's Lemma are satisfied, since $\mathcal{V}$ is $H^{-\frac{1}{2},-\frac{1}{4}}(\Gamma\times\Upsilon)$ bounded and elliptic and $S^{d_1,d_0}_{h_x,h_t}(\Gamma\times\Upsilon)$ is a conforming sub-space of $H^{-\frac{1}{2},-\frac{1}{4}}(\Gamma\times\Upsilon)$. Therefore, we have uniqueness of the approximate Galerkin solution $q_h \in S^{d_1,d_0}_{h_x,h_t}(\Gamma\times\Upsilon)$ and for $q \in H^{2,1}_{pw}(\Gamma\times\Upsilon)$ Theorem 3.1 gives an upper bound for the error in the energy norm

$$\|q-q_h\|_{H^{-\frac{1}{2},-\frac{1}{4}}(\Gamma\times\Upsilon)} \leq C(h_x^{\frac{5}{2}}+h_t^{\frac{5}{4}})\|q\|_{H^{2,1}_{pw}(\Gamma\times\Upsilon)}\,. \tag{3.14}$$

In order to derive a more practical estimate in the L_2 norm [35, Theorem 7.6], we use the triangle inequality, Theorem 3.2 and the triangle inequality again

$$\begin{aligned}
\|q-q_h\|_{L_2(\Gamma\times\Upsilon)} \leq& \|q-\mathcal{Q}_{h_x}\mathcal{Q}_{h_t}q\|_{L_2(\Gamma\times\Upsilon)} + \|\mathcal{Q}_{h_x}\mathcal{Q}_{h_t}q-q_h\|_{L_2(\Gamma\times\Upsilon)}\\
\leq& \|q-\mathcal{Q}_{h_x}\mathcal{Q}_{h_t}q\|_{L_2(\Gamma\times\Upsilon)} + C(h_x^{-\frac{1}{2}}+h_t^{-\frac{1}{4}})\|\mathcal{Q}_{h_x}\mathcal{Q}_{h_t}q-q_h\|_{H^{-\frac{1}{2},-\frac{1}{4}}(\Gamma\times\Upsilon)}\\
\leq& \|q-\mathcal{Q}_{h_x}\mathcal{Q}_{h_t}q\|_{L_2(\Gamma\times\Upsilon)}\\
&+C(h_x^{-\frac{1}{2}}+h_t^{-\frac{1}{4}})\Big(\|q-\mathcal{Q}_{h_x}\mathcal{Q}_{h_t}q\|_{H^{-\frac{1}{2},-\frac{1}{4}}(\Gamma\times\Upsilon)} + \|q-q_h\|_{H^{-\frac{1}{2},-\frac{1}{4}}(\Gamma\times\Upsilon)}\Big)\,.
\end{aligned}$$

With Theorem 3.1 for the first two terms and (3.14) for the last term we get

$$\|q-q_h\|_{L_2(\Gamma\times\Upsilon)} \leq C\left((h_x^2+h_t)+(h_x^{-\frac{1}{2}}+h_t^{-\frac{1}{4}})(h_x^{\frac{5}{2}}+h_t^{\frac{5}{4}})\right)\|q\|_{H^{2,1}_{pw}(\Gamma\times\Upsilon)}$$

and using Young's inequality to estimate $h_x^{\frac{5}{2}}h_t^{-\frac{1}{4}}$ and $h_x^{-\frac{1}{2}}h_t^{\frac{5}{4}}$ we have

$$\|q-q_h\|_{L_2(\Gamma\times\Upsilon)} \leq C(h_x^2+h_t)\|q\|_{H^{2,1}_{pw}(\Gamma\times\Upsilon)}\,. \tag{3.15}$$

However, in our numerical examples we always approximate the right hand side and, therefore, end up with a perturbed Galerkin variational formulation

$$\langle \mathcal{V}\bar{q}_h, v_h\rangle_{\Gamma\times\Upsilon} = \langle \left(\tfrac{\mathcal{I}}{2}+\mathcal{K}\right)\bar{g}_D, v_h\rangle_{\Gamma\times\Upsilon} \quad \forall v_h \in S^{d_1,d_0}_{h_x,h_t}(\Gamma\times\Upsilon)\,, \tag{3.16}$$

which is why we may not be able to verify (3.15) but observe a different behavior.

Lemma 3.1. *Let $q \in H^{2,1}_{pw}(\Gamma \times \Upsilon)$ be the solution of the variational form* (2.16)*. Then the solution $\bar{q}_h \in S^{d_1,d_t}_{h_x,h_t}(\Gamma \times \Upsilon)$ of the perturbed variational formulation* (3.16) *with $g_D \in H^{2,1}(\Gamma \times \Upsilon)$ and $\bar{g}_D = \mathcal{Q}_{h_x}\mathcal{Q}_{h_t} g_D$*

$$\|q - \bar{q}_h\|_{L_2(\Gamma\times\Upsilon)} \leq C(h_x + h_t^{\frac{1}{2}}) \left(\|q\|_{H^{2,1}_{pw}(\Gamma\times\Upsilon)} + \|g_D\|_{H^{2,1}(\Gamma\times\Upsilon)} \right) .$$

Proof. We use the triangle inequality and Theorem 3.2 to estimate

$$\begin{aligned} \|q - \bar{q}_h\|_{L_2(\Gamma\times\Upsilon)} \leq & \|q - q_h\|_{L_2(\Gamma\times\Upsilon)} + \|q_h - \bar{q}_h\|_{L_2(\Gamma\times\Upsilon)} \\ \leq & \|q - q_h\|_{L_2(\Gamma\times\Upsilon)} + C(h_x^{-\frac{1}{2}} + h_t^{-\frac{1}{4}}) \|q_h - \bar{q}_h\|_{H^{-\frac{1}{2},-\frac{1}{4}}(\Gamma\times\Upsilon)} . \end{aligned} \tag{3.17}$$

As an intermediate result obtained by subtracting (3.16) from (3.13)

$$\langle \mathcal{V}(q_h - \bar{q}_h), v_h \rangle_{\Gamma\times\Upsilon} = \langle \left(\tfrac{\mathcal{I}}{2} + \mathcal{K}\right)(g_D - \bar{g}_D), v_h \rangle_{\Gamma\times\Upsilon} = \langle \mathcal{K}(g_D - \bar{g}_D), v_h \rangle_{\Gamma\times\Upsilon}$$

we can bound the second term in (3.17) due to the boundedness of the double layer operator by the approximation error of the Dirichlet data

$$\begin{aligned} \|q_h - \bar{q}_h\|^2_{H^{-\frac{1}{2},-\frac{1}{4}}(\Gamma\times\Upsilon)} = & \langle \mathcal{V}(q_h - \bar{q}_h), (q_h - \bar{q}_h) \rangle_{\Gamma\times\Upsilon} \\ = & \langle \mathcal{K}(g_D - \bar{g}_D), (q_h - \bar{q}_h) \rangle_{\Gamma\times\Upsilon} \\ \leq & \|g_D - \bar{g}_D\|_{H^{\frac{1}{2},\frac{1}{4}}(\Gamma\times\Upsilon)} \|q_h - \bar{q}_h\|_{H^{-\frac{1}{2},-\frac{1}{4}}(\Gamma\times\Upsilon)} . \end{aligned}$$

Thus we continue using (3.15) and Theorem 3.1

$$\begin{aligned} \|q - \bar{q}_h\|_{L_2(\Gamma\times\Upsilon)} \leq & \|q - q_h\|_{L_2(\Gamma\times\Upsilon)} + C(h_x^{-\frac{1}{2}} + h_t^{-\frac{1}{4}}) \|g_D - \bar{g}_D\|_{H^{\frac{1}{2},\frac{1}{4}}(\Gamma\times\Upsilon)} \\ \leq & C(h_x^2 + h_t) \|q\|_{H^{2,1}_{pw}(\Gamma\times\Upsilon)} + C(h_x^{-\frac{1}{2}} + h_t^{-\frac{1}{4}})(h_x^{\frac{3}{2}} + h_t^{\frac{3}{4}}) \|g_D\|_{H^{2,1}(\Gamma\times\Upsilon)} \end{aligned}$$

and Young's inequality yields the assertion once again. □

Remark 3.1. *Observe that in this case there is no point in using linear spatial approximation of the solution, since the error is dominated by the approximation of the given Dirichlet data. From the last formula in the proof above it is obvious that one can achieve the same order of convergence by using $S^{d_0,d_0}_{h_x,h_t}(\Gamma \times \Upsilon)$ instead of $S^{d_1,d_0}_{h_x,h_t}(\Gamma \times \Upsilon)$. The only way to remedy this situation would be to approximate the right hand side by piece-wise quadratic functions in space.*

3.2.2 Initial Neumann Boundary Value Problem

We solve (2.17) for the approximate solution $u_h \in S^{c_1,d_0}_{h_x,h_t}(\Gamma\times\Upsilon)$

$$\langle \mathcal{D}u_h, w_h\rangle_{\Gamma\times\Upsilon} = \langle \left(\tfrac{\mathcal{I}}{2} - \mathcal{K}'\right) g_N, w_h\rangle_{\Gamma\times\Upsilon} \quad \forall w_h \in S^{c_1,d_0}_{h_x,h_t}(\Gamma\times\Upsilon)\,. \tag{3.18}$$

Since $\mathcal{D} : H^{\frac{1}{2},\frac{1}{4}}(\Gamma\times\Upsilon) \to H^{-\frac{1}{2},-\frac{1}{4}}(\Gamma\times\Upsilon)$ is bounded, $H^{\frac{1}{2},\frac{1}{4}}(\Gamma\times\Upsilon)$ elliptic and we have chosen a conforming discretization $u_h \in S^{c_1,d_0}_{h_x,h_t}(\Gamma\times\Upsilon) \subset \mathcal{D} : H^{\frac{1}{2},\frac{1}{4}}(\Gamma\times\Upsilon)$ we get uniqueness and quasi-optimality of the approximate solution. Assuming $u \in H^{2,1}(\Gamma\times\Upsilon)$ Theorem 3.1 gives the following bound

$$\|u-u_h\|_{H^{\frac{1}{2},\frac{1}{4}}(\Gamma\times\Upsilon)} \leq C(h_x^{\frac{3}{2}} + h_t^{\frac{3}{4}})\|u\|_{H^{2,1}(\Gamma\times\Upsilon)}\,. \tag{3.19}$$

Again, it is more practical to work with an L_2 error estimate. However, instead of the inverse inequality we have to use a duality argument commonly referred to as Aubin-Nitsche trick. Observe that in all our numerical examples we work with the L_2 projection $\bar{g}_N = \mathcal{Q}_{h_x}\mathcal{Q}_{h_t} g_N$ of the given Neumann data g_N and, hence, are solving the perturbed problem

$$\langle \mathcal{D}\bar{u}_h, w_h\rangle_{\Gamma\times\Upsilon} = \langle \left(\tfrac{\mathcal{I}}{2} - \mathcal{K}'\right) \bar{g}_N, w_h\rangle_{\Gamma\times\Upsilon} \quad \forall w_h \in S^{c_1,d_0}_{h_x,h_t}(\Gamma\times\Upsilon)\,. \tag{3.20}$$

Lemma 3.2. *[40, Theorem 12.10] Assume that $\mathcal{D} : H^{1,\frac{1}{2}}(\Gamma\times\Upsilon) \to L_2(\Gamma\times\Upsilon)$ is bounded and bijective and, moreover $\left(\frac{\mathcal{I}}{2} - \mathcal{K}'\right) : H^{-1,-\frac{1}{2}}(\Gamma\times\Upsilon) \to H^{-1,-\frac{1}{2}}(\Gamma\times\Upsilon)$ is bounded. Let $u \in H^{2,1}(\Gamma\times\Upsilon)$ be the unique solution of* (2.17) *and $\bar{u}_h \in S^{c_1,d_0}_{h_x,h_t}(\Gamma\times\Upsilon)$ the unique solution of* (3.20) *with $g_N \in H^{1,\frac{1}{2}}_{pw}(\Gamma\times\Upsilon)$ and $\bar{g}_N = \mathcal{Q}_{h_x}\mathcal{Q}_{h_t} g_N$, then we have*

$$\|u-\bar{u}_h\|_{L_2(\Gamma\times\Upsilon)} \leq C(h_x^2 + h_t)\left(\|u\|_{H^{2,1}(\Gamma\times\Upsilon)} + \|g_N\|_{H^{1,\frac{1}{2}}_{pw}(\Gamma\times\Upsilon)}\right)\,.$$

Proof. By duality we have

$$\|u-\bar{u}_h\|_{L_2(\Gamma\times\Upsilon)} = \sup_{0\neq w\in L_2(\Gamma\times\Upsilon)} \frac{\langle u-\bar{u}_h, w\rangle_{\Gamma\times\Upsilon}}{\|w\|_{L_2(\Gamma\times\Upsilon)}}\,.$$

Since the hyper-singular operator is an isomorphism from $H^{1,\frac{1}{2}}(\Gamma\times\Upsilon)$ to $L_2(\Gamma\times\Upsilon)$ there this is a unique $v \in H^{1,\frac{1}{2}}(\Gamma\times\Upsilon)$ such that

$$\begin{aligned}\|u-\bar{u}_h\|_{L_2(\Gamma\times\Upsilon)} &= \sup_{0\neq v\in H^{1,\frac{1}{2}}(\Gamma\times\Upsilon)} \frac{\langle u-\bar{u}_h, \mathcal{D}v\rangle_{\Gamma\times\Upsilon}}{\|\mathcal{D}v\|_{L_2(\Gamma\times\Upsilon)}} \\ &= \sup_{0\neq v\in H^{1,\frac{1}{2}}(\Gamma\times\Upsilon)} \frac{\langle \mathcal{D}(u-\bar{u}_h), v\rangle_{\Gamma\times\Upsilon}}{\|\mathcal{D}v\|_{L_2(\Gamma\times\Upsilon)}}\,.\end{aligned}$$

Subtracting (3.20) from (2.17) we have

$$\langle \mathcal{D}(u-\bar{u}_h), w_h\rangle_{\Gamma\times\Upsilon} = \langle \left(\tfrac{\mathcal{I}}{2}-\mathcal{K}'\right)(g_N-\bar{g}_N), w_h\rangle_{\Gamma\times\Upsilon}$$

and with the triangle inequality we get

$$\begin{aligned}\|u-\bar{u}_h\|_{L_2(\Gamma\times\Upsilon)} \leq & \sup_{0\neq v\in H^{1,\frac{1}{2}}(\Gamma\times\Upsilon)} \frac{\langle \mathcal{D}(u-\bar{u}_h), v-\mathcal{Q}_{h_x}\mathcal{Q}_{h_t}v\rangle_{\Gamma\times\Upsilon}}{\|\mathcal{D}v\|_{L_2(\Gamma\times\Upsilon)}} \\ & + \sup_{0\neq v\in H^{1,\frac{1}{2}}(\Gamma\times\Upsilon)} \frac{\langle \left(\tfrac{\mathcal{I}}{2}-\mathcal{K}'\right)(g_N-\bar{g}_N), \mathcal{Q}_{h_x}\mathcal{Q}_{h_t}v\rangle_{\Gamma\times\Upsilon}}{\|\mathcal{D}v\|_{L_2(\Gamma\times\Upsilon)}}\,.\end{aligned}$$

Due to the boundedness and bijectivity of the hyper-singular operator and Theorem 3.1 we can bound the first term

$$\begin{aligned}\sup_{0\neq v\in H^{1,\frac{1}{2}}(\Gamma\times\Upsilon)} \frac{\langle \mathcal{D}(u-u_h), v-\mathcal{Q}_{h_x}\mathcal{Q}_{h_t}v\rangle_{\Gamma\times\Upsilon}}{\|\mathcal{D}v\|_{L_2(\Gamma\times\Upsilon)}} &\leq \|u-u_h\|_{H^{\frac{1}{2},\frac{1}{4}}(\Gamma\times\Upsilon)} \times \\ & \sup_{0\neq v\in H^{1,\frac{1}{2}}(\Gamma\times\Upsilon)} \frac{\|v-\mathcal{Q}_{h_x}\mathcal{Q}_{h_t}v\|_{H^{\frac{1}{2},\frac{1}{4}}(\Gamma\times\Upsilon)}}{\|v\|_{H^{1,\frac{1}{2}}(\Gamma\times\Upsilon)}} \\ &\leq C(h_x^{\frac{1}{2}}+h_t^{\frac{1}{4}})\|u-u_h\|_{H^{\frac{1}{2},\frac{1}{4}}(\Gamma\times\Upsilon)}\,.\end{aligned}$$

For the second term we use the triangle inequality, the boundedness of the adjoint double layer potential and Theorem 3.1

$$\begin{aligned}\left|\langle \left(\tfrac{\mathcal{I}}{2}-\mathcal{K}'\right)(g_N-\bar{g}_N), \mathcal{Q}_{h_x}\mathcal{Q}_{h_t}v\rangle_{\Gamma\times\Upsilon}\right| \leq & \left|\langle \left(\tfrac{\mathcal{I}}{2}-\mathcal{K}'\right)(g_N-\bar{g}_N), v\rangle_{\Gamma\times\Upsilon}\right| \\ & + \left|\langle \left(\tfrac{\mathcal{I}}{2}-\mathcal{K}'\right)(g_N-\bar{g}_N), v-\mathcal{Q}_{h_x}\mathcal{Q}_{h_t}v\rangle_{\Gamma\times\Upsilon}\right| \\ \leq & C\|g_N-\bar{g}_N\|_{H^{-1,-\frac{1}{2}}(\Gamma\times\Upsilon)}\|v\|_{H^{1,\frac{1}{2}}(\Gamma\times\Upsilon)} \\ & + C\|g_N-\bar{g}_N\|_{L_2(\Gamma\times\Upsilon)}\|v-\mathcal{Q}_{h_x}\mathcal{Q}_{h_t}v\|_{L_2(\Gamma\times\Upsilon)} \\ \leq & C(h_x^2+h_t)\|g_N\|_{H^{1,\frac{1}{2}}_{pw}(\Gamma\times\Upsilon)}\|v\|_{H^{1,\frac{1}{2}}(\Gamma\times\Upsilon)} \\ & + C(h_x+h_t^{\frac{1}{2}})\|g_N\|_{H^{1,\frac{1}{2}}_{pw}(\Gamma\times\Upsilon)}(h_x+h_t^{\frac{1}{2}})\|v\|_{H^{1,\frac{1}{2}}(\Gamma\times\Upsilon)}\end{aligned}$$

and the assertion follows from these last two estimates, (3.19) and Young's inequality. □

3.2.3 Initial Robin Boundary Value Problem

If we solve the variational form (2.18) for the approximate solution $u_h \in S^{c_1,d_0}_{h_x,h_t}(\Gamma\times\Upsilon)$

$$\langle (\mathcal{S}+\kappa)\,u_h, v_h\rangle_{\Gamma\times\Upsilon} = \langle g_R, v_h\rangle_{\Gamma\times\Upsilon} \quad \forall v_h \in S^{c_1,d_0}_{h_x,h_t}(\Gamma\times\Upsilon)\,, \tag{3.21}$$

Cea's Lemma is satisfied due to the $H^{\frac{1}{2},\frac{1}{4}}(\Gamma\times\Upsilon)$ boundedness and ellipticity of $(\mathcal{S}+\kappa)$ provided by Subsection 2.4.3. Thus, assuming $u\in H^{2,1}(\Gamma\times\Upsilon)$ Theorem 3.1 gives an upper bound for the error in the energy norm

$$\|u-u_h\|_{H^{\frac{1}{2},\frac{1}{4}}(\Gamma\times\Upsilon)} \leq C(h_x^{\frac{3}{2}}+h_t^{\frac{3}{4}})\|u\|_{H^{2,1}(\Gamma\times\Upsilon)} . \tag{3.22}$$

However, due to the inverse single layer operator, we can not directly realize the Steklov Poincaré operator. Therefore, we proceed as in [40, page 284] by solving the variational problem

$$\langle \mathcal{V}q_h, w_h\rangle_{\Gamma\times\Upsilon} = \langle \left(\tfrac{\mathcal{I}}{2}+\mathcal{K}\right)u, w_h\rangle_{\Gamma\times\Upsilon} \quad \forall w_h\in S_{h_x,h_t}^{d_0,d_0}(\Gamma\times\Upsilon) \tag{3.23}$$

with $q_h\in S_{h_x,h_t}^{d_0,d_0}(\Gamma\times\Upsilon)$ first, which leads to the following approximation of the Steklov-Poincaré operator

$$\bar{\mathcal{S}}u = \left(\tfrac{\mathcal{I}}{2}+\mathcal{K}'\right)q_h + \mathcal{D}u \tag{3.24}$$

and the perturbed variational problem

$$\langle \left(\bar{\mathcal{S}}+\kappa\right)\bar{u}_h, v_h\rangle_{\Gamma\times\Upsilon} = \langle g_R, v_h\rangle_{\Gamma\times\Upsilon} \quad \forall v_h\in S_{h_x,h_t}^{c_1,d_0}(\Gamma\times\Upsilon) . \tag{3.25}$$

Lemma 3.3. *[40, Lemma 12.11] The approximated Steklov-Poincaré operator in* (3.24) $\bar{\mathcal{S}}: H^{\frac{1}{2},\frac{1}{4}}(\Gamma\times\Upsilon)\to H^{-\frac{1}{2},-\frac{1}{4}}(\Gamma\times\Upsilon)$ *is bounded*

$$\|\bar{\mathcal{S}}u\|_{H^{-\frac{1}{2},-\frac{1}{4}}(\Gamma\times\Upsilon)} \leq C\|u\|_{H^{\frac{1}{2},\frac{1}{4}}(\Gamma\times\Upsilon)}$$

and $H^{\frac{1}{2},\frac{1}{4}}(\Gamma\times\Upsilon)$ *elliptic*

$$\langle\bar{\mathcal{S}}v, v\rangle_{\Gamma\times\Upsilon} \geq C\|v\|^2_{H^{\frac{1}{2},\frac{1}{4}}(\Gamma\times\Upsilon)} \quad \forall v\in H^{\frac{1}{2},\frac{1}{4}}(\Gamma\times\Upsilon) .$$

Further, assuming that $\mathcal{V}: H^{-1+s,\frac{-1+s}{2}}(\Gamma\times\Upsilon)\to H^{s,\frac{s}{2}}(\Gamma\times\Upsilon)$ *is bounded and bijective for* $s\in[\frac{1}{2},1]$ *and* $\mathcal{S}u\in H^{1,\frac{1}{2}}_{pw}(\Gamma\times\Upsilon)$*, the approximate Steklov-Poincaré operator satisfies the estimate*

$$\|(\mathcal{S}-\bar{\mathcal{S}})u\|_{H^{-s,-\frac{s}{2}}(\Gamma\times\Upsilon)} \leq C\left(h_x^{1+s}+h_t^{\frac{1+s}{2}}\right)\|\mathcal{S}u\|_{H^{1,\frac{1}{2}}_{pw}(\Gamma\times\Upsilon)} .$$

Proof. For the solution $q_h\in S_{h_x,h_t}^{d_0,d_0}(\Gamma\times\Upsilon)$ of the variational problem (3.23) we have due to the ellipticity of the single layer operator and the boundedness of the double layer operator provided by Theorem 2.1

$$\|q_h\|_{H^{-\frac{1}{2},-\frac{1}{4}}(\Gamma\times\Upsilon)} \leq C\|u\|_{H^{\frac{1}{2},\frac{1}{4}}(\Gamma\times\Upsilon)} .$$

Thus the boundedness of the approximate Steklov-Poincaré operator follows with the triangle inequality, the boundedness of the hyper-singular operator and the adjoint operator given in Theorem 2.1

$$\begin{aligned}\|\bar{\mathcal{S}}u\|_{H^{-\frac{1}{2},-\frac{1}{4}}(\Gamma\times\Upsilon)} =& \|\mathcal{D}u+\left(\tfrac{\mathcal{I}}{2}+\mathcal{K}'\right)q_h\|_{H^{-\frac{1}{2},-\frac{1}{4}}(\Gamma\times\Upsilon)}\\ \leq& C\left(\|u\|_{H^{\frac{1}{2},\frac{1}{4}}(\Gamma\times\Upsilon)}+\|q_h\|_{H^{-\frac{1}{2},-\frac{1}{4}}(\Gamma\times\Upsilon)}\right)\\ \leq& C\|u\|_{H^{\frac{1}{2},\frac{1}{4}}(\Gamma\times\Upsilon)}.\end{aligned}$$

The ellipticity follows from the ellipticity of the hyper-singular operator and the single layer operator guaranteed by Theorem 2.1

$$\begin{aligned}\langle\bar{\mathcal{S}}v,v\rangle_{\Gamma\times\Upsilon} =& \langle\mathcal{D}v,v\rangle_{\Gamma\times\Upsilon}+\langle\left(\tfrac{\mathcal{I}}{2}+\mathcal{K}'\right)q_h,v\rangle_{\Gamma\times\Upsilon}\\ =& \langle\mathcal{D}v,v\rangle_{\Gamma\times\Upsilon}+\langle q_h,\left(\tfrac{\mathcal{I}}{2}+\mathcal{K}\right)v\rangle_{\Gamma\times\Upsilon}\\ =& \langle\mathcal{D}v,v\rangle_{\Gamma\times\Upsilon}+\langle q_h,\mathcal{V}q_h\rangle_{\Gamma\times\Upsilon}\geq C\|v\|^2_{H^{\frac{1}{2},\frac{1}{4}}(\Gamma\times\Upsilon)}.\end{aligned}$$

Taking the difference between the exact and approximated Steklov-Poincaré operator and Cea's Lemma together with Theorem 3.1 yields

$$\begin{aligned}\|\left(\mathcal{S}-\bar{\mathcal{S}}\right)u\|_{H^{-\frac{1}{2},-\frac{1}{4}}(\Gamma\times\Upsilon)} &= \|\left(\tfrac{\mathcal{I}}{2}+\mathcal{K}'\right)(q-q_h)\|_{H^{-\frac{1}{2},-\frac{1}{4}}(\Gamma\times\Upsilon)}\\ &\leq C\|q-q_h\|_{H^{-\frac{1}{2},-\frac{1}{4}}(\Gamma\times\Upsilon)}\\ &\leq C\left(h_x^{\frac{3}{2}}+h_t^{\frac{3}{4}}\right)\|\mathcal{S}u\|_{H^{1,\frac{1}{2}}_{pw}(\Gamma\times\Upsilon)}.\end{aligned}\tag{3.26}$$

With the aid of some Aubin-Nitsche duality argument for the variational Dirichlet problem (3.23) this result can be extended. We use the bijectivity and boundedness of the single layer operator $\mathcal{V}:H^{-1+s,\frac{-1+s}{2}}(\Gamma\times\Upsilon)\to H^{s,\frac{s}{2}}(\Gamma\times\Upsilon)$ for $s\in(\frac{1}{2},1]$, the Galerkin orthogonality of (3.23), Theorem 3.1, estimate (3.26), and Young's inequality to conclude the proof

$$\begin{aligned}\|\left(\mathcal{S}-\bar{\mathcal{S}}\right)u\|_{H^{-s,-\frac{s}{2}}(\Gamma\times\Upsilon)} &\leq C\|q-q_h\|_{H^{-s,-\frac{s}{2}}(\Gamma\times\Upsilon)}\\ &= C\sup_{0\neq v\in H^{s,\frac{s}{2}}(\Gamma\times\Upsilon)}\frac{\langle q-q_h,v\rangle_{\Gamma\times\Upsilon}}{\|v\|_{H^{s,\frac{s}{2}}(\Gamma\times\Upsilon)}}\\ &= C\sup_{0\neq w\in H^{-1+s,\frac{-1+s}{2}}(\Gamma\times\Upsilon)}\frac{\langle\mathcal{V}(q-q_h),w-\mathcal{Q}_{h_x}\mathcal{Q}_{h_t}w\rangle_{\Gamma\times\Upsilon}}{\|\mathcal{V}w\|_{H^{s,\frac{s}{2}}(\Gamma\times\Upsilon)}}\\ &\leq C\left(h_x^{\frac{-1+2s}{2}}+h_t^{\frac{-1+2s}{4}}\right)\|q-q_h\|_{H^{-\frac{1}{2},-\frac{1}{4}}(\Gamma\times\Upsilon)}\\ &\leq C\left(h_x^{1+s}+h_t^{\frac{1+s}{2}}\right)\|\mathcal{S}u\|_{H^{1,\frac{1}{2}}_{pw}(\Gamma\times\Upsilon)}.\end{aligned}$$

□

In order to derive an error estimate for the solution $\bar{u}_h \in S^{c_1,d_0}_{h_x,h_t}(\Gamma\times\Upsilon)$ of (3.25), we subtract (3.25) from (2.18) to obtain the Galerkin orthogonality

$$\langle (\mathcal{S}+\kappa)\, u_h - \left(\bar{\mathcal{S}}+\kappa\right)\bar{u}_h, w_h\rangle_{\Gamma\times\Upsilon} = 0\,,$$

which we use together with the $H^{\frac{1}{2},\frac{1}{4}}(\Gamma\times\Upsilon)$ ellipticity of $\bar{\mathcal{S}}$ and the positiveness of the heat transfer coefficient κ to estimate

$$\begin{aligned}\|u_h-\bar{u}_h\|^2_{H^{\frac{1}{2},\frac{1}{4}}(\Gamma\times\Upsilon)} &\le C\langle(\bar{\mathcal{S}}+\kappa)(u_h-\bar{u}_h), u_h-\bar{u}_h\rangle_{\Gamma\times\Upsilon}\\ &= C\langle(\bar{\mathcal{S}}-\mathcal{S})u_h, u_h-\bar{u}_h\rangle_{\Gamma\times\Upsilon}\\ &\le C\|(\bar{\mathcal{S}}-\mathcal{S})u_h\|_{H^{-\frac{1}{2},-\frac{1}{4}}(\Gamma\times\Upsilon)}\|u_h-\bar{u}_h\|_{H^{\frac{1}{2},\frac{1}{4}}(\Gamma\times\Upsilon)}\,.\end{aligned}$$

With the triangle inequality, the boundedness of the operators $\mathcal{S}$ and $\bar{\mathcal{S}}$, and Lemma 3.3 we get

$$\begin{aligned}\|u_h-\bar{u}_h\|_{H^{\frac{1}{2},\frac{1}{4}}(\Gamma\times\Upsilon)} &\le C\|(\bar{\mathcal{S}}-\mathcal{S})u_h\|_{H^{-\frac{1}{2},-\frac{1}{4}}(\Gamma\times\Upsilon)}\\ &\le C\left(\|(\bar{\mathcal{S}}-\mathcal{S})u\|_{H^{-\frac{1}{2},-\frac{1}{4}}(\Gamma\times\Upsilon)} + \|(\bar{\mathcal{S}}-\mathcal{S})(u_h-u)\|_{H^{-\frac{1}{2},-\frac{1}{4}}(\Gamma\times\Upsilon)}\right)\\ &\le C\left(h_x^{\frac{3}{2}}+h_t^{\frac{3}{4}}\right)\left(\|\mathcal{S}u\|_{H^{1,\frac{1}{2}}_{pw}(\Gamma\times\Upsilon)} + \|u\|_{H^{2,1}(\Gamma\times\Upsilon)}\right)\end{aligned}$$

and together with (3.22) we can bound the error for the solution of (3.25) by

$$\begin{aligned}\|u-\bar{u}_h\|_{H^{\frac{1}{2},\frac{1}{4}}(\Gamma\times\Upsilon)} &\le \|u-u_h\|_{H^{\frac{1}{2},\frac{1}{4}}(\Gamma\times\Upsilon)} + \|u_h-\bar{u}_h\|_{H^{\frac{1}{2},\frac{1}{4}}(\Gamma\times\Upsilon)}\\ &\le C\left(h_x^{\frac{3}{2}}+h_t^{\frac{3}{4}}\right)\left(\|u\|_{H^{2,1}(\Gamma\times\Upsilon)} + \|\mathcal{S}u\|_{H^{1,\frac{1}{2}}_{pw}(\Gamma\times\Upsilon)}\right)\,.\end{aligned} \tag{3.27}$$

Again, for practical reasons it is more convenient to work with the L_2 error. Thanks to the help of G. Of and O. Steinbach we provide such an estimate for the solution $\bar{u}_h \in S^{c_1,d_0}_{h_x,h_t}(\Gamma\times\Upsilon)$ of the perturbed problem (3.25) in a similar manner to Lemma 3.2.

Lemma 3.4. *Assume that* $\mathcal{S}: H^{1,\frac{1}{2}}(\Gamma\times\Upsilon)\to L_2(\Gamma\times\Upsilon)$ *is bounded and bijective, and* $0\le\kappa\le\kappa_0\in\mathbb{R}$. *Let* $u\in H^{2,1}(\Gamma\times\Upsilon)$ *be the unique solution of* (2.18) *and* $\bar{u}_h\in S^{c_1,d_0}_{h_x,h_t}(\Gamma\times\Upsilon)$ *the unique solution of* (3.25). *Further, assume that there is a* $v_h\in S^{c_1,d_0}_{h_x,h_t}(\Gamma\times\Upsilon)$ *satisfying*

$$\|v-v_h\|_{H^{\frac{1}{2},\frac{1}{4}}(\Gamma\times\Upsilon)} \le C(h_x^{\frac{1}{2}}+h_t^{\frac{1}{4}})\|v\|_{H^{1,\frac{1}{2}}(\Gamma\times\Upsilon)}$$

and

$$\|v_h\|_{H^{\frac{1}{2},\frac{1}{4}}(\Gamma\times\Upsilon)} \le C\|v\|_{H^{\frac{1}{2},\frac{1}{4}}(\Gamma\times\Upsilon)}\,,$$

then we have

$$\|u-\bar{u}_h\|_{L_2(\Gamma\times\Upsilon)} \leq C(h_x^2+h_t)\|u\|_{H^{2,1}(\Gamma\times\Upsilon)} .$$

Proof. Similar to the proof of Lemma 3.2 we have by duality

$$\|u-\bar{u}_h\|_{L_2(\Gamma\times\Upsilon)} = \sup_{0\neq w\in L_2(\Gamma\times\Upsilon)} \frac{\langle u-\bar{u}_h, w\rangle_{\Gamma\times\Upsilon}}{\|w\|_{L_2(\Gamma\times\Upsilon)}}$$

and there this is a unique $v \in H^{1,\frac{1}{2}}(\Gamma\times\Upsilon)$ such that

$$\|u-\bar{u}_h\|_{L_2(\Gamma\times\Upsilon)} = \sup_{0\neq v\in H^{1,\frac{1}{2}}(\Gamma\times\Upsilon)} \frac{\langle (u-\bar{u}_h), (\mathcal{S}+\kappa)v\rangle_{\Gamma\times\Upsilon}}{\|(\mathcal{S}+\kappa)v\|_{L_2(\Gamma\times\Upsilon)}} .$$

Subtracting (3.25) from (2.18), we have the Galerkin orthogonality

$$\langle (\mathcal{S}+\kappa)u-(\bar{\mathcal{S}}+\kappa)\bar{u}_h, w_h\rangle_{\Gamma\times\Upsilon} = 0$$

which leads to

$$\begin{aligned}
\|u-\bar{u}_h\|_{L_2(\Gamma\times\Upsilon)} &\leq \sup_{0\neq v\in H^{1,\frac{1}{2}}(\Gamma\times\Upsilon)} \left(\frac{\langle (\mathcal{S}+\kappa)(u-\bar{u}_h), v-v_h\rangle_{\Gamma\times\Upsilon}}{\|(\mathcal{S}+\kappa)v\|_{L_2(\Gamma\times\Upsilon)}} + \frac{\langle (\bar{\mathcal{S}}-\mathcal{S})\bar{u}_h, v_h\rangle_{\Gamma\times\Upsilon}}{\|(\mathcal{S}+\kappa)v\|_{L_2(\Gamma\times\Upsilon)}} \right) \\
&\leq \sup_{0\neq v\in H^{1,\frac{1}{2}}(\Gamma\times\Upsilon)} \left(\frac{\langle (\mathcal{S}+\kappa)(u-\bar{u}_h), v-v_h\rangle_{\Gamma\times\Upsilon}}{\|(\mathcal{S}+\kappa)v\|_{L_2(\Gamma\times\Upsilon)}} \right. \\
&\qquad + \frac{\langle (\bar{\mathcal{S}}-\mathcal{S})(\bar{u}_h-u), v_h\rangle_{\Gamma\times\Upsilon}}{\|(\mathcal{S}+\kappa)v\|_{L_2(\Gamma\times\Upsilon)}} \\
&\qquad \left. + \frac{\langle (\bar{\mathcal{S}}-\mathcal{S})u, v_h\rangle_{\Gamma\times\Upsilon}}{\|(\mathcal{S}+\kappa)v\|_{L_2(\Gamma\times\Upsilon)}} \right) ,
\end{aligned}$$

where the final result is obtained by an application of the triangle inequality. Due to the boundedness and bijectivity of the Steklov-Poincaré operator provided by Corollary 2.1, the assumptions on $v_h \in S^{c_1,d_0}_{h_x,h_t}(\Gamma\times\Upsilon)$, and Theorem 3.1 we can control the first term with the help of (3.22) and Young's inequality

$$\begin{aligned}
\frac{\langle (\mathcal{S}+\kappa)(u-\bar{u}_h), v-v_h\rangle_{\Gamma\times\Upsilon}}{(\|\mathcal{S}+\kappa)v\|_{L_2(\Gamma\times\Upsilon)}} &\leq \frac{\|(\mathcal{S}+\kappa)(u-\bar{u}_h)\|_{H^{-\frac{1}{2},-\frac{1}{4}}(\Gamma\times\Upsilon)} \|v-v_h\|_{H^{\frac{1}{2},\frac{1}{4}}(\Gamma\times\Upsilon)}}{\|(\mathcal{S}+\kappa)v\|_{L_2(\Gamma\times\Upsilon)}} \\
&\leq C(h_x^{\frac{1}{2}}+h_t^{\frac{1}{4}})\|u-u_h\|_{H^{\frac{1}{2},\frac{1}{4}}(\Gamma\times\Upsilon)} \\
&\leq C(h_x^2+h_t)\|u\|_{H^{2,1}(\Gamma\times\Upsilon)} .
\end{aligned}$$

For the second term we use the boundedness and bijectivity of the Steklov-Poincaré operator, Lemma 3.3, Theorem 3.1, and Young's inequality

$$\begin{aligned}\frac{\langle(\bar{\mathcal{S}}-\mathcal{S})(\bar{u}_h-u),v_h\rangle_{\Gamma\times\Upsilon}}{\|(\mathcal{S}+\kappa)v\|_{L_2(\Gamma\times\Upsilon)}} &\leq \frac{\|\bar{u}_h-u\|_{H^{\frac{1}{2},\frac{1}{4}}(\Gamma\times\Upsilon)}\|(\bar{\mathcal{S}}-\mathcal{S})v_h\|_{H^{-\frac{1}{2},-\frac{1}{4}}(\Gamma\times\Upsilon)}}{\|(\mathcal{S}+\kappa)v\|_{L_2(\Gamma\times\Upsilon)}}\\ &\leq C(h_x^{\frac{1}{2}}+h_t^{\frac{1}{4}})\|\bar{u}_h-u\|_{H^{\frac{1}{2},\frac{1}{4}}(\Gamma\times\Upsilon)}\\ &\leq C(h_x^2+h_t)\|u\|_{H^{2,1}(\Gamma\times\Upsilon)}\,.\end{aligned}$$

Finally, with the stability assumption on $v_h\in S^{c_1,d_0}_{h_x,h_t}(\Gamma\times\Upsilon)$, the boundedness of the Steklov-Poincaré operator, and Lemma 3.3 we conclude the proof by estimating the third term

$$\begin{aligned}\frac{\langle(\bar{\mathcal{S}}-\mathcal{S})u,v_h\rangle_{\Gamma\times\Upsilon}}{\|(\mathcal{S}+\kappa)v\|_{L_2(\Gamma\times\Upsilon)}} &\leq \frac{\|(\bar{\mathcal{S}}-\mathcal{S})u\|_{H^{-1,-\frac{1}{2}}(\Gamma\times\Upsilon)}\|v_h\|_{H^{1,\frac{1}{2}}(\Gamma\times\Upsilon)}}{\|(\mathcal{S}+\kappa)v\|_{L_2(\Gamma\times\Upsilon)}}\\ &\leq C\|(\bar{\mathcal{S}}-\mathcal{S})u\|_{H^{-1,-\frac{1}{2}}(\Gamma\times\Upsilon)}\\ &\leq C(h_x^2+h_t)\|u\|_{H^{2,1}(\Gamma\times\Upsilon)}\,.\end{aligned}$$

□

3.2.4 Mixed Initial Boundary Value Problems

We solve the variational form (2.19) with $\Gamma_{NR}:=\Gamma_N\cup\Gamma_R$ for the approximate solution $\tilde{u}_h\in S^{c_1,d_0}_{h_x,h_t}(\Gamma_{NR}\times\Upsilon):=S^{c_1,d_0}_{h_x,h_t}(\Gamma\times\Upsilon)\cap\widetilde{H}^{\frac{1}{2},\frac{1}{4}}(\Gamma_{NR}\times\Upsilon)$

$$\langle(\mathcal{S}+\kappa)\tilde{u}_h,v_h\rangle_{\Gamma_{NR}\times\Upsilon}=\langle g_{NR}-(\mathcal{S}+\kappa)\tilde{g}_D,v_h\rangle_{\Gamma\times\Upsilon}\quad\forall v_h\in S^{c_1,d_0}_{h_x,h_t}(\Gamma_{NR}\times\Upsilon)\,. \tag{3.28}$$

Uniqueness and solvability of the continuous problem (2.19) directly translates to the discrete problem (3.28), since we are working with conforming finite dimensional sub-spaces. Furthermore, Cea's Lemma guarantees quasi-optimality and Theorem 3.1 provides the estimate

$$\|\tilde{u}-\tilde{u}_h\|_{\widetilde{H}^{\frac{1}{2},\frac{1}{4}}(\Gamma_{NR}\times\Upsilon)}\leq C(h_x^{\frac{3}{2}}+h_t^{\frac{3}{4}})\|u\|_{H^{2,1}(\Gamma\times\Upsilon)}\,.$$

Again, since we work with an approximation of the right hand side $\bar{g}_{NR}=\mathcal{Q}_{h_x}\mathcal{Q}_{h_t}g_{NR}$ and $\bar{\tilde{g}}_D=\mathcal{Q}_{h_x}\mathcal{Q}_{h_t}\tilde{g}_D$ we solve the perturbed problem for $\bar{\tilde{u}}_h\in S^{c_1,d_0}_{h_x,h_t}(\Gamma_{NR}\times\Upsilon)$

$$\langle(\mathcal{S}+\kappa)\,\bar{\tilde{u}}_h,v_h\rangle_{\Gamma\times\Upsilon}=\langle\bar{g}_{NR}-(\mathcal{S}+\kappa)\bar{\tilde{g}}_D,v_h\rangle_{\Gamma\times\Upsilon}\quad v_h\in S^{c_1,d_0}_{h_x,h_t}(\Gamma_{NR}\times\Upsilon)\,, \tag{3.29}$$

which the following lemma gives an $L_2(\Gamma\times\Upsilon)$ error estimate for.

Lemma 3.5. *Assume that* $(\mathcal{S}+\kappa) : H^{1,\frac{1}{2}}(\Gamma\times\Upsilon) \to L_2(\Gamma\times\Upsilon)$ *is bounded and bijective. Let* $\tilde{u} \in \widetilde{H}^{2,1}(\Gamma_{NR}\times\Upsilon)$ *be the unique solution of* (2.19) *with* $\Gamma := \Gamma_D \cup \Gamma_{NR}$ *and* $\tilde{\bar{u}}_h \in S^{c_1,d_0}_{h_x,h_t}(\Gamma_{NR}\times\Upsilon) := S^{c_1,d_0}_{h_x,h_t}(\Gamma\times\Upsilon) \cap \widetilde{H}^{\frac{1}{2},\frac{1}{4}}(\Gamma_{NR}\times\Upsilon)$ *the unique solution of* (3.29)*, then we have*

$$\|\tilde{u} - \tilde{\bar{u}}_h\|_{L_2(\Gamma\times\Upsilon)} \leq C(h_x^2 + h_t)\|u\|_{H^{2,1}(\Gamma\times\Upsilon)} .$$

Proof. Due to $\widetilde{H}^{\frac{1}{2},\frac{1}{4}}(\Gamma_{NR}\times\Upsilon) \subset H^{\frac{1}{2},\frac{1}{4}}(\Gamma\times\Upsilon)$ Lemma 3.4 applies. □

Remark 3.2. *Due to the definition of the boundary element space* $S^{c_1,d_0}_{h_x,h_t}(\Gamma_{NR}\times\Upsilon) := S^{c_1,d_0}_{h_x,h_t}(\Gamma\times\Upsilon) \cap \widetilde{H}^{\frac{1}{2},\frac{1}{4}}(\Gamma_{NR}\times\Upsilon)$ *with* $\Gamma_{NR} := \Gamma_N \cup \Gamma_R$ *it is clear that the elimination of a boundary part* Γ_i *with* $i \in \{D,N,R\}$ *of the continuous problem in Subsection 2.4.4 carries directly over to the discrete problem.*

4 THE PARABOLIC FAST MULTIPOLE METHOD

The Fast Multipole Method (FMM) [17] was originally developed to solve many body problems in two-dimensional potential field theory. Its name stems from the multipole expansion of an electrostatic point charge in the original paper. Ever since the algorithm has been extended to higher dimensions, further improved by using different expansions and applied to different physical problems [9, 18, 34]. Even though the panel clustering method [22] had appeared almost contemporaneously to the original FMM publication, we follow the common misuse of terminology and use the term FMM in connection with boundary element methods. This combination has seen quite some success in the elliptic [21, 29, 36] and lately also in the parabolic case [31, 43, 45].

It has become customary to refer to efficient evaluation schemes for point-point interaction, based on a hierarchical clustering of the computational domain and separation of variables for well separated clusters through some sort of kernel expansion, as FMM algorithms. In this context Galerkin boundary element methods may be conceived as weighted and integrated point-point interactions problems. The basic idea of such algorithms is to collect the influence of sources in clusters and evaluate their collective influence on all admissible target clusters, i.e. clusters where the expansion converges. This way the otherwise $\mathcal{O}(N^2)$ cost for the evaluation of the point-point interaction problem is reduced to $\mathcal{O}(N)$, where N is the number of unknowns.

Since these general ideas are kernel depended, we need to elaborate on those details next. The heat kernel is asymptotically smooth for $t-\tau>0$ and exponentially decaying in space (see Figure 4.1a and 4.1b, respectively). We call the FMM adapted to this kind of kernel the parabolic FMM [43] (pFMM). One may perceive it as a combination of a one-dimensional causal FMM [45] (cFMM) in time with a Fast Gauss Transform [20] (FGT) applied to the spatial variable. Based on this observation we will explain these two algorithms by themselves first, before joining them together to the pFMM algorithm.

Since it is of major importance for the remainder of this chapter, we would like to emphasize at this point that the spatial variable of the heat kernel naturally separates due to basic properties of the exponential function

$$G(\mathbf{r},d)=\prod_{i=1}^{3}\frac{1}{(4\pi\alpha d)^{\frac{1}{2}}}\exp\left(-\frac{|r_i|^2}{4\alpha d}\right)=\prod_{i=1}^{3}G(r_i,d)\ . \tag{4.1}$$

Hence for the most part it is sufficient to look at properties of the one-dimensional heat kernel with the multi-dimensional case following from this Gaussian structure. This idea

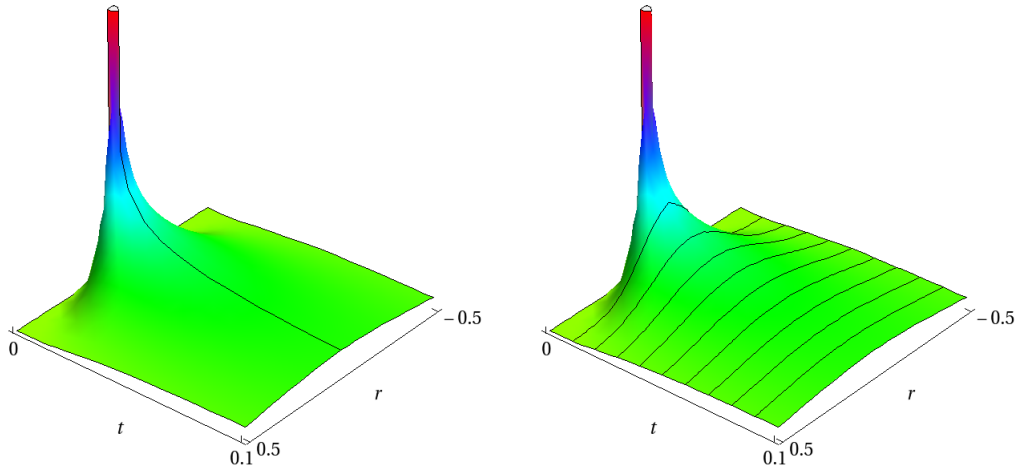

(a) The heat kernel is asymptotically smooth in time – see curve at $r = 0$.

(b) For fixed time variables the heat kernel is a Gaussian in space – see set of curves.

Figure 4.1: One-dimensional heat kernel $G(r,t)$ for $r \times t \in (-0.5,0.5) \times (0,0.1)$.

is pursued throughout the entire pFMM algorithm, be it in the spatial clustering or kernel expansion of the spatial variables. As a matter of fact, the spatial dimension of the algorithm is not limited to three space dimensions, however, since we only deal with three-dimensional heat diffusion problems we develop the algorithm for that special case. Another important property of the heat kernel that we will frequently encounter is the space-time scaling property

$$G(\mathbf{r}, \delta d) = \delta^{-\frac{3}{2}} G\left(\frac{\mathbf{r}}{\sqrt{\delta}}, d\right) , \tag{4.2}$$

which tells us that the heat kernel gets more and more peaked the smaller the variance.

To set the stage, we introduce a hierarchical space-time clustering in Section 4.1 and recall some basics from multi-variate approximation theory in Section 4.2. From there we proceed as follows: In Section 4.3, we construct space independent thermal layer potentials and evaluate them via the cFMM, in Section 4.4 we present an efficient realization of thermal layer potentials with fixed time variable through the FGT and in Section 4.5 we combine the ideas of Section 4.3 and Section 4.4 to efficiently solve Galerkin space-time discretized boundary integral equations of the heat equation via the pFMM. Sections 4.2 through 4.5 are a presentation of [43, 45, 46] from the authors perspective with an adaption to the Galerkin method whenever necessary. Finally, due to the temporal nearfield being so expensive, whenever the space-time scaling is not optimal, we present some more recent results in Section 4.6 to improve the spatial evaluation of the temporal nearfield [31].

4.1 Space-Time Clustering

In this section, we introduce a hierarchical clustering of the computational domain as the first basic ingredient for the any FMM algorithm to be established. We distinguish between the temporal and spatial cluster tree due to the different build of the temporal respectively spatial dimension of the space-time cylinder $\Gamma_{h_x} \times \Upsilon$. While the spatial discretization is rather unstructured, the temporal discretization has a very simple and clear nature that we seek to conserve.

4.1.1 Temporal Cluster-Tree

We want the temporal cluster tree to inherit the uniformity of time discretization (3.2). Moreover, since time is a one-dimensional and ordered manifold in $\mathbb{R}_0^+$, there will be no empty temporal clusters which allows a simple cluster structure without geometric sorting (see Figure 4.2).

Definition 4.1. *We define the temporal root cluster to coincide with the time interval of interest $I_0^0 := \Upsilon = [0,T]$ with center $c^{I_0^0} = T/2$ and cluster half length $h_t^0 = T/2$. Then we choose a leaf level L_t and split all clusters $I_k^{\ell_t}$ recursively into two equal sized children*

$$\mathfrak{C}(I_k^{\ell_t}) = \{I_{2k+i}^{\ell_t+1}\}_{i=0}^{1}, \quad \ell_t = 0,\dots L_t - 1, \quad k = 0,\dots 2^{\ell_t} - 1.$$

This way we end up with 2^{ℓ_t} uniform clusters with half interval length $h_t^{\ell_t} = T/2^{\ell_t+1}$ in each level. In particular we have 2^{L_t} temporal leaf clusters which we split into n_t uniform time steps of step size $h_t = 2h_t^{L_t}/n_t$. Hence we can introduce the panel list

$$\mathfrak{P}(I_k^{\ell_t}) = \bigcup_{i=0}^{n_t-1} 2^{L_t-\ell_t}k + i \tag{4.3}$$

containing the indexes of all time steps belonging to a temporal cluster $I_k^{\ell_t}$.

4.1.2 Spatial Cluster-Tree

The spatial dimension of the computational domain is more involved than the temporal one for the following reason: We are dealing with polyhedral triangulations Γ_{h_x} of an arbitrary Lipschitz domain's boundary, i.e. two-dimensional Lipschitz manifolds embedded in three-dimensional space. We can not expect the spatial clustering to be uniform like in time, since there will be empty clusters, i.e. clusters not intersecting with Γ_{h_x} (see Figure 4.3 and 4.4). Nevertheless, we restrict ourselves to a very simple structure only,

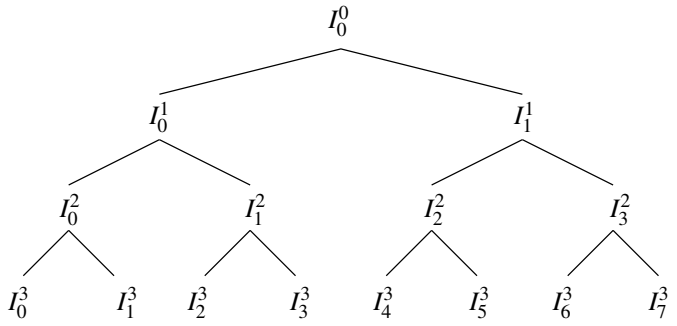

Figure 4.2: Completely uniform temporal binary tree.

namely a regular, axis parallel and thus tensorial cluster-tree. This choice facilitates an FMM algorithm, whose translation operators inherit the tensor structure of the heat kernel (4.1) – a feature that in general would not be possible with more sophisticated clustering strategies.

Definition 4.2. *We define the root cluster X_0^0 to be the cubic bounding box with half-side length*

$$h_x^0 = \frac{\|\tilde{\mathbf{x}} - \bar{\mathbf{x}}\|_\infty}{2}, \quad \tilde{\mathbf{x}}, \bar{\mathbf{x}} \in \Gamma_{h_x}$$

and center

$$c_i^{X_0^0} = \max_{\tilde{\mathbf{x}}, \bar{\mathbf{x}} \in \Gamma_{h_x}} \left(\frac{|\tilde{x}_i| + |\bar{x}_i|}{2} \right), \quad i \in \{1,2,3\}.$$

The spatial cluster tree is constructed by a recursive splitting of all $X_k^{\ell_x}$ into eight equal sized child cubes

$$\mathfrak{C}(X_k^{\ell_t}) = \{X_{8k+i}^{\ell_t+1}\}_{i=0}^7, \quad \ell_x = 0, \dots L_x - 1, \quad k = 0, \dots 8^{\ell_x} - 1$$

with half-side length $h_x^{\ell_x+1} = h_x^0 / 2^{\ell_x+1}$. Throughout this process test- and trial functions φ_j are assigned to the panel list $\mathfrak{P}(X_k^{\ell_x})$ of one and only one cluster $X_k^{\ell_x}$ in each level

$$\mathfrak{P}(X_k^{\ell_x}) = \{ j : \mathbf{c}^{\varphi_j} \in X_k^{\ell_x} \}.$$

We drop all $X_k^{\ell_x}$ with $\mathfrak{P}(X_k^{\ell_x}) = \emptyset$ while we collect all nonempty clusters per level in a cluster list

$$\mathfrak{X}(\ell_x) = \{k : \mathfrak{P}(X_k^{\ell_x}) \neq \emptyset\}$$

and stop at level ℓ_x once $N_x = n_x \dim(\mathfrak{X}(\ell_x))$ with a pre-specified n_x is reached.

Since we work with Galerkin discretized boundary integral operators, we have to evaluate their bilinear forms (3.5), (3.6), (3.7) and (3.8) cluster wise over the support of test- and trial functions. This requires that we define our kernel expansions in such that they hold true for the entire support of the respective test- and trial function. Since Definition 4.2 does not ensure that (see Figure 4.3, where the boundary is not completely contained in the union of all leaf clusters), we define an extension of all clusters as follows.

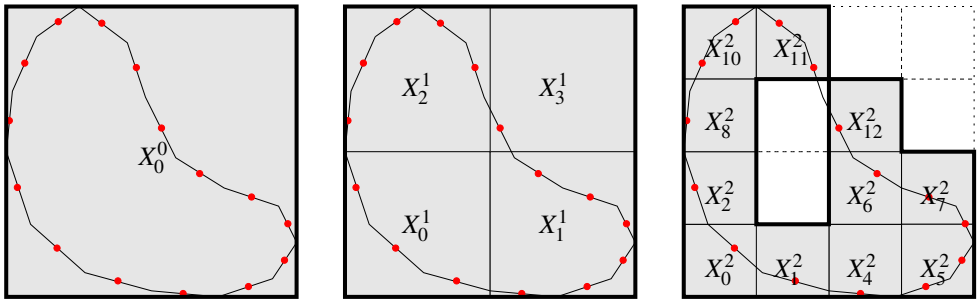

Figure 4.3: Cross-section through spatial cluster structure (• are $\mathbf{c}^{\varphi_j}$).

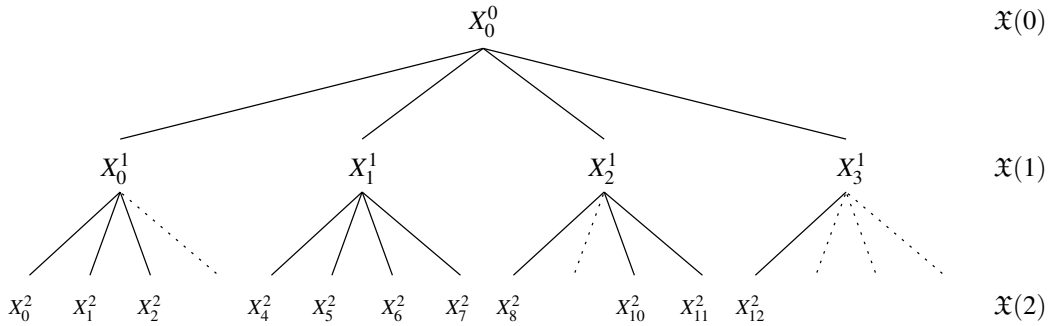

Figure 4.4: Spatial cluster-tree corresponding to Figure 4.3.

Definition 4.3. *Find the maximal bounding box of all test- or trial functions assigned to each leaf cluster*

$$\bar{h}_x^{L_x} = \max_k \|\mathbf{c}^{X_k^{L_x}} - \mathbf{x}\|_\infty \,, \quad \mathbf{x} \in \bigcup_{j \in \mathfrak{P}(X_k^{L_x})} supp\,(\varphi_j)$$

and uniformly extend all clusters $X_k^{\ell_x} \to \bar{X}_k^{\ell_x}$ *in all levels* $\ell_x = 0, \ldots L_x$ *by*

$$\bar{h}_x^{\ell_x} = h_x^{\ell_x} + \left(\bar{h}_x^{L_x} - h_x^{L_x}\right) \,.$$

Observe that after the extension described in Definition 4.3 $\bigcup \bar{X}_k^{\ell_x}$ covers the entire computational domain Γ_{h_x} (see Figure 4.5) while this was not ensured by $\bigcup X_k^{\ell_x}$ (see Figure 4.3).

4.2 Multivariate Lagrange Interpolation and Chebyshev Expansion

The second major ingredient required for any FMM is a separation of variables through an appropriate kernel expansion. Here we recall the basics from Lagrange interpolation

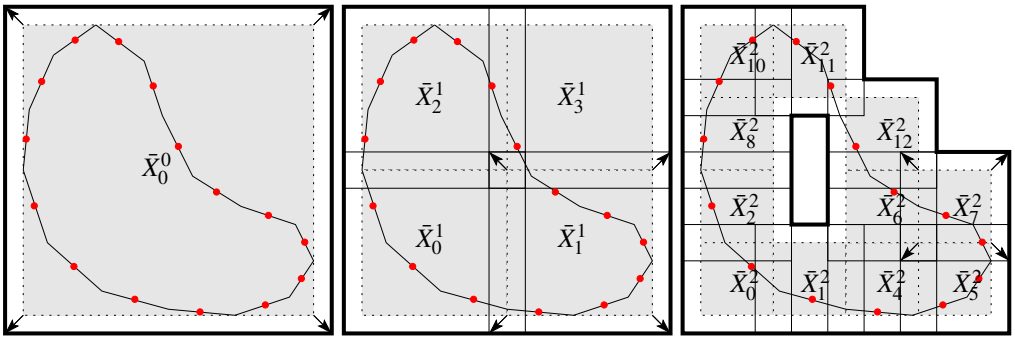

Figure 4.5: Spatial cluster extension as described in Definition 4.3.

and Chebyshev expansion theory that we will need for the kernel expansions later on. Throughout this section we make use of the linear transformation $\Phi(\hat{z}) : [-1,1] \to [a,b]$ defined by

$$\Phi(\hat{z}) = \frac{a+b}{2} + \frac{b-a}{2}\hat{z}\,.$$

It is understood that in the multi-dimensional case $\Phi(\hat{\mathbf{z}}) : [-1,1]^d \to [\mathbf{a},\mathbf{b}]$ is equivalent to $\{\Phi(\hat{z}_i) : [-1,1] \to [a_i,b_i]\}_{i=1}^d$ with $[\mathbf{a},\mathbf{b}] = [a_1,b_1] \times [\ldots] \times [a_d,b_d]$. Furthermore, due to Definitions 4.1 through 4.3 we will always have $b_1 - a_1 = \cdots = b_d - a_d$ and thus write $(b-a)$ instead of $(b_i - a_i)$. Finally, to be clarify the notation, let α be a d-dimensional multi-index, e.g. $\alpha = (\alpha_1,\ldots,\alpha_d)$ then we have $|\alpha| = \alpha_1 + \cdots + \alpha_d$, $\alpha! = \alpha_1! + \cdots + \alpha_d!$ and $\alpha^2 = (\alpha_1^2,\ldots,\alpha_d^2)$.

4.2.1 Lagrange Interpolation

Let us assume a continuous function $f(t) : [a,b] \to \mathbb{R}$, then we may write its interpolation on the nodes $\{\omega_i^p\}_{i=0}^p \in [-1,1]$

$$\mathcal{J}_p f(t) = \sum_{i=0}^{p} f\left(\Phi(\omega_i^p)\right) L_i\left(\Phi^{-1}(t)\right) \tag{4.4}$$

in terms of the Lagrange polynomials

$$L_i(\hat{t}) = \prod_{k \neq i} \frac{\hat{t} - \omega_k^p}{\omega_i^p - \omega_k^p}\,, \quad \hat{t} \in [-1,1]\,.$$

We chose the roots of the $(p+1)^{st}$ Chebyshev polynomial as interpolation nodes

$$\omega_k^p = \cos\left(\frac{\pi}{2}\frac{2k+1}{p+1}\right)$$

because they minimize the interpolation error thus bounded by

$$|(\mathcal{I}-\mathcal{J}_p)f(t)| \leq \frac{\|D_t^{(p+1)}f(t)\|_\infty}{(p+1)!}\left(\frac{b-a}{4}\right)^{p+1} . \tag{4.5}$$

Multi-Variate Interpolation The interpolation of $f(\mathbf{t}) : [\mathbf{a},\mathbf{b}] \to \mathbb{R}$ on a tensor grid of interpolation nodes $\{\omega_\alpha^p\}_{\alpha=0}^p = \{\{\omega_{\alpha_1}^p\}_{\alpha_1=0}^p \times \cdots \times \{\omega_{\alpha_d}^p\}_{\alpha_d=0}^p\} \in [-1,1]^d$

$$\mathcal{J}_p^d f(\mathbf{t}) = \sum_{\alpha=0}^{p} f\left(\Phi(\omega_\alpha^p)\right) L_\alpha\left(\Phi^{-1}(\mathbf{t})\right) \tag{4.6}$$

induces an error [21] bounded by

$$|(\mathcal{I}-\mathcal{J}_p^d)f(\mathbf{t})| \leq \sum_{\|\alpha\|_\infty=1} \frac{\|D_{\mathbf{t}}^{\alpha(p+1)}f(\mathbf{t})\|_\infty}{(|\alpha|(p+1))!}\left(\frac{b-a}{4}\right)^{|\alpha|(p+1)} . \tag{4.7}$$

4.2.2 Chebyshev Expansion

Let us assume an analytic function $f(x) : [a,b] \to \mathbb{R}$, then we may write its Chebyshev expansion

$$\mathcal{S}_\infty f(x) = \sum_{i=0}^{\infty} c_i T_i\left(\Phi^{-1}(x)\right) \tag{4.8}$$

with the Chebyshev polynomials of the first kind

$$T_i(\hat{x}) = \cos\left(i \arccos(\hat{x})\right) , \quad \hat{x} \in [-1,1] .$$

Due to their $L_w^2[-1,1]$ orthogonality with respect to the weight function $w(\hat{x}) = \sqrt{1-\hat{x}^2}$

$$\int_{-1}^{1} T_m(\hat{x})T_n(\hat{x})w(\hat{x})\mathrm{d}\hat{x} = \frac{\pi}{\gamma_n}\delta_{mn} , \quad \gamma_n = \begin{cases} 1 & n=0 \\ 2 & n \geq 1 \end{cases} \tag{4.9}$$

it is easily verified that the coefficients c_i in (4.8) are given by

$$c_i = \frac{\gamma_i}{\pi}\int_{-1}^{1} f\left(\Phi(\hat{x})\right) T_i(\hat{x})w(\hat{x})\mathrm{d}\hat{x} . \tag{4.10}$$

After expanding the function $f(x)$ itself in a Chebyshev series, we are interested in the expansion of its derivative

$$\mathcal{S}_\infty \frac{\partial}{\partial x} f(x) = \frac{\partial}{\partial x}\mathcal{S}_\infty f(x) = \frac{\partial}{\partial x}\sum_{i=0}^{\infty} c_i T_i\left(\Phi^{-1}(x)\right) = \sum_{i=0}^{\infty} c_i \frac{\partial}{\partial x} T_i\left(\Phi^{-1}(x)\right) , \tag{4.11}$$

what turns out to be a rather straightforward task, because we do not have to change the expansion coefficients (4.10). We simply shift the derivative over to the Chebyshev polynomials and replace them by their derivatives, which are given in terms of the Chebyshev polynomials of the second kind

$$\frac{\partial}{\partial \hat{x}} T_i(\hat{x}) = iU_{i-1}(\hat{x}) \quad \text{with} \quad U_{i-1}(\hat{x}) = \frac{\sin(i \arccos(\hat{x}))}{\sqrt{1-\hat{x}^2}} , \tag{4.12}$$

thus we may write

$$\mathcal{S}_\infty \frac{\partial}{\partial x} f(x) = \sum_{i=0}^{\infty} c_i \, iU_{i-1}\left(\Phi^{-1}(x)\right) \frac{\partial}{\partial x} \Phi^{-1}(x) . \tag{4.13}$$

Multi-Variate Expansion The expansion of $f(\mathbf{x}) : [\mathbf{a}, \mathbf{b}] \to \mathbb{R}$ is given by

$$\mathcal{S}_\infty^d f(\mathbf{x}) = \sum_{\alpha=0}^{\infty} c_\alpha T_\alpha \left(\Phi^{-1}(\mathbf{x})\right)$$

with the coefficients

$$c_\alpha = \frac{\gamma_\alpha}{\pi^d} \int\limits_{[-1,1]^d} f\left(\Phi(\hat{\mathbf{x}})\right) T_\alpha(\hat{\mathbf{x}}) w_\alpha(\hat{\mathbf{x}}) \mathrm{d}\hat{\mathbf{x}} .$$

In the same manner as for the derivative (4.11) in the one-dimensional case we introduce the Chebyshev expansion of the gradient

$$\mathcal{S}_\infty^d \nabla_{\mathbf{x}} f(\mathbf{x}) = \nabla_{\mathbf{x}} \mathcal{S}_\infty^d f(\mathbf{x}) = \nabla_{\mathbf{x}} \sum_{\alpha=0}^{\infty} c_\alpha T_\alpha \left(\Phi^{-1}(\mathbf{x})\right) = \sum_{\alpha=0}^{\infty} c_\alpha \nabla_{\mathbf{x}} T_\alpha \left(\Phi^{-1}(\mathbf{x})\right) \tag{4.14}$$

with

$$\nabla_{\mathbf{x}} T_\alpha \left(\Phi^{-1}(\mathbf{x})\right) = \begin{pmatrix} \alpha_1 U_{\alpha_1 - 1}(x_1) T_{\alpha_2}(x_2) \dots T_{\alpha_d}(x_d) \\ T_{\alpha_1}(x_1) \alpha_2 U_{\alpha_2 - 1}(x_2) \dots T_{\alpha_d}(x_d) \\ \vdots \\ T_{\alpha_1}(x_1) T_{\alpha_2}(x_2) \dots \alpha_d U_{\alpha_d - 1}(x_d) \end{pmatrix} \frac{1}{\det\left(\mathbf{J}_\Phi(\mathbf{x})\right)} . \tag{4.15}$$

Remark 4.1. *Assume that we truncate* (4.8) *after* $q+1$ *terms and compute the coefficients in* (4.10) *by replacing the integral with a* q^{th} *order Gauss-Chebyshev quadrature rule*

$$\check{\mathcal{S}}_q f(x) = \sum_{i=0}^{q} \check{c}_i T_i \left(\Phi^{-1}(x)\right) \quad \textit{and} \quad \check{c}_i \approx \frac{\gamma_i}{q+1} \sum_{k=0}^{q} T_i(\omega_k^q) f\left(\Phi(\omega_k^q)\right) ,$$

then we obtain $\check{\mathcal{S}}_q f = \mathcal{J}_q f$.

Remark 4.1 shows us how to convert a truncated Chebyshev expansion into a Lagrange interpolation formula. The extension of this idea to the multi-dimensional case would give us an estimate of the truncation error with coefficients in a hyper-cubic region. However, this is not optimal because the tensor product space spanned by the Lagrange polynomials does not span the full polynomial space of the hyper-cube's dimension. As we will see later, we can find a better truncation criterion with coefficients in a hyper-simplicial region by estimating the specific truncation error of the heat kernel itself.

4.3 Purely Time Dependent Thermal Layer Potentials – Causal FMM

In the case of a purely time dependent density $q(\tau)$ on a sphere one can perform the spatial integration in the thermal layer potentials analytically, resulting in the layer potentials being Volterra integral operators. We chose this special case as a starting point for the derivation of the parabolic FMM, because it allows us to isolate the temporal aspect of the algorithm, the causal FMM. For simplicity we choose a unit-sphere, then the single layer potential due to $q(\tau)$ becomes

$$\begin{aligned}
\mathcal{V}q(t) &= \int_0^t \int_{|\mathbf{y}|=1} \frac{1}{(4\pi(t-\tau))^{\frac{3}{2}}} \exp\left(-\frac{|\mathbf{x}-\mathbf{y}|^2}{4(t-\tau)}\right) \mathrm{d}s_{\mathbf{y}} q(\tau)\mathrm{d}\tau \\
&= \int_0^t \frac{1}{\sqrt{\pi(t-\tau)}} \left[1-\exp\left(-\frac{1}{(t-\tau)}\right)\right] q(\tau)\mathrm{d}\tau \\
&:= \int_0^t \left(V_1(t-\tau)-V_2(t-\tau)\right) q(\tau)\mathrm{d}\tau := \int_0^t V(t-\tau)q(\tau)\mathrm{d}\tau\,. \qquad (4.16)
\end{aligned}$$

In the remainder of this section we dedicate ourselves to effectively apply the Galerkin discretized operator of (4.16) by means of the causal FMM [45]. Splitting Υ into N_t equidistant time steps according to Subsection 3.1.1 yields the Galerkin discretized Volterra integral equation

$$\langle \mathcal{V}q_h, w_h\rangle = \langle f, w_h\rangle \quad \forall w_h \in T_{h_t}^{d_{d_t}}(\Upsilon)\,, \qquad (4.17)$$

which eventually leads to the linear system

$$\mathbf{V}\,\mathbf{q} = \mathbf{f}$$

with $f_i := \langle f, \phi_i\rangle$ and the lower triangular Toeplitz matrix $V_{ij} = V_{i-j} := \langle \mathcal{V}\phi_j, \phi_i\rangle$. Clearly the computation of the right hand side is $\mathcal{O}(N_t)$ whereas the application of the lower triangular Toeplitz matrix on the left hand side is $\mathcal{O}(N_t^2)$ even if applied by forward substitution. We seek to reduce this prohibitively large amount of work to almost optimal complexity by means of the cFMM algorithm.

4.3.1 Lagrange Interpolation of the Time Dependent Kernel

Based on the hierarchical clustering of Υ as described in Subsection 4.1.1 we interpolate the time dependent kernel in (4.16) with $t \in I_m^{\ell_t} \subset \Upsilon$ and $\tau \in J_n^{\ell_t} \subset \Upsilon$. For this purpose we introduce local variables $\hat{t}, \hat{\tau} \in [-1,1]$

$$t = \Phi_{I_m^{\ell_t}}(\hat{t}) = c_{I_m^{\ell_t}} + h_t^{\ell_t}\hat{t} \quad \text{and} \quad \tau = \Phi_{J_n^{\ell_t}}(\hat{\tau}) = c_{J_n^{\ell_t}} + h_t^{\ell_t}\hat{\tau}\,,$$

then we may write

$$V(t-\tau) = V\left(\Phi_{I_m^{\ell_t}}(\hat{t}) - \Phi_{J_n^{\ell_t}}(\hat{\tau})\right) = V\left((d_{mn}^{\ell_t} + \hat{t} - \hat{\tau})h_t^{\ell_t}\right)$$

with $d_{mn}^{\ell_t} = (c_{I_m^{\ell_t}} - c_{J_n^{\ell_t}})/h_t^{\ell_t}$.

Lemma 4.1. *Let $t \in I_m^{\ell_t}$ and $\tau \in J_m^{\ell_t}$, then the interpolation error of the kernel in* (4.16) *by a bi-variate interpolation ($\mathcal{J}_p^2 = \mathcal{J}_{p,t} \circ \mathcal{J}_{p,\tau} \equiv \mathcal{J}_{p,\tau} \circ \mathcal{J}_{p,t}$) as described in Subsection 4.2.1*

$$\mathcal{J}_p^2 V(t-\tau) = \sum_{a,b=0}^{p} V\left(\Phi_{I_m^{\ell_t}}(\omega_a^p) - \Phi_{J_n^{\ell_t}}(\omega_b^p)\right) L_a\left(\Phi_{I_m^{\ell_t}}^{-1}(t)\right) L_b\left(\Phi_{J_n^{\ell_t}}^{-1}(\tau)\right)$$

for two well separated clusters

$$\eta\, dist(I_m^{\ell_t}, J_n^{\ell_t}) \geq \tfrac{1}{2} max\{diam(I_m^{\ell_t}), diam(J_n^{\ell_t})\}\,, \quad \eta \in (0,1) \tag{4.18}$$

is bounded by

$$|(\mathcal{I} - \mathcal{J}_p^2)V(t-\tau)| \leq C\left(h_t^{\ell_t}\right)^{-\frac{1}{2}} \eta^{p+1}\,. \tag{4.19}$$

Proof. In order to prove (4.19) using estimate (4.7) we need to show that the kernel in (4.16) is asymptotically smooth. It is easily seen that the first part $V_1(t-\tau)$ fulfills

$$\left|\frac{D_t^i D_\tau^j V_1(t-\tau)}{(i+j)!}\right| \leq \frac{C_1}{|t-\tau|^{i+j+\frac{1}{2}}}\,.$$

However, for the second part $V_2(t-\tau)$ such a relation is not so obvious. For this purpose we define $\delta := t - \tau$ and use Cauchy's integral formula to estimate

$$\frac{V_2^{(n)}(\delta)}{n!} = \frac{(-1)^n}{2\pi\imath}\int_\gamma \frac{1}{\sqrt{\pi\zeta}}\exp\left(-\frac{1}{\zeta}\right)\frac{1}{(\delta-\zeta)^{n+1}}\mathrm{d}\zeta\,.$$

We chose the contour γ to be a circle with positive radius $a < \delta$ centered at δ

$$\gamma = \{\zeta : |\delta - \zeta| = a\}\,.$$

For this choice we obtain the estimates

$$|\delta-\zeta| = a\,, \quad \mathfrak{Re}\left(\tfrac{1}{\zeta}\right) \geq 0 \quad \text{and} \quad |\zeta| \geq \delta - a\,,$$

which lead to

$$\left|\frac{V_2^{(n)}(\delta)}{n!}\right| \leq (\pi(\delta-a))^{-\frac{1}{2}}\, a^{-n}\,.$$

We maximize $(\delta-a)^{-\frac{1}{2}}a^{-n}$ for the optimal radius $a = 2n\delta/(2n+1)$ resulting in

$$\left|\frac{D_t^i D_\tau^j V_2(t-\tau)}{(i+j)!}\right| \leq \frac{C_2(i+j)^{\frac{1}{2}}}{|t-\tau|^{i+j+\frac{1}{2}}}\,.$$

Thus we may state the asymptotic smoothness condition for the kernel in (4.16) as

$$\frac{|D_t^i D_\tau^j V(t-\tau)|}{(i+j)!} \leq \frac{C(i+j)^{\frac{1}{2}}}{|t-\tau|^{i+j+\frac{1}{2}}} \tag{4.20}$$

with $C := C_1 + C_2$. Hence from estimate (4.7), the well separation condition (4.18), Definition 4.1 and condition (4.20) the assertion follows immediately

$$\begin{aligned}
|(\mathcal{I}-\mathcal{J}_p^2)V(t-\tau)| &\leq \sum_{i,j\in\{0,p+1\}} \frac{\|D_t^i D_\tau^j V(t-\tau)\|_\infty}{(i+j)!}\left(\frac{h_t^{\ell_t}}{2}\right)^{i+j} \\
&\leq \sum_{i,j\in\{0,p+1\}} \frac{C(i+j)^{\frac{1}{2}}}{\left|(d_{mn}^{\ell_t}-2)h_t^{\ell_t}\right|^{i+j+\frac{1}{2}}}\left(\frac{h_t^{\ell_t}}{2}\right)^{i+j} \\
&\leq C\left((d_{mn}^{\ell_t}-2)h_t^{\ell_t}\right)^{-\frac{1}{2}} \sum_{i,j\in\{0,p+1\}} \frac{(i+j)^{\frac{1}{2}}}{2^{i+j}}\eta^{i+j} \\
&\leq C\left(h_t^{\ell_t}\right)^{-\frac{1}{2}}\eta^{p+1}\,.
\end{aligned}$$

□

Except for the mild influence of the first term, Lemma 4.1 bounds the interpolation error independently of the temporal level ℓ_t. Next we use this estimate to show how the interpolation order p has to be chosen such that it does not interfere with the discretization error of the Galerkin scheme.

Lemma 4.2. *Let us assume the Galerkin bilinear form $\langle \mathcal{V}\phi_j, \phi_i\rangle$ as given in* (4.17) *and furthermore the approximated bilinear form $\langle \check{\mathcal{V}}\phi_j, \phi_i\rangle$, where we replace the kernel of* (4.17)

by a bi-variate Lagrange interpolation as described in Lemma 4.1. Choosing the interpolation order to be $p = \mathcal{O}(\log N_t)$ we can guarantee a point-wise approximation error of order σ_t

$$|\langle \mathcal{V}\phi_j, \phi_i\rangle - \langle \check{\mathcal{V}}\phi_j, \phi_i\rangle| \leq C h_t^{\sigma_t} \|\phi_j\|_{L_2} \|\phi_i\|_{L_2} .$$

Proof. By Definition 4.1 we have $h_t^{\ell_t} > h_t$ thus together with the Cauchy-Schwarz inequality we have

$$\begin{aligned}
|\langle \mathcal{V}\phi_j, \phi_i\rangle - \langle \check{\mathcal{V}}\phi_j, \phi_i\rangle| &\leq \int_{t=ih_t}^{(i+1)h_t} \int_{\tau=jh_t}^{(j+1)h_t} \left|(\mathcal{I} - \mathcal{J}_p^2) V(t-\tau)\phi_j(\tau)\phi_i(t)\right| \mathrm{d}\tau \mathrm{d}t \\
&\leq C \left(h_t^{\ell_t}\right)^{-\frac{1}{2}} \eta^{p+1} \int_{t=ih_t}^{(i+1)h_t} \int_{\tau=jh_t}^{(j+1)h_t} \left|\phi_j(\tau)\phi_i(t)\right| \mathrm{d}\tau \mathrm{d}t \\
&\leq C \eta^{p+1} h_t^{\frac{3}{2}} \|\phi_j\|_{L_2} \|\phi_i\|_{L_2} ,
\end{aligned}$$

which trivialy holds for the nearfield, too. Claiming $\mathcal{O}(\eta^{p+1} h_t^{\frac{3}{2}}) = \mathcal{O}(h_t^{\sigma_t})$ we get

$$p = \mathcal{O}\left(\left(\sigma_t - \frac{3}{2}\right) \frac{\log(1/h_t)}{\log(1/\eta)}\right) = \mathcal{O}(\log N_t) ,$$

which concludes the proof. □

4.3.2 Temporal Multi-Level Structure

Lemma 4.2 tells us how to establish a temporal multilevel structure similar to a classic one-dimensional multilevel FMM. However, we additionally incorporate the causality of the Volterra type integral operator in time by only regarding clusters from the past within the neighbor and interaction lists.

Definition 4.4. *From Definition 4.1, Lemma 4.1 and causality of the kernel it follows that each cluster has the following neighbor list, which is all clusters of the same level sharing at least one point*

$$\mathfrak{N}(I_m^{\ell_t}) = \begin{cases} \{m\} & m = 0 \\ \{m-1, m\} & m > 0 \end{cases}$$

and interaction list

$$\mathfrak{I}(I_m^{\ell_t}) = \bigcup_{n \in \mathfrak{N}\left(I_{\lfloor m/2 \rfloor}^{\ell_t - 1}\right)} \bigcup_{k \in \left\{\mathfrak{C}\left(I_n^{\ell_t - 1}\right) : I_k^{\ell_t} \cap I_m^{\ell_t} = \emptyset\right\}} I_k^{\ell_t} \tag{4.21}$$

containing all parent's neighbors children that are not neighbors of the cluster itself.

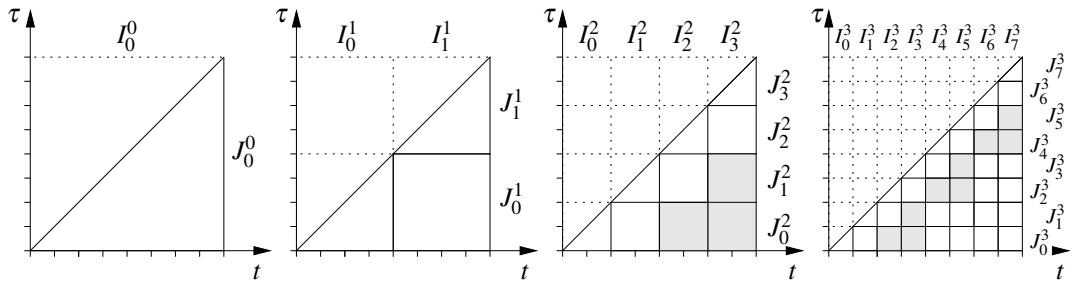

Figure 4.6: Illustration of $\mathfrak{I}(I_m^{\ell_t})$ in gray with $\eta \in (0.5, 1)$.

4.3.3 The Causal FMM

We use the interaction lists (4.21) to split the discrete bilinear form (4.17) into a near- and farfield. Assuming that $i \in \mathfrak{P}(I_m^{L_t})$ and $m \geq 2$ we may rewrite (4.17)

$$\sum_{j \in \{\mathfrak{P}(I_m^{L_t}) \cup \mathfrak{P}(I_{m-1}^{L_t}) | j \leq i\}} \langle \mathcal{V}\phi_j, \phi_i \rangle q_j + \sum_{2 \leq \ell_t \leq L_t} \sum_{J_n^{\ell_t} \in \mathfrak{I}(I_{m^{\ell_t}}^{\ell_t})} \sum_{j \in \mathfrak{P}(J_n^{\ell_t})} \langle \mathcal{V}\phi_j, \phi_i \rangle q_j = \langle f, \phi_i \rangle$$

$$\forall i = 0, \ldots N_t - 1 \,, \quad (4.22)$$

where the level ℓ_t parent of $I_m^{L_t}$ has the index $m^{\ell_t} = \lfloor m/2^{L_t - \ell_t} \rfloor$. The first term on the left hand side of (4.22) is the temporal nearfield containing the singularity and the second term is the farfield or smooth part of the layer potential. The nearfield contribution is computed by direct evaluation (see Appendix B), while in the farfield we replace the kernel by a two-variate Lagrange interpolation as described in Subsection 4.2.1. This yields the approximate farfield contribution of a cluster $J_n^{\ell_t}$ to the i^{th} time step

$$\sum_{j \in \mathfrak{P}(J_n^{\ell_t})} \langle \breve{\mathcal{V}}\phi_j, \phi_i \rangle q_j = \sum_{a=0}^{p} \left(\int_{t=ih_t}^{(i+1)h_t} L_a \left(\Phi_{I_{m^{\ell_t}}^{\ell_t}}^{-1}(t) \right) \phi_i(t) \mathrm{d}t \right) \lambda_a^{\ell_t}(I_{m^{\ell_t}}^{\ell_t}) \quad (4.23)$$

with the local expansions

$$\lambda_a^{\ell_t}(I_{m^{\ell_t}}^{\ell_t}) = \sum_{b=0}^{p} V \left(\Phi_{I_m^{\ell_t}}(\omega_a^p) - \Phi_{J_n^{\ell_t}}(\omega_b^p) \right) \mu_b^{\ell_t}(J_n^{\ell_t}) \quad (4.24)$$

and moment expansions

$$\mu_b^{\ell_t}(J_n^{\ell_t}) = \sum_{j \in \mathfrak{P}(J_n^{\ell_t})} \left(\int_{\tau=jh_t}^{(j+1)h_t} L_b \left(\Phi_{J_n^{\ell_t}}^{-1}(\tau) \right) \phi_j(\tau) \mathrm{d}\tau \right) q_j \,. \quad (4.25)$$

We call (4.25) Q2M (source to moment), (4.24) M2L (moment to local) and (4.23) L2P (local to potential) translations. If we collect the contributions of all $I_m^{L_t}$'s parents $\{I_{m^{\ell_t}}^{\ell_t}\}_{\ell_t=2}^{L_t}$ interaction lists according to (4.22), we end up with the cFMM approximated farfield. However, the straight forward way of doing that can be improved in two ways.

First, we neither want to compute moments from scratch in all levels nor convert local expansions to potential contributions in all levels. The following interpolation relation between Lagrange polynomials in the parent and child level

$$L_b(\hat{\tau}^{\ell_t}) = L_b\left(\frac{1}{2}\hat{\tau}^{\ell_t+1} \pm \frac{1}{2}\right) = \sum_{a=0}^{p} \mathfrak{q}_{a,b}^{\pm} L_a(\hat{\tau}^{\ell_t+1}) \,, \quad \mathfrak{q}_{a,b}^{\pm} = L_b\left(\frac{1}{2}\omega_a^p \pm \frac{1}{2}\right)$$

helps us to avoid this by shifting finer level moment expansions to coarser levels. This procedure is called upward path and involves M2M (moment to moment) translations

$$\mu_b^{\ell_t}(J_n^{\ell_t}) = \sum_{j \in \mathfrak{C}(J_n^{\ell_t})} \sum_{a=0}^{p} \mathfrak{q}_{a,b}^{\pm} \mu_a^{\ell_t+1}(J_j^{\ell_t+1}) \tag{4.26}$$

In the very same manner, coarser level local expansions can be shifted to finer levels, which is called downward path and involves L2L (local to local) translations

$$\lambda_a^{\ell_t+1}(I_i^{\ell_t+1}) = \sum_{b=0}^{p} \mathfrak{q}_{a,b}^{\pm} \lambda_b^{\ell_t}(I_m^{\ell_t}) \quad \forall i \in \mathfrak{C}(I_m^{\ell_t}) \,. \tag{4.27}$$

Notice that M2M and L2L are the transposed operators of one another where the directions $(\pm)$ are resolved by the child lists.

Second, the interaction list (4.21) incorporates causality, however, it does not enable forward substitution/elimination of the Toeplitz system, yet. In a classical FMM we would compute all leaf level moment expansions, perform the upward sweep, evaluate all interactions, perform the downward sweep and add the potential contributions of all leaf level local expansions to the directly evaluated nearfield. For a forward elimination we need to be able to compute the whole time history as time progresses. We modify the order in which moments are computed, interactions are evaluated and contributions to the potential are calculated to provide this feature. Moment expansions, interactions and local expansions are computed in the order they are required in a forward substitution (see Algorithm 1). In each time step we evaluate moments, interactions and local expansions up to the last level ℓ_t^*, where the parent $I_{m^{\ell_t}}^{\ell_t}$ of the current leaf level cluster $I_m^{L_t}$ does not change any more. This is sufficient, because everything higher up in the hierarchy does not change and is available from previous steps. The evaluation of the whole ancestry involves the evaluation of one interaction list per level. Since this list is bounded by two, we only need to keep track of two moment expansion vectors in each level at each time. In an attempt to symmetrize the algorithm, we also store two local expansions in each level (see Algorithm 1).

Complexity Due to the equidistant time discretization we have $\dim\left(\mathfrak{P}(J_n^{L_t})\right) = n_t = N_t/2^{L_t}$ time steps in each leaf level cluster. The total number of $2^{L_t+1}-1$ clusters is $\mathcal{O}(N_t)$ thus the number of arithmetic operations of the presented algorithm comes down to $\mathcal{O}(p^2 N_t)$ and is composed by

- 2^{L_t} Q2M/L2P's at $\mathcal{O}(pn_t)$ each, which results in $\mathcal{O}(pN_t)$ work for the computation of all leaf level moment/local expansions.
- $\mathcal{O}(N_t)$ M2M/L2L's of $\mathcal{O}(p^2)$, resulting in a total cost of $\mathcal{O}(p^2 N_t)$ for all M2M/L2L's.
- $\mathcal{O}(p^2 N_t)$ work for all M2L's, since the number of interactions per cluster is bounded by two and the cost of one M2L is $\mathcal{O}(p^2)$.
- $\mathcal{O}(1)$ work for the nearfield.

Since we only changed the order in which expansions are evaluated, the arithmetic work remains the same as in a classical FMM. However, the amount of memory requirement changes drastically, it amounts in $\mathcal{O}(p^2 \log_2 N_t)$ composed by

- $\mathcal{O}(p^2 \log_2 N_t)$ moment/local expansions, since we only need to keep track of two clusters in each level.
- $\mathcal{O}(1)$ for the expansion coefficients of all Q2M/L2P's and M2M/L2L's, due to the uniform time discretization.
- $\mathcal{O}(p^2 \log_2 N_t)$ coefficients for all M2L's, since the number of M2L's in each level is bounded by two.
- $\mathcal{O}(1)$ memory for the nearfield.

We use matrix notation to describe the algorithm in pseudo code. Due to the uniform time discretization we only need the following matrices:

- one $\mathbf{Q2M} = (\mathbf{L2P})^\top \in \mathbb{R}^{(p+1)\times n_t}$ matrix – (4.25) and (4.23)
- one $\mathbf{M2M}^+ = (\mathbf{L2L}^+)^\top \in \mathbb{R}^{(p+1)\times(p+1)}$ matrix – (4.26) and (4.27)
- one $\mathbf{M2M}^- = (\mathbf{L2L}^-)^\top \in \mathbb{R}^{(p+1)\times(p+1)}$ matrix – (4.26) and (4.27)
- two $\mathbf{M2L}(d^{\ell_t}_{m_t^\ell n}) \in \mathbb{R}^{(p+1)\times(p+1)}$ matrices in each level – (4.24)

Algorithm 1: The causal Fast Multipole Method

```
for m = 0 to 2^{L_t} do
    %% find ℓ_t^*, i.e. coarsest level where parents change
    m̄ = m − 1
    for ℓ_t = 2 to L_t − 1 do
        if I^{ℓ_t}_{m^{ℓ_t}} = I^{ℓ_t}_{m̄^{ℓ_t}} then ℓ_t^* = ℓ_t + 1
    end for

    %% compute moments
    m(J^{L_t}_{m−2}) = q2m q(J^{L_t}_{m−2})

    %% upward path
    for ℓ_t = L_t − 1 to ℓ_t^* do
        for j ∈ 𝔠(J^{ℓ_t}_{m^{ℓ_t}−2}) do
            m(J^{ℓ_t}_{m^{ℓ_t}−2}) = m(J^{ℓ_t}_{m^{ℓ_t}−2}) + m2m^{±} m(J_j^{ℓ_t+1})
        end for
    end for

    %% interaction phase
    for ℓ_t = L_t to ℓ_t^* do
        for n ∈ 𝔍(I^{ℓ_t}_{m^{ℓ_t}}) do
            l(I^{ℓ_t}_{m^{ℓ_t}}) = l(I^{ℓ_t}_{m^{ℓ_t}}) + m2l(d^{ℓ_t}_{m^{ℓ_t} n}) m(J_n^{ℓ_t})
        end for
    end for

    %% downward path
    for ℓ_t = ℓ_t^* to L_t − 1 do
        for i ∈ 𝔠(I^{ℓ_t}_{m^{ℓ_t}}) do
            l(I_i^{ℓ_t+1}) = l(I_i^{ℓ_t+1}) + l2l^{±} l(I^{ℓ_t}_{m^{ℓ_t}})
        end for
    end for

    %% evaluate potential
    f^{FF}(I^{L_t}_m) = l2p l(I^{L_t}_m)

    %% add nearfield
    f(I^{L_t}_m) = f^{FF}(I^{L_t}_m) + f^{NF}(I^{L_t}_m)
end for
```

4.4 Thermal Layer Potential at a Fixed Time – Fast Gauss Transform

In an attempt to isolate the spatial aspect of the pFMM algorithm we assume the thermal single layer potential for a fixed variance $\delta := t - \tau > 0$ and end up with a Gauss transform

$$\mathcal{V}q(\mathbf{x}) = \int_\Gamma G(\mathbf{x}-\mathbf{y},\delta)q(\mathbf{y})\mathrm{d}s_\mathbf{y} = \frac{1}{(4\pi\delta)^{\frac{3}{2}}}\int_\Gamma \exp\left(-\frac{|\mathbf{x}-\mathbf{y}|^2}{4\delta}\right)q(\mathbf{y})\mathrm{d}s_\mathbf{y} = f(\mathbf{x})\,. \quad (4.28)$$

This problem is not only interesting from an explanatory point of view but also from a practical one – as a matter of fact we will encounter it again, when dealing with the efficient nearfield evaluation of thermal layer potentials in Section 4.6. Again we are not interested in applying the continuous operator (4.28) but its Galerkin discretized bilinear form according to Subsection 3.1.1

$$\langle \mathcal{V}q_h, w_h\rangle = \langle f, w_h\rangle\,, \quad \forall w_h \in X_{h_x}^{d_{d_x}}(\Gamma)_{h_x}\,, \quad (4.29)$$

which is equivalent to the application of the dense matrix vector product

$$\mathbf{V}\,\mathbf{q} = \mathbf{f}\,,$$

with $V_{k\ell} := \langle \mathcal{V}\varphi_\ell, \varphi_k\rangle$ and $f_k := \langle f, \varphi_k\rangle$. Throughout this section we devote ourselves to reduce this otherwise $\mathcal{O}(N_x^2)$ task to $\mathcal{O}(N_x \log N_x)$ by means of the Fast Gauss Transform [20, 44].

4.4.1 Truncated Chebyshev Expansion

Based on the hierarchical clustering of Γ_{h_x} described in Subsection 4.1.2 we interpolate the heat kernel with $\mathbf{x} \in X_u^{\ell_x}$ and $\mathbf{y} \in Y_v^{\ell_x}$. For this purpose we introduce local variables $\hat{\mathbf{x}}, \hat{\mathbf{y}} \in [-1,1]^3$

$$\mathbf{x} = \Phi_{X_u^{\ell_x}}(\hat{\mathbf{x}}) = \mathbf{c}_{X_u^{\ell_x}} + \hat{\mathbf{x}}h_x^{\ell_x} \quad \text{and} \quad \mathbf{y} = \Phi_{Y_v^{\ell_x}}(\hat{\mathbf{y}}) = \mathbf{c}_{Y_v^{\ell_x}} + \hat{\mathbf{y}}h_x^{\ell_x}\,.$$

Hence we may write the heat kernel in local coordinates

$$G(\mathbf{x}-\mathbf{y},\delta) = G\left(\Phi_{X_u^{\ell_x}}(\hat{\mathbf{x}}) - \Phi_{Y_v^{\ell_x}}(\hat{\mathbf{y}}),\delta\right) = G\left(h_x^{\ell_x}(\mathbf{d}_{uv}^{\ell_x} + \hat{\mathbf{x}} - \hat{\mathbf{y}}),\delta\right)$$

with $\mathbf{d}_{uv}^{\ell_x} = (\mathbf{c}_{X_u^{\ell_x}} - \mathbf{c}_{Y_m^{\ell_x}})/h_x^{\ell_x}$. Remember that the heat kernel naturally separates into a tensor product of three one-dimensional heat kernels (4.1). Hence we start by investigating the Chebyshev expansion of the one-dimensional heat kernel with $\mathbf{x} \in X_u^{\ell_x}$ and $\mathbf{y} \in Y_v^{\ell_x}$

$$\mathcal{S}_\infty^2 G(x_i - y_i,\delta) = \sum_{k,\ell=0}^{\infty} G_{k,\ell}(\delta)T_k\left(\Phi_{X_u^{\ell_x}}^{-1}(x_i)\right)T_\ell\left(\Phi_{Y_v^{\ell_x}}^{-1}(y_i)\right)\,, \quad (4.30)$$

where $\mathcal{S}_\infty^2 = \mathcal{S}_{\infty,x} \circ \mathcal{S}_{\infty,y} \equiv \mathcal{S}_{\infty,y} \circ \mathcal{S}_{\infty,x}$ with the coefficients

$$G_{k,\ell}(\delta) = \frac{\gamma_k \gamma_\ell}{\pi^2} \int_{-1}^{1} \int_{-1}^{1} G\left(\Phi_{X_u^{\ell_x}}(\hat{x}) - \Phi_{Y_v^{\ell_x}}(\hat{y}), \delta\right) T_k(\hat{x}) T_\ell(\hat{y}) w(\hat{x}) w(\hat{y}) \mathrm{d}\hat{x}\mathrm{d}\hat{y} \,. \tag{4.31}$$

Lemma 4.3. *Assume we truncate the Chebyshev expansion* (4.30) *of the one-dimensional heat kernel with fixed variance $\delta > 0$ after $n := k + \ell > q$ terms*

$$\mathcal{S}_q^2 G(x_i - y_i, \delta) = \sum_{n=0}^{q} \sum_{k+\ell=n} G_{k,\ell}(\delta) T_k\left(\Phi_{X_u^{\ell_x}}^{-1}(x_i)\right) T_\ell\left(\Phi_{Y_v^{\ell_x}}^{-1}(y_i)\right) \,,$$

with $\mathbf{x} \in X_u^{\ell_x}$ and $\mathbf{y} \in Y_v^{\ell_x}$ in any two clusters $X_u^{\ell_x}$ and $Y_v^{\ell_x}$, then we can bound the error by

$$\left|(\mathcal{I} - \mathcal{S}_q^2) G(x_i - y_i, \delta)\right| \lesssim \left(\frac{8}{\delta q}\right)^{q/2} \,,$$

where $A \lesssim B$ means that there is a constant $c > 1$ such that $A \leq cB$.

Proof. Since the Chebyshev polynomials are bounded by one, the truncation error of the expansion only depends on the magnitude of the coefficients $G_{k,\ell}(\delta)$. We use the following estimate [45, Lemma 1] that holds for every $a > 1$

$$|G_{k,\ell}(\delta)| \leq \frac{2}{\sqrt{\pi\delta}} \frac{1}{a^n} \exp\left(\frac{4}{\delta}\left(a - \frac{1}{a}\right)^2\right) \,,$$

and minimize it for the optimal one

$$a = \left(\frac{\delta n}{16} + \sqrt{\left(\frac{\delta n}{16}\right)^2 + 1}\right)^{\frac{1}{2}} \,.$$

Thus we get

$$\left|G_{k,\ell}(\delta)\right| \leq \frac{2}{\sqrt{\pi\delta}} \exp\left(-n\kappa\left(\frac{\delta n}{16}\right)\right) \tag{4.32}$$

with

$$\kappa(t) = \frac{1}{2}\log\left(t + \sqrt{t^2+1}\right) - \frac{1}{4t}\left[\left(t + \sqrt{t^2+1}\right)^{\frac{1}{2}} - \left(t + \sqrt{t^2+1}\right)^{-\frac{1}{2}}\right] \,. \tag{4.33}$$

This result allows us to further estimate

$$\begin{aligned}
\left|(\mathcal{I} - \mathcal{S}_q^2) G(x_i - y_i, \delta)\right| &\leq \sum_{n=q+1}^{\infty} \sum_{n=k+\ell} |G_{k,\ell}(\delta)| \\
&\leq \frac{2}{\sqrt{\pi\delta}} \sum_{n=q+1}^{\infty} (n+1) \exp\left(-n\kappa\left(\frac{\delta n}{16}\right)\right) \\
&\leq \frac{2}{\sqrt{\pi\delta}} \sum_{n=q+1}^{\infty} (n+1) b^n
\end{aligned}$$

with $b = \exp(-\kappa(\delta(q+1)/16))$, where the last inequality holds since $\kappa(t)$ is monotonically increasing. Hence with the remainder of a geometric series's derivative we have

$$\left|(\mathcal{I}-\mathcal{S}_q^2)G(x_i-y_i,\delta)\right| \leq \frac{2(q+2)}{\sqrt{\pi\delta}}\left(\frac{b}{1-b}\right)^{q+1},$$

and with $\kappa(t) \to \log(\sqrt{2t})$ for $t \to \infty$ we get the assertion

$$\left|(\mathcal{I}-\mathcal{S}_q^2)G(x_i-y_i,\delta)\right| \leq \frac{2(q+2)}{\sqrt{\pi\delta}}\left(\frac{\delta(q+1)}{8}\right)^{-(q+1)/2}.$$

□

According to Lemma 4.3 we can bound the truncation error for any $\delta > 0$ independently of the spatial variables. We observe that it decays super-exponentially in the sum of the indexes rather than their individual value. Thus we only have to retain coefficients from a triangular index set

$$\mathfrak{S}(\mathcal{S}_q^2) = \{k,\ell : 0 \leq k+\ell \leq q\} =: S_q^2$$

with about half as many coefficients as we would have in the rectangular index set

$$\mathfrak{S}(\mathcal{J}_q^2) = \{k,\ell : 0 \leq k,\ell \leq q\}$$

if we had used the interpolation scheme (4.6). This constant becomes more significant in higher dimensions. Due to the tensor product structure (4.1) the truncated Chebyshev expansion of the three-dimensional Gaussian is given by

$$\mathcal{S}_q^6 G(\mathbf{x}-\mathbf{y},\delta) = \sum_{n=0}^{q}\sum_{|\alpha+\beta|=n} G_{\alpha,\beta}(\delta)T_\alpha\left(\Phi_{X_u^{\ell_x}}^{-1}(\mathbf{x})\right)T_\beta\left(\Phi_{Y_v^{\ell_x}}^{-1}(\mathbf{y})\right) \tag{4.34}$$

with coefficients

$$G_{\alpha,\beta}(\delta) = G_{\alpha_1,\beta_1}(\delta)G_{\alpha_2,\beta_2}(\delta)G_{\alpha_3,\beta_3}(\delta)\,. \tag{4.35}$$

Obviously the cardinality of the index set $\mathfrak{S}(\mathcal{S}_q^6)$ required for the truncated Chebyshev expansion is much less than the cardinality of the index set $\mathfrak{S}(\mathcal{J}_q^6)$ required for the corresponding interpolation approximation, i.e.

$$\#\mathfrak{S}(\mathcal{S}_q^6) = \binom{q+6}{q} \ll (q+1)^6 = \#\mathfrak{S}(\mathcal{J}_q^6)\,.$$

Corollary 4.1. *By construction we can bound the truncation error of the three-dimensional Chebyshev expansion similar to Lemma 4.3. For* $\mathbf{x} \in X_u^{\ell_x}$ *and* $\mathbf{y} \in Y_v^{\ell_x}$ *in any two clusters* $X_u^{\ell_x}$ *and* $Y_v^{\ell_x}$ *we have*

$$\left|(\mathcal{I}-\mathcal{S}_q^6)G(\mathbf{x}-\mathbf{y},\delta)\right| \lesssim \left(\frac{8}{\delta q}\right)^{3q/2}.$$

Proof. We estimate the three-dimensional expansion coefficients (4.35) using (4.32) and the fact that $\kappa(t)$ given in (4.33) is monotonically increasing

$$\begin{aligned}\left|(\mathcal{I}-\mathcal{S}_q^6)G(\mathbf{x}-\mathbf{y},\delta)\right| &\leq \sum_{n=q+1}^{\infty}\sum_{|\alpha+\beta|=n}|G_{\alpha,\beta}(\delta)| \\ &\leq \left(\frac{2}{\sqrt{\pi\delta}}\right)^3 \sum_{n=q+1}^{\infty}\binom{n+5}{n}\exp\left(-3n\kappa\left(\frac{\delta n}{16}\right)\right) \\ &\leq \left(\frac{2}{\sqrt{\pi\delta}}\right)^3 \sum_{n=q+1}^{\infty}\binom{n+5}{n} b^n\end{aligned}$$

with $b = \exp(-3\kappa(\delta(q+1)/16))$. Estimating the remainder of a geometric series's fifth derivative we get

$$\left|(\mathcal{I}-\mathcal{S}_q^6)G(\mathbf{x}-\mathbf{y},\delta)\right| \leq \left(\frac{2}{\sqrt{\pi\delta}}\right)^3 \binom{q+6}{q+1}\left(\frac{b}{1-b}\right)^{q+1}$$

and with $\kappa(t) \to \log(\sqrt{2t})$ for $t \to \infty$ we obtain the assertion

$$\left|(\mathcal{I}-\mathcal{S}_q^6)G(\mathbf{x}-\mathbf{y},\delta)\right| \leq \left(\frac{2}{\sqrt{\pi\delta}}\right)^3 \binom{q+6}{q+1}\left(\frac{\delta(q+1)}{8}\right)^{-3(q+1)/2}.$$

□

After we have estimated the truncation error for the Chebyshev expansion of the heat kernel itself, we still need to estimate the truncation error for its derivatives.

Corollary 4.2. *Let us assume $\delta > 0$ and $\mathbf{x} \in X_u^{\ell_x}$ and $\mathbf{y} \in Y_v^{\ell_x}$ in any two clusters $X_u^{\ell_x}$ and $Y_v^{\ell_x}$, then we can bound the truncation error related to the Chebyshev expansion of the heat kernel's gradient by*

$$|(\mathcal{I}-\mathcal{S}_q^6)\nabla_{\mathbf{x}}G(\mathbf{x}-\mathbf{y},\delta)| \lesssim \left(\frac{1}{h_x^{\ell_x}}\right)^3\left(\frac{8}{\delta q}\right)^{3q/2}.$$

Proof. Remember that for $\delta > 0$ the heat kernel is analytic thus we can expand it in a Chebyshev series for any $\mathbf{x} \in X_u^{\ell_x}$ and $\mathbf{y} \in Y_v^{\ell_x}$ and we have due to (4.14)

$$\begin{aligned}\mathcal{S}_q^6\nabla_{\mathbf{x}}G(\mathbf{x}-\mathbf{y},\delta) &= \nabla_{\mathbf{x}}\mathcal{S}_q^6 G(\mathbf{x}-\mathbf{y},\delta) \\ &= \sum_{n=0}^{q}\sum_{|\alpha+\beta|=n} G_{\alpha,\beta}(\delta)\nabla_{\mathbf{x}}T_\alpha\left(\Phi_{X_u^{\ell_x}}^{-1}(\mathbf{x})\right)T_\beta\left(\Phi_{Y_v^{\ell_x}}^{-1}(\mathbf{y})\right).\end{aligned}$$

Observe that the gradient of the first kind Chebyshev polynomials (4.15) is not bounded by one any more. However, simple calculus shows that

$$\max_{\hat{x}\in[-1,1]} \frac{\partial}{\partial \hat{x}} T_n(\hat{x}) = nU_{n-1}(\pm 1) = n^2$$

and, therefore,

$$\nabla_{\mathbf{x}} T_\alpha \left(\Phi^{-1}_{X_u^{\ell_x}}(\mathbf{x}) \right) \leq \frac{|\alpha^2|}{\det(\mathbf{J}_\Phi(\mathbf{x}))} \leq \frac{3(q+1)^2}{(h_x^{\ell_x})^3}$$

and the assertion follows from

$$\left| (\mathcal{I} - \mathcal{S}_q^6) \nabla_{\mathbf{x}} G(\mathbf{x}-\mathbf{y},\delta) \right| \leq \sum_{n=q+1}^{\infty} \sum_{|\alpha+\beta|=n} \left| G_{\alpha,\beta}(\delta) \right| \left| \nabla_{\mathbf{x}} T_\alpha \left(\Phi^{-1}_{X_u^{\ell_x}}(\mathbf{x}) \right) \right| .$$

□

Corollary 4.1 and 4.2 show the super-exponential convergence of the truncated Chebyshev expansion of the heat kernel and its derivatives, respectively. We use these results to show how the truncation parameter q has to be chosen in order to maintain the properties of the Galerkin discretization.

Lemma 4.4. *Assume we approximate the discrete Galerkin bilinear form* (4.29) *replacing the heat kernel by its truncated Chebyshev expansion* (4.34)*. If we choose the truncation parameter $q = \mathcal{O}(\log N_x)$ then we obtain a point-wise approximation error for $k \in \mathfrak{P}(X_u^{\ell_x})$ and $\ell \in \mathfrak{P}(Y_v^{\ell_x})$ of order σ_x*

$$\left| \langle \mathcal{V}\varphi_\ell, \varphi_k \rangle - \langle \check{\mathcal{V}}\varphi_\ell, \varphi_k \rangle \right| \leq C h_x^{\sigma_x} \|\varphi_k\|_{L_2} \|\varphi_\ell\|_{L_2} .$$

Proof. We estimate

$$\begin{aligned}
\left| \langle \mathcal{V}\varphi_\ell, \varphi_k \rangle - \langle \check{\mathcal{V}}\varphi_\ell, \varphi_k \rangle \right| &= \int_{\mathrm{supp}(\varphi_k)} \int_{\mathrm{supp}(\varphi_\ell)} \left| (\mathcal{I} - \mathcal{S}_q^6) G(\mathbf{x}-\mathbf{y},\delta) \varphi_\ell(\mathbf{y}) \varphi_k(\mathbf{x}) \right| \mathrm{d}s_{\mathbf{y}} \mathrm{d}s_{\mathbf{x}} \\
&\leq C \left(\frac{8}{\delta q} \right)^{3q/2} \frac{1}{h_x^3} \int_{\mathrm{supp}(\varphi_k)} \int_{\mathrm{supp}(\varphi_\ell)} |\varphi_\ell(\mathbf{y}) \varphi_k(\mathbf{x})| \, \mathrm{d}s_{\mathbf{y}} \mathrm{d}s_{\mathbf{x}} \\
&\leq C \left(\frac{8}{\delta q} \right)^{3q/2} h_x \|\varphi_k\|_{L_2} \|\varphi_\ell\|_{L_2}
\end{aligned}$$

and, with the observation that the choice $q = \mathcal{O}(\log N_x)$ is more than sufficient to guarantee $(8/(\delta q))^{3q/2} = \mathcal{O}(h_x^{\sigma_x - 1})$, we conclude the proof. □

4.4.2 Spatial Single-Level Structure

Corollaries 4.1 and 4.2 give us a bound for the truncation error of the three-dimensional Chebyshev expansion independent of the spatial variable. Due to the exponential decay of the heat kernel for $|\mathbf{x}-\mathbf{y}| \to \infty$ and the space-time scaling (4.2) we can derive an admissibility criterion that allows to control the approximation error for any fixed variance $\delta > 0$ by taking an almost constant number of cluster interactions in one and only one level into consideration.

Lemma 4.5. *Let us assume $\delta > 0$, then we choose the spatial cluster level ℓ_x according to Definition 4.2 such that $h_x^{\ell_x} = C\sqrt{\delta}$. Taking only cluster interactions between two clusters $X_u^{\ell_x}$ and $Y_v^{\ell_x}$ into account that are separated by less or equal than*

$$n_x = \frac{1}{C}\left[\log\left(\frac{1}{\varepsilon}\right) + \frac{3}{2}\log\left(\frac{1}{4\pi\delta}\right)\right]^{\frac{1}{2}}$$

clusters, we can approximate the Gauss transformation in (4.28) *by*

$$\mathcal{V}_{B(\mathbf{x})}q(\mathbf{x},t) := \int\limits_{\{\mathbf{y}\in\Gamma:\|\mathbf{x}-\mathbf{y}\|_\infty \le 2h_x^{\ell_x} n_x\}} G(\mathbf{x}-\mathbf{y},\delta)q(\mathbf{y})ds_{\mathbf{y}}$$

which leads to a cut-off error of

$$|\mathcal{V}q(\mathbf{x},t) - \mathcal{V}_{B(\mathbf{x})}q(\mathbf{x},t)| \le \varepsilon\|q(\mathbf{x})\|_{L_1(\Gamma)} .$$

Proof. With a separation of n_x clusters in the $\|\cdot\|_\infty$ norm, the estimate directly follows

$$\begin{aligned}
|\mathcal{V}_{B(\mathbf{x})}q(\mathbf{x},t) - \mathcal{V}q(\mathbf{x},t)| &\le \int\limits_{\{\mathbf{y}\in\Gamma:\|\mathbf{x}-\mathbf{y}\|_\infty \ge 2h_x^{\ell_x} n_x\}} |G(\mathbf{x}-\mathbf{y},\delta)q(\mathbf{y})|\mathrm{d}s_{\mathbf{y}} \\
&\le \max_{\|\mathbf{x}-\mathbf{y}\|_\infty \ge 2h_x^{\ell_x} n_x} |G(\mathbf{x}-\mathbf{y},\delta)| \int\limits_\Gamma |q(\mathbf{y})|\mathrm{d}s_{\mathbf{y}} \\
&= \varepsilon \int\limits_\Gamma |q(\mathbf{y})|\mathrm{d}s_{\mathbf{y}} .
\end{aligned}$$

□

Provided a fixed variance $\delta > 0$ Lemma 4.5 helps us to choose the right spatial cluster half-side length $h_x^{\ell_x}$ and cut-off parameter n_x. It constitutes an admissibility criterion that allows us to define the FGT's interaction lists.

Definition 4.5. *Choose L_x such that $2^{-L_x}h_x^0 \ge h_x^{\ell_x} \ge 2^{-(L_x+1)}h_x^0$ with $h_x^{\ell_x} = C\sqrt{\delta}$ to ensure that the estimate of Lemma 4.5 still holds. Then the interaction list for the FGT is given by*

$$\mathfrak{I}(X_u^{L_x}) = \bigcup_{Y_v^{L_x}:\|\mathbf{d}_{uv}^{L_x}\|_\infty \le 2(n_x+1)} v . \tag{4.36}$$

4.4.3 The Fast Gauss Transform

The structure of the Fast Gauss transform is very simple. We choose the spatial level L_x according to Lemma 4.5 and the interaction list as proposed in (4.36). Assuming that $k \in \mathfrak{P}(X_u^{L_x})$ we write the discrete bilinear form (4.29) for $\varphi_k(\mathbf{x})$ with $\mathrm{supp}\,(\varphi_k(\mathbf{x})) \subset X_u^{L_x}$

$$\sum_{Y_v^{L_x} \in \mathfrak{I}(X_u^{L_x})} \sum_{\ell \in \mathfrak{P}(Y_v^{L_x})} \langle \mathcal{V}_{B(\mathbf{x})} \varphi_\ell, \varphi_k \rangle q_\ell = \langle f, \varphi_k \rangle \ .$$

Next we replace the heat kernel by its truncated Chebyshev expansion (4.34), which separates the variables. Thus we get φ_ℓ with $\ell \in \mathfrak{P}(Y_v^{L_x})$ contributions to the Galerkin bilinear form tested with φ_k through L2P translations

$$\sum_{\ell \in \mathfrak{P}(Y_v^{L_x})} \langle \breve{\mathcal{V}}_{B(\mathbf{x})} \varphi_\ell, \varphi_k \rangle q_\ell = \sum_{|\alpha|=0}^{q} \int_{\mathrm{supp}(\varphi_k)} T_\alpha \left(\Phi^{-1}_{X_u^{L_x}}(\mathbf{x}) \right) \varphi_k(\mathbf{x}) \mathrm{d}s_{\mathbf{x}} \, \lambda_\alpha(X_u^{L_x}) \ , \tag{4.37}$$

local expansions λ_α via M2L translations

$$\lambda_\alpha(X_u^{L_x}) = \sum_{|\beta|=0}^{q-|\alpha|} G_{\alpha,\beta}(\delta) \mu_\beta(Y_v^{L_x}) \tag{4.38}$$

and moment expansions μ_α via Q2M translations

$$\mu_\beta(Y_v^{L_x}) = \sum_{\ell \in \mathfrak{P}(Y_v^{L_x})} \int_{\mathrm{supp}(\varphi_\ell)} T_\beta \left(\Phi^{-1}_{Y_v^{L_x}}(\mathbf{y}) \right) \varphi_\ell(\mathbf{y}) \mathrm{d}s_{\mathbf{y}} \, q_\ell \ . \tag{4.39}$$

Furthermore, we observe that such a M2L translation (4.38) does not maintain the Gaussian structure of the heat kernel. This becomes evident when writing out the M2L translation in more detail [44], namely

$$\lambda_{\alpha_1,\alpha_2,\alpha_3}(X_u^{L_x}) = \sum_{\beta_3=0}^{q-|\alpha|} G_{\alpha_3,\beta_3}(\delta) \sum_{\beta_2=0}^{q-|\alpha|-\beta_3} G_{\alpha_2,\beta_2}(\delta) \sum_{\beta_1=0}^{q-|\alpha|-\beta_2-\beta_3} G_{\alpha_1,\beta_1}(\delta) \mu_{\beta_1,\beta_2,\beta_3}(Y_v^{L_x}) \ .$$

Setting $\lambda^{(0)} = \mu(Y_v^{L_x})$ and $\lambda^{(3)} = \lambda(X_u^{L_x})$ we have

$$\begin{aligned}
\lambda^{(1)}_{\alpha_1,\alpha_2,\alpha_3,\beta_2,\beta_3} &= \sum_{\beta_1=0}^{q-|\alpha|-\beta_2-\beta_3} G_{\alpha_1,\beta_1}(\delta) \lambda^{(0)}_{\beta_1,\beta_2,\beta_3} \\
\lambda^{(2)}_{\alpha_1,\alpha_2,\alpha_3,\beta_3} &= \sum_{\beta_2=0}^{q-|\alpha|-\beta_3} G_{\alpha_2,\beta_2}(\delta) \lambda^{(1)}_{\alpha_1,\alpha_2,\alpha_3,\beta_2,\beta_3} \\
\lambda^{(3)}_{\alpha_1,\alpha_2,\alpha_3} &= \sum_{\beta_3=0}^{q-|\alpha|} G_{\alpha_3,\beta_3}(\delta) \lambda^{(2)}_{\alpha_1,\alpha_2,\alpha_3,\beta_3}
\end{aligned}$$

and a close inspection reveals that from the outer to the inner loop we are dealing with three one-dimensional M2L's whose number of terms are $\#\mathfrak{S}(\mathcal{S}_q^5)$, $\#\mathfrak{S}(\mathcal{S}_q^4)$ and $\#\mathfrak{S}(\mathcal{S}_q^3)$, respectively. Since each sum is bounded by $q+1$ terms, this results in a total cost of $\mathcal{O}(q^6)$. Including more terms in each sum

$$\begin{aligned}
\lambda^{(1)}_{\alpha_1,\beta_2,\beta_3} &= \sum_{\beta_1=0}^{q-\beta_2-\beta_3} G_{\alpha_1,\beta_1}(\delta)\lambda^{(0)}_{\beta_1,\beta_2,\beta_3} \\
\lambda^{(2)}_{\alpha_1,\alpha_2,\beta_3} &= \sum_{\beta_2=0}^{q-\alpha_1-\beta_3} G_{\alpha_2,\beta_2}(\delta)\lambda^{(1)}_{\alpha_1,\beta_2,\beta_3} \\
\lambda^{(3)}_{\alpha_1,\alpha_2,\alpha_3} &= \sum_{\beta_3=0}^{q-\alpha_1-\alpha_2} G_{\alpha_3,\beta_3}(\delta)\lambda^{(2)}_{\alpha_1,\alpha_2,\beta_3}
\end{aligned}$$

leads to each one-dimensional M2L consisting of $\#\mathfrak{S}(\mathcal{S}_q^3)$ terms only. Hence for a three-dimensional M2L translation of the form

$$\lambda_{\alpha_1,\alpha_2,\alpha_3}(X) = \sum_{\beta_3=0}^{q-\alpha_1-\alpha_2} G_{\alpha_3,\beta_3}(\delta) \sum_{\beta_2=0}^{q-\alpha_1-\beta_3} G_{\alpha_2,\beta_2}(\delta) \sum_{\beta_1=0}^{q-\beta_2-\beta_3} G_{\alpha_1,\beta_1}(\delta)\mu_{\beta_1,\beta_2,\beta_3}(Y)$$

we have reduced the total cost to $3(q+1)\#\mathfrak{S}(\mathcal{S}_q^3) = \mathcal{O}(q^4)$ arithmetic operations.

Remark 4.2. *If we replace the kernel of* (4.28) *by its normal derivative with respect to* $\mathbf{y}$*, we simply shift the derivative to the moment expansions and end up with modified Q2M translations*

$$\mu_\beta(Y_v^{L_x}) = \sum_{\ell\in\mathfrak{P}(Y_v^{L_x})_{supp(\varphi_\ell)}} \int \mathbf{n}_\mathbf{y}{}^\top \nabla_\mathbf{y} T_\beta\left(\Phi^{-1}_{Y_v^{L_x}}(\mathbf{y})\right)\varphi_\ell(\mathbf{y})ds_\mathbf{y}\, q_\ell\ .$$

The same holds true in case the normal derivative is applied with respect to $\mathbf{x}$*, except that then the L2P translations are affected.*

Remark 4.3. *For implementation purpose we find it sufficient to replace the integrals in* (4.31) *by a* q^{th} *order Gauss-Chebyshev quadrature. This way we compute the one-dimensional expansion coefficients for the M2L translations by*

$$G_{k,\ell}(\delta) \approx \frac{\gamma_k\gamma_\ell}{(q+1)^2}\sum_{m,n=0}^{q} G\left(\Phi_{X_u^{\ell_x}}(\omega_m^q) - \Phi_{Y_v^{\ell_x}}(\omega_n^q),\delta\right)T_k(\omega_m^q)T_\ell(\omega_n^q)\ .$$

Algorithm 2: The Fast Gauss Transform

%% compute moments
`for` v `in` $\mathfrak{Y}(L_x)$ `do`
    $\mathbf{m}(Y_v^{L_x}) = \mathbf{Q2M}(Y_v^{L_x})\mathbf{g}(Y_v^{L_x})$
`end for`

%% interaction phase
`for` u `in` $\mathfrak{X}(L_x)$ `do`
    `for` v `in` $\mathfrak{I}(X_u^{L_x})$ `do`
        $\mathbf{l}(X_u^{L_x}) = \mathbf{l}(X_u^{L_x}) + \mathbf{M2L}(\mathbf{d}_{uv}^{L_x})\mathbf{m}(Y_v^{L_x})$
    `end for`
`end for`

%% evaluate potential
`for` u `in` $\mathfrak{X}(L_x)$ `do`
    $\mathbf{f}(X_u^{L_x}) = \mathbf{L2P}(X_u^{L_x})\mathbf{l}(X_u^{L_x})$
`end for`

Complexity Unlike in the causal FMM where we had only a constant number of translation operators due to the uniform time discretization, we need many more translation operators for the FGT since we are dealing with unstructured triangulations Γ_{h_x}. The algorithm requires

- one $\mathbf{Q2M}(Y_v^{L_x}) \in \mathbb{R}^{\#S_q^3 \times \#\mathfrak{P}(Y_v^{L_x})}$ matrix $\forall v \in \mathfrak{X}(L_x)$ and one $\mathbf{L2P}(X_u^{L_x}) \in \mathbb{R}^{\#\mathfrak{P}(X_u^{L_x}) \times \#S_q^3}$ matrix $\forall u \in \mathfrak{Y}(L_x)$.
- $2(n_x+1)+1$ one-dimensional M2Ls $\in \mathbb{R}^{\#S_q^2}$ to define all possible $\mathbf{M2L}(\mathbf{d}_{uv}^{L_x})$.

The arithmetic cost of the algorithm becomes $\mathcal{O}(q^4 N_x \log N_x)$ due to

- a total cost of Q2M/L2P translations is $\mathcal{O}(q^3 N_x)$.
- a cost for one M2L is $\mathcal{O}(q^4)$, the number of M2L's per cluster is $\mathcal{O}(\log N_x)$ and the number of clusters is $\mathcal{O}(N_x)$ which leads to a total cost of $\mathcal{O}(q^4 N_x \log N_x)$.

In terms of storage the algorithm requires $\mathcal{O}(q^3 N_x)$ due to

- $\mathcal{O}(q^3 N_x)$ memory for all Q2M/L2P expansion coefficients.
- $\mathcal{O}(q^2)$ for all M2L expansion coefficients since we only need to store a constant number of one dimensional M2L translation coefficients.

4.5 Thermal Layer Potentials – The Parabolic FMM

In Section 4.3, we have investigated the temporal aspect of thermal layer potentials by itself leading to Volterra integral operators and the causal FMM as an algorithm to enforce their efficient application. In an attempt to isolate the spatial aspect of thermal layer potentials in Section 4.4 we came across what is called the Gauss transform with the Fast Gauss Transform enabling its fast application. Now we are in the nice position to pick those plums and put them together to form the parabolic FMM [43, 45], an almost optimal algorithm to accelerate the application of arbitrary thermal layer potentials. Let us recall the thermal single layer potential as the model potential we use throughout this section

$$\mathcal{V}q(\mathbf{x},t) = f(\mathbf{x},t) \; .$$

Again we are not dealing with the continuous potential, but with its Galerkin discretized bilinear form according to Subsection 3.1.1

$$\langle \mathcal{V}q_h, w_h \rangle = \langle f, w_h \rangle \quad w_h \in S_{h_x,h_t}^{d_{d_x},d_{d_t}}(\Gamma_{h_x} \times \Upsilon) \; . \tag{4.40}$$

4.5.1 Lagrange-Chebyshev Kernel Approximation

Based on the hierarchical space-time clustering of Section 4.1, we want to approximate the heat kernel in a space-time cluster-pair with $\mathbf{x} \in X_u^{\ell_x}$, $\mathbf{y} \in Y_v^{\ell_x}$, $t \in I_m^{\ell_t}$ and $\tau \in J_n^{\ell_t}$. For this purpose we define local coordinates $\hat{\mathbf{x}}, \hat{\mathbf{y}} \in [-1,1]^3$ and $\hat{t}, \hat{\tau} \in [-1,1]$

$$\begin{aligned} \mathbf{x} &= \mathbf{c}_{X_u^{\ell_x}} + \hat{\mathbf{x}} h_x^{\ell_x} \; , \quad \mathbf{y} = \mathbf{c}_{Y_v^{\ell_x}} + \hat{\mathbf{y}} h_x^{\ell_x} \; , \\ t &= c_{I_m^{\ell_t}} + \hat{t} h_t^{\ell_t} \; , \qquad \tau = c_{J_n^{\ell_t}} + \hat{\tau} h_t^{\ell_t} \; . \end{aligned}$$

Now we can write the heat kernel in local coordinates

$$G(\mathbf{x}-\mathbf{y}, t-\tau) = G\left(\Phi_{X_u^{\ell_x}}(\hat{\mathbf{x}}) - \Phi_{Y_v^{\ell_x}}(\hat{\mathbf{y}}), \Phi_{I_m^{\ell_t}}(\hat{t}) - \Phi_{J_n^{\ell_t}}(\hat{\tau}) \right) = G\left(h_x^{\ell_x}(\mathbf{d}_{uv}^{\ell_x} + \hat{\mathbf{x}} - \hat{\mathbf{y}}), h_t^{\ell_t}(d_{mn}^{\ell_t} + \hat{t} - \hat{\tau}) \right)$$

with

$$\mathbf{d}_{uv}^{\ell_x} = \frac{\mathbf{c}_{X_u^{\ell_x}} - \mathbf{c}_{Y_m^{\ell_x}}}{h_x^{\ell_x}} \quad \text{and} \quad d_{mn}^{\ell_t} = \frac{c_{I_m^{\ell_t}} - c_{J_n^{\ell_t}}}{h_t^{\ell_t}} \; .$$

Lagrange Interpolation in Time. We use Lagrange interpolation for the temporal approximation of the heat kernel, because it conserves its spatial Gaussian structure, which otherwise would be destroyed by a Chebyshev expansion. Hence we end up with the time interpolated heat kernel

$$\mathcal{J}_p^2 G(\mathbf{x}-\mathbf{y},t-\tau) = \sum_{a,b=0}^{p} G\left(\mathbf{x}-\mathbf{y}, \Phi_{I_m^{\ell_t}}(\omega_a^p) - \Phi_{J_n^{\ell_t}}(\omega_b^p)\right) \times L_a\left(\Phi_{I_m^{\ell_t}}^{-1}(t)\right) L_b\left(\Phi_{J_n^{\ell_t}}^{-1}(\tau)\right) . \quad (4.41)$$

By the same argument as used in proof of Lemma 4.1 one can show that the heat kernel satisfies the temporal smoothness condition for $t-\tau > 0$

$$\frac{|D_t^i D_\tau^j G(\mathbf{x}-\mathbf{y},t-\tau)|}{i!\,j!} \leq \frac{c\,(i+j)^{\frac{3}{2}}}{|t-\tau|^{i+j+\frac{3}{2}}} ,$$

which allows to estimate the temporal interpolation error of the heat kernel in the same manner as done in Lemma 4.1

$$|(\mathcal{I}-\mathcal{J}_p^2)G(\mathbf{x}-\mathbf{y},t-\tau)| \leq C\left(h_t^{\ell_t}\right)^{-\frac{3}{2}} \eta^{p+1} . \quad (4.42)$$

Truncated Spatial Chebyshev Expansion of the Time Interpolated Heat Kernel. For the reasons elaborated in Section 4.4 we do not use the same interpolation scheme in space, but expand the spatial variables of the time interpolated heat kernel (4.41) in a truncated Chebyshev series

$$\mathcal{S}_q^6 \mathcal{J}_p^2 G(\mathbf{x}-\mathbf{y},t-\tau) = \sum_{a,b=0}^{p} L_a\left(\Phi_{I_m^{\ell_t}}^{-1}(t)\right) L_b\left(\Phi_{J_n^{\ell_t}}^{-1}(\tau)\right) \times \sum_{|\alpha+\beta|=0}^{q} G_{\alpha,\beta}\left(\Phi_{I_m^{\ell_t}}(\omega_a^p) - \Phi_{J_n^{\ell_t}}(\omega_b^p)\right) T_\alpha\left(\Phi_{X_u^{\ell_x}}^{-1}(\mathbf{x})\right) T_\beta\left(\Phi_{Y_v^{\ell_x}}^{-1}(\mathbf{y})\right) . \quad (4.43)$$

Lemma 4.6. *Assume we choose $t \in I_m^{\ell_t}$ and $\tau \in J_n^{\ell_t}$ to be well separated* (4.18) *and $\mathbf{x} \in X_u^{\ell_x}$ and $\mathbf{y} \in Y_v^{\ell_x}$, then we can bound the error of the Lagrange-Chebyshev approximation* (4.43) *by*

$$\left|(\mathcal{I}-\mathcal{S}_q^6\mathcal{J}_p^2)G(\mathbf{x}-\mathbf{y},t-\tau)\right| \leq C\left(\left(h_t^{\ell_t}\right)^{-\frac{3}{2}}\eta^{p+1} + \left(\frac{4}{(q+1)h_t^{\ell_t}}\right)^{\frac{3(q+1)}{2}}\right) .$$

Proof. In order to get a handle on the approximation error we plug

$$G(\mathbf{x}-\mathbf{y},t-\tau) = \mathcal{J}_p^2 G(\mathbf{x}-\mathbf{y},t-\tau) + (\mathcal{I}-\mathcal{J}_p^2)G(\mathbf{x}-\mathbf{y},t-\tau)$$

into the right hand side of

$$G(\mathbf{x}-\mathbf{y},t-\tau) = \mathcal{S}_q^6 G(\mathbf{x}-\mathbf{y},t-\tau) + (\mathcal{I}-\mathcal{S}_q^6)G(\mathbf{x}-\mathbf{y},t-\tau)$$

and end up with the remainder of the Chebyshev-Lagrange approximation

$$(\mathcal{I}-\mathcal{S}_q^6\mathcal{J}_p^2)G(\mathbf{x}-\mathbf{y},t-\tau) = \left((\mathcal{I}-\mathcal{J}_p^2)+(\mathcal{I}-\mathcal{S}_q^6)\mathcal{J}_p^2\right)G(\mathbf{x}-\mathbf{y},t-\tau)\,.$$

Then we apply the triangle inequality to this expression

$$\left|(\mathcal{I}-\mathcal{S}_q^6\mathcal{J}_p^2)G(\mathbf{x}-\mathbf{y},t-\tau)\right| \le \left|(\mathcal{I}-\mathcal{J}_p^2)G(\mathbf{x}-\mathbf{y},t-\tau)\right| + \left|(\mathcal{I}-\mathcal{S}_q^6)\mathcal{J}_p^2 G(\mathbf{x}-\mathbf{y},t-\tau)\right|\,,$$

and simply estimate the interpolation error using (4.42)

$$\left|(\mathcal{I}-\mathcal{J}_p^2)G(\mathbf{x}-\mathbf{y},t-\tau)\right| \le C'\left(h_t^{\ell_t}\right)^{-\frac{3}{2}}\eta^{p+1}\,.$$

while for the second term we have

$$\begin{aligned}
\left|(\mathcal{I}-\mathcal{S}_q^6)\mathcal{J}_p^2 G(\mathbf{x}-\mathbf{y},t-\tau)\right| &\le \Big|\sum_{a,b=0}^{p}(\mathcal{I}-\mathcal{S}_q^6)G\left(\mathbf{x}-\mathbf{y},\Phi_{I_m^{\ell_t}}(\omega_a^p)-\Phi_{J_n^{\ell_t}}(\omega_b^p)\right)\times \\
&\qquad\qquad L_a\left(\Phi_{I_m^{\ell_t}}^{-1}(t)\right)L_b\left(\Phi_{J_n^{\ell_t}}^{-1}(\tau)\right)\Big| \\
&\le \left|(\mathcal{I}-\mathcal{S}_q^6)G\left(\mathbf{x}-\mathbf{y},2h_t^{\ell_t}\right)\right|\times \\
&\qquad\qquad \left|\sum_{a=0}^{p}L_a\left(\Phi_{I_m^{\ell_t}}^{-1}(t)\right)\right|\left|\sum_{a=0}^{p}L_b\left(\Phi_{J_n^{\ell_t}}^{-1}(\tau)\right)\right| \\
&= \left|(\mathcal{I}-\mathcal{S}_q^6)G\left(\mathbf{x}-\mathbf{y},2h_t^{\ell_t}\right)\right|\,.
\end{aligned}$$

This shows that the truncation error of the time interpolated heat kernel can be bounded by the truncation error of the heat kernel itself via Corollary 4.1

$$\left|(\mathcal{I}-\mathcal{S}_q^6)\mathcal{J}_p^2 G(\mathbf{x}-\mathbf{y},t-\tau)\right| \le C\left(\frac{4}{(q+1)h_t^{\ell_t}}\right)^{3(q+1)/2}\,.$$

□

Lemma 4.6 provides exponential convergence in time and super-exponential convergence in space, hence the same ideas as in Lemma 4.2 and Lemma 4.4 can be used to show that choosing $p=\mathcal{O}(\log N_t)$ and $q=\mathcal{O}(\log N_x)$ are sufficient to maintain the approximation property of the underlying Galerkin scheme

$$\left|\langle\mathcal{V}\phi_j\varphi_\ell,\phi_i\varphi_k\rangle - \langle\breve{\mathcal{V}}\phi_j\varphi_\ell,\phi_i\varphi_k\rangle\right| \le C\left(h_t^{\sigma_t}\|\phi_i\|_{L_2}\|\phi_j\|_{L_2} + h_x^{\sigma_x}\|\varphi_k\|_{L_2}\|\varphi_\ell\|_{L_2}\right)\,. \tag{4.44}$$

4.5.2 The Space-Time Multi-Level Structure

We start by choosing the number n_t of time steps per leaf cluster, which defines the temporal leaf level L_t according to Definition 4.1. Next we us Lemma 4.5, where we set $\delta = 2h_t^{L_t}$, to find the spatial leaf level L_x as stated in Definition 4.2. Finally, we assign a spatial level to each temporal level such that the Lagrange-Chebyshev approximation according to Lemma 4.6 is independent of the respective space-time level combination. Due to the constraint $h_x^{\ell_x} = \mathcal{O}(\sqrt{\delta})$ chosen in Lemma 4.5 and $\delta = \mathcal{O}(h_t^{\ell_t})$ it turns out that we only have to coarsen the spatial level with every other temporal level.

Not very surprisingly the Lagrange-Chebyshev approximation error estimate in Lemma 4.6 dictates that the temporal interaction list of the parabolic FMM must be the same as for the causal FMM described in Subsection 4.3.2. Furthermore, it requires the spatial interaction lists to be identical with the FGT's interaction list in Subsection 4.4.2.

Definition 4.6. *Based on a space-time clustering of $\Gamma_{h_x} \times \Upsilon$ according to Section 4.1 with given spatial- and temporal leaf levels L_x and L_t, we link the spatial level ℓ_x to the temporal level ℓ_t by*

$$\ell_x = max\left(L_x - \left\lfloor \frac{L_t - \ell_t}{2} \right\rfloor, 0\right)$$

and define the space-time interaction lists

$$\mathfrak{I}(X_u^{\ell_x} \times I_m^{\ell_t}) = \mathfrak{I}(X_u^{\ell_x}) \times \mathfrak{I}(I_m^{\ell_t}) \tag{4.45}$$

with $\mathfrak{I}(X_u^{\ell_x})$ and $\mathfrak{I}(I_m^{\ell_t})$ defined in (4.36) *and* (4.21)*, respectively.*

Remark 4.4. *Observe that the spatial interaction list implies a truncation after n_x neighboring clusters. Even though in Lemma 4.5 this cut-off is only described for the kernel of the single layer potential, it holds for all other operators in a similar manner, too.*

4.5.3 The Parabolic Fast Multipole Algorithm

Assuming that $i \in \mathfrak{P}(I_m^{L_t})$ and $m \geq 2$ and $k \in \mathfrak{P}(X_u^{L_x})$ we use the interaction list (4.45) to split the discrete Galerkin bilinear form (4.40) into a near- and farfield

$$\sum_{j \in \{\mathfrak{P}(I_m^{L_t}) \cup \mathfrak{P}(I_{m-1}^{L_t}) | j \leq i\}} \sum_{u \in \mathfrak{X}(L_x)} \sum_{v \in \mathfrak{I}(X_u^{L_x})} \sum_{\ell \in \mathfrak{P}(Y_v^{L_x})} \langle \mathcal{V}\phi_j\varphi_\ell, \phi_i\varphi_k\rangle q_{\ell j} +$$
$$\sum_{2 \leq \ell_t \leq L_t} \sum_{n \in \mathfrak{I}(I_{m^{\ell_t}}^{\ell_t})} \sum_{j \in \mathfrak{P}(J_n^{\ell_t})} \sum_{u \in \mathfrak{X}(\ell_x)} \sum_{v \in \mathfrak{I}(X_u)} \sum_{\ell \in \mathfrak{P}(Y_v^{\ell_x})} \langle \mathcal{V}\phi_j\varphi_\ell, \phi_i\varphi_k\rangle q_{\ell j} = \langle f, \phi_i\varphi_k\rangle \,. \tag{4.46}$$

We call the first term on the left hand side the nearfield and evaluate it directly for the time being. The second expression is the farfield, where we replace the kernel by the Lagrange-Chebyshev approximation (4.43). Since the variables of the approximate kernel separate,

this allows us to compute an approximate farfield contribution of all sources $\varphi_\ell(\mathbf{y}) \times \phi_j(\tau)$ with $\ell \times j \in \mathfrak{P}(Y_v^{\ell_x}) \times \mathfrak{P}(J_n^{\ell_t})$ tested by $\varphi_k(\mathbf{x}) \times \phi_i(t)$ via L2P translation

$$\sum_{j \in \mathfrak{P}(J_n^{\ell_t})} \sum_{\ell \in \mathfrak{P}(Y_v^{\ell_x})} \langle \breve{\mathcal{V}}_{B(\mathbf{x})} \phi_j \varphi_\ell, \phi_i \varphi_k \rangle q_{\ell j} = \sum_{a=0}^{p} \left(\int_{ih_t}^{(i+1)h_t} L_a \left(\Phi^{-1}_{I^{\ell_t}_{m^{\ell_t}}}(t) \right) \phi_i(t) \mathrm{d}t \right) \times \sum_{|\alpha|=0}^{q} \left(\int_{\mathrm{supp}(\varphi_k)} T_\alpha \left(\Phi^{-1}_{X_u^{\ell_x}}(\mathbf{x}) \right) \varphi_k(\mathbf{x}) \mathrm{d}s_{\mathbf{x}} \right) \lambda_{\alpha,a} \left(X_u^{\ell_x} \times I_{m^{\ell_t}}^{\ell_t} \right) . \quad (4.47)$$

Local expansions are computed via M2L translations

$$\lambda_{\alpha,a} \left(X_u^{\ell_x} \times I_{m^{\ell_t}}^{\ell_t} \right) = \sum_{b=0}^{p} \sum_{|\beta|=0}^{q-|\alpha|} G_{\alpha,\beta} \left(\Phi_{I_m^{\ell_t}}(\omega_a^p) - \Phi_{J_n^{\ell_t}}(\omega_b^p) \right) \mu_{\beta,b} \left(Y_v^{\ell_x} \times J_n^{\ell_t} \right) \quad (4.48)$$

and moment expansions through Q2M translations

$$\mu_{\beta,b} \left(Y_v^{\ell_x} \times J_n^{\ell_t} \right) = \sum_{j \in \mathfrak{P}(J_n^{\ell_t})} \sum_{\ell \in \mathfrak{P}(Y_v^{\ell_x})} \left(\int_{jh_t}^{(j+1)h_t} L_b \left(\Phi^{-1}_{J_n^{\ell_t}}(t) \right) \phi_j(\tau) \mathrm{d}\tau \right) \times \left(\int_{\mathrm{supp}(\varphi_\ell)} T_\beta \left(\Phi^{-1}_{Y_v^{\ell_x}}(\mathbf{y}) \right) \varphi_\ell(\mathbf{y}) \mathrm{d}s_{\mathbf{y}} \right) q_{\ell j} . \quad (4.49)$$

Similar to the causal FMM we do not want to compute moment expansions nor evaluate local expansions in all levels directly, as an evaluation of the farfield as presented above would require. Therefore, we introduce M2M translations that allow the computation of space-time moment expansions in coarser space-time combinations from finer levels and vice-versa for local expansions via L2L translations. We observe that there are two kinds of M2M/L2L required. Due to the fact that the spatial level only changes with every other temporal level, we need M2M/L2L translations that shift expansions only between temporal levels, they are identical with the temporal M2M/L2L translation operators (4.26) and (4.27), respectively. In case the spatial level also changes, we have to enrich those translation operators with the capability to shift the moment expansions between spatial levels, too. Since the multi-dimensional Chebyshev expansion is based on a Gaussian structure, we will use the discrete orthogonality of the Chebyshev polynomials to formulate the multi-dimensional translation operators. Due to the cluster extension described in Definition 4.3 we may write a Chebyshev polynomials in the parent level in terms of the Chebyshev polynomials in the child level

$$T_\ell(\hat{x}^{\ell_x}) = T_\ell \left(\frac{\bar{h}_x^{\ell_x+1}}{\bar{h}_x^{\ell_x}} \hat{x}^{\ell_x+1} \pm \left(1 - \frac{\bar{h}_x^{\ell_x+1}}{\bar{h}_x^{\ell_x}} \right) \right) = \sum_{k=0}^{\ell} \mathfrak{a}_{k,\ell}^{\ell_x \pm} T_k(\hat{x}^{\ell_x+1}) ,$$

where we have

$$\mathfrak{a}_{k,\ell}^{\pm\ell_x} = \frac{\gamma_k}{\pi}\int_{-1}^{1} T_\ell\left(\frac{\bar{h}_x^{\ell_x+1}}{\bar{h}_x^{\ell_x}}\hat{x} \pm \left(1-\frac{\bar{h}_x^{\ell_x+1}}{\bar{h}_x^{\ell_x}}\right)\right) T_k(\hat{x})w(\hat{x})\mathrm{d}\hat{x}$$
$$= \frac{\gamma_k}{q+1}\sum_{n=0}^{q} T_\ell\left(\frac{\bar{h}_x^{\ell_x+1}}{\bar{h}_x^{\ell_x}}\omega_n^q \pm \left(1-\frac{\bar{h}_x^{\ell_x+1}}{\bar{h}_x^{\ell_x}}\right)\right) T_k(\omega_n^q)$$

due to orthogonality (4.9). The second equality holds since $k \le \ell \le q$, which allows to compute the integral exactly by a q^{th} order Gauss Chebyshev quadrature rule. It is easily seen that

$$T_\beta(\hat{\mathbf{x}}^{\ell_x}) = \sum_{\alpha=0}^{q} \mathfrak{a}_{\alpha,\beta}^{\ell_x\pm} T_\alpha(\hat{\mathbf{x}}^{\ell_x+1})$$

and hence a space-time M2M translation is given by

$$\mu_{\beta,b}(Y_v^{\ell_x}\times J_n^{\ell_t}) = \sum_{j\in\mathfrak{C}(J_n^{\ell_t})}\sum_{\ell\in\mathfrak{C}(Y_v^{\ell_x})}\sum_{a=0}^{p}\mathfrak{q}_{a,b}^{\pm}\sum_{\alpha=0}^{q}\mathfrak{a}_{\alpha,\beta}^{\ell_x\pm}\mu_{\alpha,a}(Y_\ell^{\ell_x+1}\times J_j^{\ell_t+1}) \tag{4.50}$$

where spatial directions are resolved by the child lists. In order to understand what exactly happens here, we write out the inner most sum in more detail, where we set $\mu_\alpha^{(0)} = \mu_{\alpha,a}(Y^{\ell_x+1}\times J_{2n}^{\ell_t+1})$ and $\mu_\beta^{(3)} = \mu_{\beta,a}(Y_v^{\ell_x}\times J_{2n}^{\ell_t+1})$ and neglect the direction $\pm$ and level dependence ℓ_x for sake of clarity. Thus we get

$$\mu_{\beta_1,\beta_2,\beta_3}^{(3)} = \sum_{\alpha_3=0}^{q}\mathfrak{a}_{\alpha_3,\beta_3}\sum_{\alpha_2=0}^{q}\mathfrak{a}_{\alpha_2,\beta_2}\sum_{\alpha_1=0}^{q}\mathfrak{a}_{\alpha_1,\beta_1}\mu_{\alpha_1,\alpha_2,\alpha_3}^{(0)}$$

what entangles into three one-dimensional M2M's

$$\mu_{\beta_1,\alpha_2,\alpha_3}^{(1)} = \sum_{\alpha_1=0}^{q}\mathfrak{a}_{\alpha_1,\beta_1}\mu_{\alpha_1,\alpha_2,\alpha_3}^{(0)}$$
$$\mu_{\beta_1,\beta_2,\alpha_3}^{(2)} = \sum_{\alpha_2=0}^{q}\mathfrak{a}_{\alpha_2,\beta_2}\mu_{\beta_1,\alpha_2,\alpha_3}^{(1)}$$
$$\mu_{\beta_1,\beta_2,\beta_3}^{(3)} = \sum_{\alpha_2=0}^{q}\mathfrak{a}_{\alpha_3,\beta_3}\mu_{\beta_1,\beta_2,\alpha_3}^{(2)}$$

adding up to $3(q+1)\#S_q^3 = \mathcal{O}(q^4)$. Since the number of possible children in space and time is bounded this leads to $\mathcal{O}(p^2q^4)$ for the space-time M2M translation in (4.50). On the other hand, if the spatial level remains the same, the M2M translation simplifies to

$$\mu_{\beta,b}(Y_v^{\ell_x}\times J_n^{\ell_t}) = \sum_{j\in\mathfrak{C}(J_n^{\ell_t})}\sum_{a=0}^{p}\mathfrak{q}_{a,b}^{\pm}\mu_{\alpha,a}(Y_v^{\ell_x}\times J_j^{\ell_t+1})$$

with reduced complexity of $\mathcal{O}(p^2q^3)$. In a similar fashion we can shift local expansions from coarser levels to finer levels all the way down to the leaf level, such that we can restrict potential evaluations to this level only. Again we need to distinguish, whether only a time shift is required or a space shift, too. The space-time L2L translations are given by

$$\lambda_{\alpha,a}(X_k^{\ell_x+1} \times I_i^{\ell_t+1}) = \sum_{b=0}^{p} \mathfrak{q}_{a,b}^{-} \sum_{\beta=0}^{q} \mathfrak{a}_{\alpha,\beta}^{\ell_x \pm} \lambda_{\beta,b}(X_v^{\ell_x} \times I_m^{\ell_t}) \quad \forall k \in \mathfrak{C}(X_v^{\ell_x}) \quad \forall i \in \mathfrak{I}(I_m^{\ell_t}) \,. \tag{4.51}$$

The complexity of $\mathcal{O}(p^2q^4)$ for the space-time M2M reduces to $\mathcal{O}(p^2q^3)$ for the pure temporal L2L translation

$$\lambda_{\alpha,a}(X_v^{\ell_x} \times I_i^{\ell_t+1}) = \sum_{b=0}^{p} \mathfrak{q}_{a,b}^{\pm} \lambda_{\beta,b}(X_v^{\ell_x} \times I_m^{\ell_t}) \quad \forall i \in \mathfrak{C}(I_m^{\ell_t}) \,.$$

Complexity Due to fact that we do a FGT at every interpolation-point combination in time, the arithmetic complexity results in $\mathcal{O}(p^2q^4N_tN_x\log N_x)$ composed by

- $\mathcal{O}(pN_t)$ times $\mathcal{O}(q^3N_x)$ for all Q2M/L2P translations.
- $\mathcal{O}(p^2N_t)$ times $\mathcal{O}(q^4N_x)$ for all M2M/L2L translations.
- $\mathcal{O}(p^2N_t)$ times $\mathcal{O}(q^4N_x\log N_x)$ M2L translations.
- $\mathcal{O}(N_x)$ work for the nearfield.

The storage requirement $\mathcal{O}(p^2q^3N_x\log_2 N_t)$ on the other side results from

- $\mathcal{O}(p^2\log_2 N_t)$ times $\mathcal{O}(q^3N_x)$ moment/local expansions.
- $\mathcal{O}(1)$ for all Q2M/L2P and M2M/L2L translation coefficients due to the uniform space-time clustering.
- $\mathcal{O}(p^2\log_2 N_t)$ times $\mathcal{O}(q^2N_x)$ for all M2L translation coefficients.
- $\mathcal{O}(N_x)$ memory for the nearfield.

In the description of the algorithm below the FGT translations are performed inside the cFMM loops. Except of the spatial $\mathbf{M2M}^{\pm}(\ell_x)$ and $\mathbf{L2L}^{\pm}(\ell_x)$ translations defined in (4.50) and (4.51) all matrices are defined in the previous sections.

Algorithm 3: The parabolic Fast Multipole Method

```
for m = 0 to 2^{L_t} do
    %% find ℓ_t, i.e. coarsest level where parents change
    for ℓ_t = 2 to L_t − 1 do
        if I^{ℓ_t}_{m^{ℓ_t}} = I^{ℓ_t}_{(m−1)^{ℓ_t}} then ℓ_t = ℓ_t + 1
    end for

    %% compute moments
    for v ∈ 𝔓(Y_v^{L_x}) do
        m(Y_v^{L_x} × J^{L_t}_{m−2}) = q2m Q2M(Y_v^{L_x}) q(Y_v^{L_x} × J^{L_t}_{m−2})
    end for

    %% upward path
    for ℓ_t = L_t − 1 to ℓ_t do
        for j ∈ 𝔈(J^{ℓ_t}_{m^{ℓ_t}−2}) do
            if ((L_t − ℓ_t)/2)%1 = 0
               for v ∈ 𝔛(ℓ_x) and ℓ ∈ 𝔈(Y_v^{ℓ_t}) do
                   m(Y_v^{ℓ_x} × J^{ℓ_t}_{m^{ℓ_t}−2}) = m(Y_v^{ℓ_x} × J^{ℓ_t}_{m^{ℓ_t}−2}) + m2m^±M2M^±(ℓ_x)m(Y_ℓ^{ℓ_x+1} × J_j^{ℓ_t+1})
               end for
            else
               for v ∈ 𝔛(ℓ_x) do
                   m(Y_v^{ℓ_x} × J^{ℓ_t}_{m^{ℓ_t}−2}) = m(Y_v^{ℓ_x} × J^{ℓ_t}_{m^{ℓ_t}−2}) + m2m^±m(Y_v^{ℓ_x} × J_j^{ℓ_t+1})
               end for
            end if
        end for
    end for

    %% interaction phase
    for ℓ_t = L_t to ℓ_t do
        for n ∈ 𝔍(I^{ℓ_t}_{m^{ℓ_t}}) do
            for u ∈ 𝔛(ℓ_x) and v ∈ 𝔍(X_u^{ℓ_x}) do
                l(X_u × I^{ℓ_t}_{m^{ℓ_t}}) = l(X_u × I^{ℓ_t}_{m^{ℓ_t}}) + m2l(d^{ℓ_t}_{m^{ℓ_t} n})M2L(d^{ℓ_x}_{uv}) m(Y_v^{ℓ_x} × J_n^{ℓ_t})
            end for
        end for
    end for
```

continues ...

Algorithm 3: The parabolic Fast Multipole Method

continue ...

```
%% downward path
for ℓ_t = ℓ_t to L_t − 1 do
    for i ∈ 𝔠(I^{ℓ_t}_{m^{ℓ_t}}) do
        if ((L_t − ℓ_t)/2)%1 = 0
            for u ∈ 𝔛(ℓ_x) and k ∈ 𝔠(X_u^{ℓ_t}) do
                l(X_k^{ℓ_x+1} × I_i^{ℓ_t+1}) = l(X_k^{ℓ_x} × I_i^{ℓ_t+1}) + l2l^± L2L^±(ℓ_x) l(X_u × I^{ℓ_t}_{m^{ℓ_t}})
            end for
        else
            for u ∈ 𝔛(ℓ_x) do
                l(X_u × I_i^{ℓ_t+1}) = l(X_u × I_i^{ℓ_t+1}) + l2l^± l(X_u × I^{ℓ_t}_{m^{ℓ_t}})
            end for
        end if
    end for
end for

%% evaluate potential
for u ∈ 𝔛(L_x) do
    f^{FF}(X_u^{L_x} × I_m^{L_t}) = l2p L2P(X_u^{L_x}) l(X_u^{L_x} × I_m^{L_t})
end for

%% add nearfield
for u ∈ 𝔛(L_x) do
    f(X_u^{L_x} × I_m^{L_t}) = f^{FF}(X_u^{L_x} × I_m^{L_t}) + f^{NF}(X_u^{L_x} × I_m^{L_t})
end for
end for
```

Remark 4.5. *We observe that even though the complexity estimate suggests optimality of the nearfield, there is space for improvement. First of all one can decrease the constant, since there are time steps in the nearfield where the kernel is not singular (that is always the case if $n_t > 1$). Second, we notice that the complexity estimate for the nearfield only holds as long as $h_x = \mathcal{O}(h_t^a)$ with $a \leq \frac{1}{2}$, however in many practical applications this might not be the case. Just imagine an problem, where the spatial resolution of the domain has to be much higher than the temporal one, the same holds true for problems, where the spatial cut-off does not kick in yet. Thus we split the nearfield into the real nearfield and the midfield that is the range where we apply numerical quadrature in combination with the FGT in space to deal with these issues.*

4.6 Acceleration of the Temporal Nearfield

Here we address the observations of Remark 4.5 by the techniques presented in [31], namely we accelerate the application of the parabolic nearfield. We have to give up the interpolation in time, because the well separation condition (4.18) is not satisfied any more. However, as depicted in Figure 4.7 the singularity of the heat kernel (2.9) is only limited to the diagonal $t = \tau$. In a naive way one would just use the explicit kernels expressions of Subsection 3.1.4 to evaluate the whole nearfield directly. However, since these kernels are time integrated versions of the heat kernel they still exhibit exponential decay for $\mathbf{x} - \mathbf{y} \to \infty$. Moreover, for $d > 1$ they are infinitely smooth as stated in Subsection 3.1.4 and, therefore, one could accelerate them by some modified FGT algorithm. Although this strategy sounds promising, the downside of such an approach would be that these time integrated kernels in Subsection 3.1.4 have lost the Gaussian structure (4.1) of the heat kernel, with the consequence that an efficient form of the translation operators as in Subsection 4.4.3 is not possible anymore. Therefore, we resort to a different approach. We apply an efficient quadrature in time, which leaves the structure of the heat kernel unchanged and apply the FGT to accelerate the spatial interactions at each Gauss point.

In Subsection 4.6.1, we provide the appropriate lemmas to control the error, which stems from the Gauss-Legendre quadrature we presented in Subsection 4.6.2 to accelerate the application of all time steps in the temporal nearfield. We start with the time steps where the kernel is regular, then we proceed with those where the kernel is singular (see Figure 4.7). In order for this idea to succeed, we split these time steps into smaller and smaller parts and accelerate those that are far enough away from the singularity. Due to the space-time scaling (4.2) of the heat kernel this temporal localization leads to a spatial localization of the required direct evaluations and thus to an optimal algorithm.

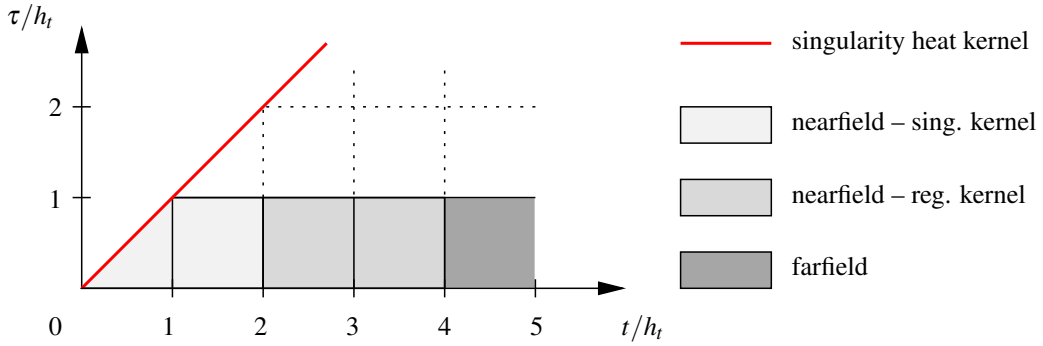

Figure 4.7: Temporal midfield splitting.

4.6.1 Gauss Legendre Quadrature

Estimates of the error of the Gauss-Legendre quadrature applied to functions with analytic extension into the complex plane have been derived in [8]. Unfortunately, the results there assume that either the quadrature order or the region of analyticity are sufficiently large and are thus not directly applicable when these values are specified, as needed in this work. However, the methodology can be modified to derive a similar result which is more suitable for the following discussion.

For a function $f : [-1,1] \to \mathbb{R}$ that has an analytic extension into the complex plane the error E_g of the Gauss-Legendre rule

$$\int_{-1}^{1} f(\xi)\mathrm{d}\xi = \sum_{j=0}^{g-1} f(\xi_j)w_j + E_g(f)$$

can be expressed in terms of an integral over a simply closed contour γ that encloses the interval $[-1,1]$ and is contained in a region of the complex plane where f is analytic

$$E_g(f) = \frac{1}{\pi i}\int_{\gamma} \frac{Q_g(z)}{P_g(z)} f(z)\mathrm{d}z\,. \tag{4.52}$$

with the Legendre function of the second kind

$$Q_g(z) = \frac{1}{2}\int_{-1}^{1} \frac{P_g(\xi)}{z-\xi}\mathrm{d}\xi, \quad z \notin [-1,1].$$

Because of the properties of the Legendre polynomials P_g [13, Section 12.4] it is convenient to let the contour γ be the ellipse ϵ_ρ that is the image of the circle of radius ρ in the complex plane under the transformation $z = \frac{1}{2}(\zeta + \frac{1}{\zeta})$, i.e.

$$\epsilon_\rho = \left\{ \tfrac{1}{2}\left(\zeta + \tfrac{1}{\zeta}\right) \,:\, |\zeta| = \rho \right\}. \tag{4.53}$$

Lemma 4.7. *Let $f(z)$ be analytic in a domain that contains the ellipse ϵ_ρ in* (4.53) *for some $\rho > \sqrt{2}$, then the error of the Gauss-Legendre quadrature can be bounded by*

$$\left|E_g(f)\right| \leq C_0\sqrt{g}\frac{\rho^2}{\rho^2-2}M(\rho)\rho^{-2g}.$$

where $M(\rho) = \max|f(z)|$ on ϵ_ρ and $C_0 = \frac{3\sqrt{\pi}}{2} exp\left(\frac{1}{6}\right) = 3.1408\ldots$.

Proof. It is well known that for $z \in \epsilon_\rho$ (4.53) the Legendre polynomials have the representation [13, Lemma 12.4.1]

$$P_g(z) = \sum_{j=0}^{g} a_{g-j} a_j \zeta^{g-2j} , \quad a_j = \frac{(2j)!}{(j!)^2 4^j} \tag{4.54}$$

with $a_{g-j}a_j \le a_g$ [13, eq. (12.4.5)]. Thus we have

$$P_g(z) = a_g \zeta^g \left(1 + \sum_{j=1}^{g} \frac{a_{g-j}a_j}{a_g} \zeta^{-2j} \right)$$

and with $\rho > \sqrt{2}$

$$\left|P_g(z)\right| \ge a_g \rho^g \left(1 - \sum_{j=1}^{g} \rho^{-2j} \right) \ge a_g \rho^g \frac{\rho^2 - 2}{\rho^2 - 1} .$$

An estimate for the Legendre functions of the second kind is given in [8, eq. (15)]

$$\left|Q_g(z)\right| \le \frac{2\rho}{\rho^2 - 1} \rho^{-g} , \quad z \in \epsilon_\rho .$$

From the contour integral formula (4.52) it follows with the length $\ell(\epsilon_\rho)$ of ϵ_ρ that

$$\left|E_g(f)\right| \le \frac{\ell(\epsilon_\rho)}{\pi} \frac{2}{a_g} \frac{\rho}{\rho^2 - 2} M(\rho) \rho^{-2g} = C_g^\rho \sqrt{g} \frac{\rho^2}{\rho^2 - 2} M(\rho) \rho^{-2g} ,$$

where the factor

$$C_\rho^g = \frac{\ell(\epsilon_\rho)}{\pi\rho} \frac{2}{\sqrt{g} a_g}$$

is uniformly bounded in g and ρ, which can be seen by using Stirling's formula [1] to estimate a_g defined in (4.54)

$$\frac{1}{\sqrt{\pi g}} e^{-\frac{1}{6g}} \le a_g \le \frac{1}{\sqrt{\pi g}} e^{\frac{1}{24g}} , \quad g \ge 1 .$$

The upper bound $C_0 = \frac{3\sqrt{\pi}}{2} \exp\left(\frac{1}{6}\right)$ is derived by elementary arguments. □

Lemma 4.8. *Let $d \ge 3$, $g \ge 1$ and $\sigma(\xi) = a + b\xi$ be a linear function with coefficients $|a| \le 1$ and $|b| \le 1$. Then for $f(\xi) = G(\mathbf{r}, d + \xi)\sigma(\xi)$ the estimate*

$$\left|E_g(f)\right| \le C_1 g^2 d \left(d + \sqrt{d^2 - 1} \right)^{-2g}$$

holds, where $C_1 = \frac{192}{7} C_0$ with $C_0 = \frac{3\sqrt{\pi}}{2} exp\left(\frac{1}{6}\right)$.

Proof. Since $f(\xi)$ has a singularity at $\xi = -d$ we must choose $\rho \in (\sqrt{2}, d+\sqrt{d^2-1})$ for the extension into the complex plane according to Lemma 4.7. To obtain a tight error bound we must minimize $M(\rho)\rho^{-2g}$. We observe that for $z \in \epsilon_\rho$

$$\left|\frac{1}{(d+z)^{\frac{3}{2}}}\right| \exp\left(-\frac{|\mathbf{r}|^2}{d+z}\right) \leq \left(d - \frac{1}{2}\left(\rho + \frac{1}{\rho}\right)\right)^{-\frac{3}{2}}$$

holds for any $\mathbf{r}$. Therefore, it is sufficient to minimize $(d - \frac{1}{2}(\rho + \frac{1}{\rho}))^{-\frac{3}{2}}\rho^{-2g}$ and simple calculus shows that the optimal ρ is $\rho^*(\theta)$

$$\rho^*(\theta) = \frac{d + \sqrt{d^2 - 1 + \theta^2}}{1+\theta}\,, \quad \theta := \tfrac{3}{4g} \in \left[0, \tfrac{3}{4}\right] \subset [0,1]\,.$$

It is easy to see that the function $\rho^*(\theta)$ is monotonically decreasing for positive θ, hence $\rho^*(\theta)$ is in the aforementioned interval of ρ. Moreover, $\rho^*(\theta)$ is concave up thus we have

$$\rho^*(\theta) \geq \left(d + \sqrt{d^2-1}\right)(1-\theta)\,,$$

where the right hand side is the linearization of $\rho^*(\theta)$ at $\theta = 0$, which gives us the estimate

$$(\rho^*(\theta))^{-2g} \leq \left(d+\sqrt{d^2-1}\right)^{-2g}\left(1 - \frac{3}{4g}\right)^{-2g} \leq 16\left(d+\sqrt{d^2-1}\right)^{-2g}\,, \quad g \geq 1\,. \tag{4.55}$$

Since $t \to \frac{1}{2}(t + \frac{1}{t})$ for $t > 1$ and $\rho^*(\theta)$ are concave up, it follows that the composition $\frac{1}{2}(\rho^*(\theta) + \frac{1}{\rho^*(\theta)}) =: d^*(\theta)$ is concave up, too. Thus we have the estimate

$$d^*(\theta) \leq d^*(0) + (d^*(1) - d^*(0))\,\theta = d - \frac{\theta}{2}\left(d - \frac{1}{d}\right)\,,$$

which implies that

$$(d - d^*(\theta))^{-\frac{3}{2}} \leq \theta^{-\frac{3}{2}}\left(\frac{1}{2}\left(d - \frac{1}{d}\right)\right)^{-\frac{3}{2}} = g^{\frac{3}{2}}\left(\frac{3}{8}\left(d - \frac{1}{d}\right)\right)^{-\frac{3}{2}} \leq g^{\frac{3}{2}}\,, \quad d \geq 3\,. \tag{4.56}$$

Furthermore, we have $\rho^*(\theta) > \rho^*(1) = d$ with the estimate

$$\frac{(\rho^*(\theta))^2}{(\rho^*(\theta))^2 - 2} \leq \frac{d^2}{d^2-2} \leq \frac{9}{7}\,, \quad d \geq 3 \tag{4.57}$$

and for $z \in \epsilon_\rho$, $|a| \leq 1$ and $|b| \leq 1$ we also have

$$\begin{aligned} |\sigma(z)| &= |a + bz| \leq 1 + |z| \leq 1 + \frac{1}{2}\left(\rho^*(\theta) + \frac{1}{\rho^*(\theta)}\right) = 1 + d^*(\theta) \\ &\leq 1 + d^*(0) = 1 + d = \left(1 + \frac{1}{d}\right)d \leq \frac{4d}{3}\,, \quad d \geq 3\,. \end{aligned} \tag{4.58}$$

Finally, the assertion follows from Lemma 4.7 and (4.55), (4.56), (4.57) and (4.58). □

4.6.2 Temporal Nearfield Splitting

Since the heat kernel only depends on the difference $t-\tau = (d+\hat{t}-\hat{\tau})h_t$, we define

$$\xi = 2\,(\hat{t}-\hat{\tau})\;, \quad \eta = 2\,(\hat{t}-\hat{\tau}-1)$$

for the transformation of (3.10), which yields

$$V_d(\mathbf{r}) = \begin{cases} \sqrt{\frac{h_t}{8}} \int_{-1}^{1} \int_{-(1-\xi)}^{(1-\xi)} G\left(\mathbf{r}\sqrt{\frac{2}{h_t}}, 2d+1+\xi\right) \mathrm{d}\eta\mathrm{d}\xi & d=0\,, \\ \sqrt{\frac{h_t}{8}} \int_{-1}^{1} \int_{-(1+\xi)}^{(1+\xi)} G\left(\mathbf{r}\sqrt{\frac{2}{h_t}}, 2d-1+\xi\right) \mathrm{d}\eta\mathrm{d}\xi & \\ \quad + \sqrt{\frac{h_t}{8}} \int_{-1}^{1} \int_{-(1-\xi)}^{(1-\xi)} G\left(\mathbf{r}\sqrt{\frac{2}{h_t}}, 2d+1+\xi\right) \mathrm{d}\eta\mathrm{d}\xi & d \geq 1\,. \end{cases}$$

After such a rotation we can perform the inner integration explicitly

$$V_d(\mathbf{r}) = \begin{cases} V_d^+(\mathbf{r}) & d=0\,, \\ V_d^-(\mathbf{r}) + V_d^+(\mathbf{r}) & d \geq 1\,, \end{cases} \tag{4.59}$$

with

$$V_d^{\pm}(\mathbf{r}) = \sqrt{2h_t} \int_{-1}^{1} G\left(\boldsymbol{r}(\mathbf{r}), \mathfrak{d}^{\pm}(d)+\xi\right) \sigma^{\pm}(\xi)\,\mathrm{d}\xi \tag{4.60}$$

and the definitions

$$\boldsymbol{r}(\mathbf{r}) := \mathbf{r}\sqrt{\frac{2}{h_t}}\;, \quad \sigma^{\pm}(\xi) := \frac{1\mp\xi}{2}\;, \quad \mathfrak{d}^{\pm}(d) := 2d\pm 1\;.$$

For $\mathfrak{d}^{\pm}(d) \geq 3$ we observe that the kernel in (4.60) is $C^{\infty}(\mathbb{R}^3 \times [-1,1])$, hence we can apply a Gauss-Legendre quadrature rule of order g

$$V_d^{\pm}(\mathbf{r}) = \sqrt{2h_t} \left\{ \sum_{i=0}^{g-1} G\left(\boldsymbol{r}(\mathbf{r}), \mathfrak{d}^{\pm}(d)+\xi_i\right) \sigma^{\pm}(\xi_i) w_i + E_g^{\pm}\left(\boldsymbol{r}(\mathbf{r}), \mathfrak{d}^{\pm}(d)\right) \right\}\;, \tag{4.61}$$

where $\{\xi_i\}_{i=0}^{g-1}$ and $\{w_i\}_{i=0}^{g-1}$ are the Gauss-Legendre quadrature points and weights, respectively. Note that the quadrature error $E_g^{\pm}$ is bounded by Lemma 4.8 with the largest value obviously occurring at $\mathbf{r}=\mathbf{0}$, which is where we have numerically verified the error by the semi-logarithmic plots in Figure 4.8.

Remark 4.6. *Time integration was performed by Gauss-Legendre quadrature for* $V_d(\mathbf{r})$ *with* $V_d^{\pm}(\mathbf{r})$ *and* $d^{\pm} \geq 3$ *instead of analytic integration as in Subsection 3.1.4. This approach directly translates to* $K_d(\mathbf{r})$, $K'_d(\mathbf{r})$ *and* $D_d(\mathbf{r})$ *simply by exchanging the kernel.*

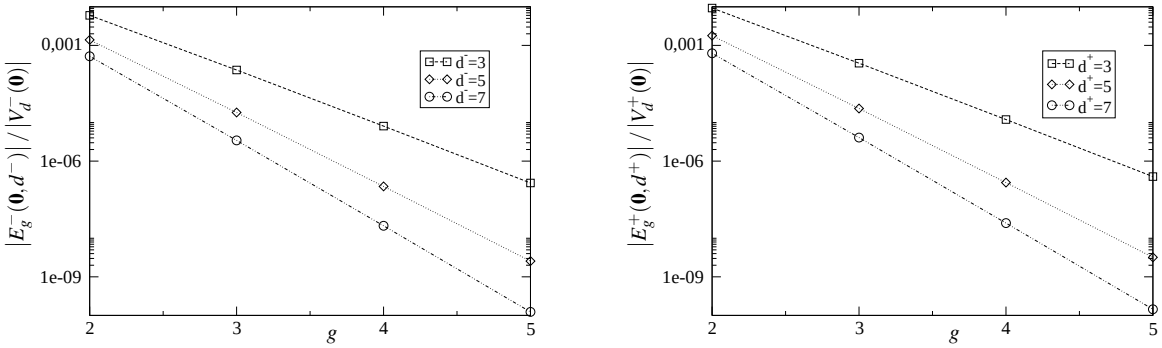

(a) $\left|E_g^-(\mathbf{0},d^-)\right| / \left|V_d^-(\mathbf{0})\right|$ vs. g (b) $\left|E_g^+(\mathbf{0},d^+)\right| / \left|V_d^+(\mathbf{0})\right|$ vs. g

Figure 4.8: Quadrature error at $\boldsymbol{r}(\mathbf{r}) = \mathbf{0}$ vs. quadrature order g.

For $\mathfrak{d}^{\pm}(d) = 1$ the integrands are singular and a composite quadrature rule must be applied. To this end, we introduce a new parameter $0 < \mu < 1$ and consider the following dyadic splitting of the interval

$$[-1,1] = \bigcup_{m=0}^{M} \mathscr{I}_m$$

where

$$\mathscr{I}_M = [-1, 2\mu^M - 1] \quad \text{and} \quad \mathscr{I}_m = \left[2\mu^{m+1} - 1, 2\mu^m - 1\right] , \quad m = 0, \dots M-1 .$$

The kernel $V_d^{\pm}(\mathbf{r})$ with $\mathfrak{d}^{\pm} = 1$ can now be written as a sum of the kernels

$$V_{1,m}^{\pm}(\mathbf{r}) := \sqrt{2h_t} \int_{\mathscr{I}_m} G\left(\mathbf{r}\sqrt{\tfrac{2}{h_t}}, 1+\xi\right) \sigma^{\pm}(\xi)\, \mathrm{d}\xi , \quad m = 0, \dots M .$$

The factor M is selected such that the kernel $V_{1,M}^{\pm}(\mathbf{r})$ is sufficiently local in space and, hence, the layer potentials with this kernel can be evaluated directly with $O(N_x)$ cost because only interactions with n_x neighboring clusters in each direction must be evaluated due to Lemma 4.5. The integrands of the remaining kernels $V_{1,m}^{\pm}(\mathbf{r})$ for $m < M$ are smooth, and approximated by a Gauss-Legendre quadrature rule, similar to (4.61). Transforming $\mathscr{I}_m$ to the standard interval leads to

$$\begin{aligned} V_{1,m}^{\pm}(\mathbf{r}) &= \frac{\sqrt{2h_t}}{\sqrt{\mu^m - \mu^{m+1}}} \int_{-1}^{1} G(\boldsymbol{r}_m(\mathbf{r}), \mathfrak{d} + \xi) \sigma_m^{\pm}(\xi)\, \mathrm{d}\xi \\ &= \frac{\sqrt{2h_t}}{\sqrt{\mu^m - \mu^{m+1}}} \left\{ \sum_{j=0}^{g-1} G(\boldsymbol{r}_m(\mathbf{r}), \mathfrak{d} + \xi_j) \sigma_m^{\pm}(\xi_j) w_j + E_{g,m}^{\pm}(\boldsymbol{r}_m(\mathbf{r}), \mathfrak{d}) \right\} , \end{aligned} \tag{4.62}$$

where

$$\boldsymbol{r}_m(\mathbf{r}) := \mathbf{r}\sqrt{\frac{2}{h_t(\mu^m - \mu^{m+1})}}, \quad \mathfrak{d} := \frac{1+\mu}{1-\mu}$$

and

$$\sigma_m^+(\xi) := 1 - \left(\frac{\mu^m + \mu^{m+1}}{2} + \frac{\mu^m - \mu^{m+1}}{2}\xi\right),$$
$$\sigma_m^-(\xi) := \frac{\mu^m + \mu^{m+1}}{2} + \frac{\mu^m - \mu^{m+1}}{2}\xi .$$

We choose $\mu = 1/2$ leading to $\mathfrak{d} = 3$ to reproduce the same error as for $\mathfrak{d}^{\pm} = 3$, then the error in (4.62) is also bounded by Lemma 4.8. However, we also have to account for the factor $(\mu^m - \mu^{m+1})^{-\frac{1}{2}}$ in (4.62), which we do in Table 4.1 by investigating

$$\sqrt{2h_t}\sum_{m=0}^{M-1}\left(\mu^m - \mu^{m+1}\right)^{-\frac{1}{2}}\left|E_{g,m}^-(\mathbf{0},\mathfrak{d})\right| / \left|V_{1,m}^-(\mathbf{0})\right| , \quad \mu = \tfrac{1}{2} .$$

It is not surprising that the error decays exponentially in g as predicted by Lemma 4.8 and seems to be bounded in M since $\mathcal{O}(d^{-2g})$ from Lemma 4.8 is stronger than the pre-factor's $\mathcal{O}(\mu^m)$.

	$M=1$	$M=4$	$M=7$	$M=10$	$M=13$
$g=2$	9.70×10^{-5}	2.48×10^{-4}	3.02×10^{-4}	3.21×10^{-4}	3.27×10^{-4}
$g=3$	2.42×10^{-6}	6.21×10^{-6}	7.55×10^{-6}	8.02×10^{-6}	8.19×10^{-6}
$g=4$	6.31×10^{-8}	1.61×10^{-7}	1.96×10^{-7}	2.08×10^{-7}	2.13×10^{-7}
$g=5$	1.68×10^{-9}	4.31×10^{-9}	5.24×10^{-9}	5.57×10^{-9}	5.69×10^{-9}

Table 4.1: Quadrature error at $\boldsymbol{r}_m(\mathbf{r}) = \mathbf{0}$ vs. order g and splitting parameter M.

The operators $V_{1,M}^{\pm}(\mathbf{r})$ still need to be evaluated directly, thus to limit their complexity to $\mathcal{O}(N_x)$, only contributions in a neighborhood of radius proportional to h_x should be considered. Since the heat kernel decays in space like $\mathcal{O}(\sqrt{\mu^M h_t})$, as can be seen from (4.2) this leads to

$$M = \mathcal{O}\left(\log_\mu\left(\frac{h_x^2}{h_t}\right)\right) . \tag{4.63}$$

Remark 4.7. *Observe that for $K_{1,m}^{\pm}(\mathbf{r})$, $K'^{\pm}_{1,m}(\mathbf{r})$ and $D_{1,m}^{\pm}(\mathbf{r})$ the same strategy applies, however, the explicit expressions for $V_{1,M}^{\pm}(\mathbf{r})$, $K_{1,M}^{\pm}(\mathbf{r})$, $K'^{\pm}_{1,M}(\mathbf{r})$ and $D_{1,M}^{\pm}(\mathbf{r})$ must be computed separately and can be found in Appendix B. Observe that the hyper-singular bilinear form exhibits the form of* (3.8) *where $V_{1,M}^{\pm}(\mathbf{r})$ can be recycled.*

4.6.3 Spatial Levels for the FGT

From the previous discussion it follows that the kernel $V_d(\mathbf{r})$ can be approximated by some composite of the Gauss-Legendre quadrature rule. We write this as

$$V_d(\mathbf{r}) \approx \begin{cases} \sum_{j=0}^{g-1} G\left(\boldsymbol{r}(\mathbf{r}), \mathfrak{d}^-(d) + \xi_j\right) \mathfrak{w}_j^- + \sum_{j=0}^{g-1} G\left(\boldsymbol{r}(\mathbf{r}), \mathfrak{d}^+(d) + \xi_j\right) \mathfrak{w}_j^+ & d \geq 2\,, \\ V_{0,M}^-(\mathbf{r}) + \sum_{m=0}^{M-1} \sum_{j=0}^{g-1} G\left(\boldsymbol{r}_m(\mathbf{r}), \mathfrak{d} + \xi_j\right) \mathfrak{w}_{j,m}^- & \\ \qquad + \sum_{j=0}^{g-1} G\left(\boldsymbol{r}(\mathbf{r}), 3 + \xi_j\right) \mathfrak{w}_j & d = 1\,, \\ V_{0,M}^+(\mathbf{r}) + \sum_{m=0}^{M-1} \sum_{j=0}^{g-1} G\left(\boldsymbol{r}_m(\mathbf{r}), \mathfrak{d} + \xi_j\right) \mathfrak{w}_{j,m}^+ & d = 0\,. \end{cases}$$

where $\xi_j \in [-1,1]$ are the Gauss points, while $\mathfrak{w}_j^\pm$ and $\mathfrak{w}_{j,m}^\pm$ combine the Gauss weights w_j with the functions $\sigma^\pm(\xi_j)$ and $\sigma_m^\pm(\xi_j)$ and the pre-factors in (4.61) and (4.62), respectively. The layer operators with singular kernels $V_{0,M}^\pm(\mathbf{r})$ are local and evaluated directly, while the kernels $G(\boldsymbol{r}(\mathbf{r}), \mathfrak{d}^\pm + \xi_j)$ and $G(\boldsymbol{r}_m(\mathbf{r}), \mathfrak{d} + \xi_j)$ are Gaussians and evaluated using the FGT. Since the temporal proximity of interactions in these cases is closer than in the parabolic farfield, they have to be computed in a finer spatial levels than the smooth part of the pFMM. Therefore, we introduce uniform refinements above level L_x by simply adding more levels $\mathsf{L}_\mathsf{x} > L_x$ to the spatial cluster-tree in Subsection 4.1.2 and choose the appropriate level for the FGT such that the truncation error of exponential function's argument

$$\frac{|x-y|^2}{\mathfrak{d}} \geq \frac{\left(h_x^{\mathsf{L}_\mathsf{x}}(2n_x)\right)^2}{\mathfrak{d}}$$

is less or equal to the corresponding value for the pFMM

$$\frac{|x-y|^2}{\mathfrak{d}} \geq \frac{1}{2} \frac{\left(h_x^{L_x}(2n_x)\right)^2}{4h_t^{L_t}(d+2)}\,,$$

where the factor $1/2$ is due to Definition 4.6 and the fact that the spatial level only changes with every other temporal level. Thus with $h_t^{L_t} = n_t h_t/2$ due to Definition 4.1 and $d \in \{4,6\}$ due to (4.18) we get

$$\mathsf{L}_\mathsf{x} \leq L_x + \log_4\left(\frac{32 n_t h_t}{\mathfrak{d}}\right). \tag{4.64}$$

By setting

$$\mathfrak{d} = \begin{cases} 4h_t(d+1) & d \geq 1 \\ 4h_t\mu^m & d = 0 \end{cases}$$

as an upper bound in (4.64) for all quadrature nodes we finally get

$$\mathsf{L}_\mathsf{x} = \begin{cases} L_x + \left\lfloor \log_4\left(\frac{8n_t}{d+1}\right)\right\rfloor & d \geq 1\,, \\ L_x + \left\lfloor \log_4\left(\frac{8n_t}{\mu^m}\right)\right\rfloor & d = 0\,. \end{cases} \tag{4.65}$$

5 NUMERICAL EXAMPLES

5.1 Benchmark Tests

We solve some homogeneous initial boundary value problems as described in Section 2.4 for $\Omega = [-0.5, 0.5]^3$ and $t \in \Upsilon = [0, 0.5]$. In all cases we choose the boundary data corresponding to a heat point source $g_D(\mathbf{x},t) = G(\mathbf{x}-\mathbf{x}_0,t)$, $g_N(\mathbf{x},t) = \partial_{\mathbf{n}_\mathbf{x}} G(\mathbf{x}-\mathbf{x}_0,t)$, and $g_R(\mathbf{x},t) = \partial_{\mathbf{n}_\mathbf{x}} G(\mathbf{x}-\mathbf{x}_0,t) + \kappa(\mathbf{x})G(\mathbf{x}-\mathbf{x}_0,t)$ located at $x_0 := (1.5, 1.5, 1.5)^\top$. Since all systems are elliptic, their related Galerkin discretized matrices (sub matrices of the block Töplitz system) turn out to be symmetric and positive definite. Therefore, we use a Conjugate Gradient (CG) solver with a block diagonal preconditioner.

The coarsest discretization of $\Gamma \times \Upsilon$ consists of a uniform mesh with 194 vertices and $N_x = 384$ triangles of mesh-width $h_x = 1/4$. In order to satisfy $h_t = h_x^2$ we subdivide Υ into $N_t = 8$ equidistant time steps of $h_t = 1/16$. With $n_t = 1$ this leads to $L_t = 3$ while we start with the spatial root cluster $L_x = 0$. Thus in the leaf level of our space-time cluster tree we get $h_t^{(3)} = 1/32$ and $h_x^{(0)} = 1/2$. It turns out that we can control the truncation error by neglecting all interactions from spatial cubes further apart than $n_x = 3$ and the interpolation error by choosing the spatial- and temporal expansion orders to be $q = 29$ and $p = 6$, respectively.

5.1.1 Initial Dirichlet BVP

In our first example we solve the pFMM approximated variational form related to the initial Dirichlet boundary value problem (3.16)

$$\langle \check{\mathcal{V}} \bar{q}_h, v_h \rangle_{\Gamma\times\Upsilon} = \langle \big(\tfrac{\mathcal{I}}{2} + \check{\mathcal{K}}\big)\, \bar{g}_D, v_h \rangle_{\Gamma\times\Upsilon} \quad \forall v_h \in S^{d_0,d_0}_{h_x,h_t}(\Gamma\times\Upsilon)$$

for the approximate solution $\bar{q}_h \in S^{d_0,d_0}_{h_x,h_t}(\Gamma\times\Upsilon)$ with the perturbed right hand side $S^{c_1,d_0}_{h_x,h_t}(\Gamma\times\Upsilon) \ni \bar{g}_D = \mathcal{Q}_{h_t}\mathcal{Q}_{h_x} g_D$. Since this benchmark problem is based on the first BIE, we use it as a test case for the single- and double layer operator.

$N_x \backslash N_t$	8	32	128	512
384	$1.47\ 10^{-1}$	$1.23\ 10^{-1}$	$1.21\ 10^{-1}$	$1.20\ 10^{-1}$
1,536	$1.02\ 10^{-1}$	$6.33\ 10^{-2}$	$6.02\ 10^{-2}$	$6.00\ 10^{-2}$
6,144	$8.81\ 10^{-2}$	$3.60\ 10^{-2}$	$3.03\ 10^{-2}$	$2.99\ 10^{-2}$
24,576	$8.42\ 10^{-2}$	$2.52\ 10^{-2}$	$1.58\ 10^{-2}$	$1.50\ 10^{-2}$

Table 5.1: Relative Neumann $L_2(\Gamma \times \Upsilon)$ error.

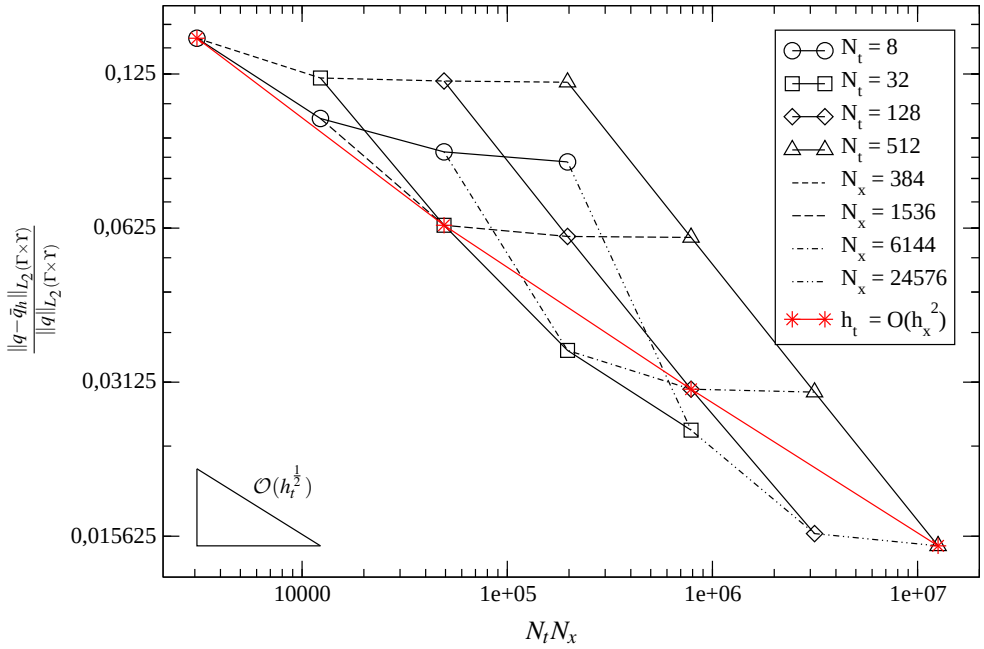

Figure 5.1: Relative Neumann $L_2(\Gamma \times \Upsilon)$ error for various space-time discretizations.

In Table 5.1 and Figure 5.1 we report the relative $L_2(\Gamma \times \Upsilon)$ error for various space-time discretizations. Note that for $h_t = \mathcal{O}(h_x^2)$ we obtain the $\mathcal{O}(\sqrt{h_t})$ behavior provided by Lemma 3.1. While these results match perfectly with the theoretically derived behavior in Subsection 3.2.1, they reveal another interesting fact. Recall that due to the perturbed right hand side and Remark 3.1 we could not reach the optimal convergence rate for the combination $\bar{q}_h \in S^{d_1,d_0}_{h_x,h_t}(\Gamma \times \Upsilon)$ and $h_t = \mathcal{O}(h_x^2)$. Instead we sought $\bar{q}_h \in S^{d_0,d_0}_{h_x,h_t}(\Gamma \times \Upsilon)$ because it yields the same asymptotic behavior as the richer space for $h_t = \mathcal{O}(h_x^2)$. However, the slope of the envelope in Figure 5.1 reveals that for this awkward ansatz space there is a better choice, namely $h_t = \mathcal{O}(h_x^\beta)$ with some $\beta < 2$. Further inspection of Table 5.1 and Figure 5.1 reveals that for a very fine spatial discretization we initially obtain the optimal $\mathcal{O}(h_t)$ behavior of the Galerkin scheme, i.e. in this case the discretization error is completely dominated by the temporal discretization. Of course, keeping one of the dis-

cretization parameters fixed, sooner or later the convergence rate breaks down, because the related contribution to the error remains constant.

In Table 5.2 we present some more details for the discretization parameters on the main diagonal of Table 5.1. Despite the previous argument regarding the awkwardness of $\bar{q}_h \in S^{d_0,d_0}_{h_x,h_t}(\Gamma \times \Upsilon)$ in combination with $h_t = \mathcal{O}(h_x^2)$ these results show that our fast scheme is optimal in the number of total unknowns $N_x N_t$ regardless the space-time refinement scheme. In Table 5.2, Figure 5.2, and Figure 5.3 one may observe that this holds true, both with respect to time and memory consumption. Further, we observe that the block diagonal preconditioner seems to work well, as the number of iterations seems to be independent of the refinement level.

lev.	$N_x N_t$	L_x/L_t	rel. $L_2(\Gamma \times \Upsilon)$	iter.	time[sec]	memory[GB]
0	3,072	0/3	$1.47\ 10^{-1}$	8	$6.12\ 10^{1}$	$1.08\ 10^{-1}$
1	49,152	1/5	$6.33\ 10^{-2}$	8	$2.12\ 10^{2}$	$4.12\ 10^{-1}$
2	786,432	2/7	$3.03\ 10^{-2}$	8	$3.02\ 10^{3}$	$1.65\ 10^{0}$
3	12,582,912	3/9	$1.50\ 10^{-2}$	8	$6.58\ 10^{4}$	$6.99\ 10^{0}$

Table 5.2: Dirichlet IBVP with uniform space-time refinement – $h_t = \mathcal{O}(h_x^2)$.

Finally, in Table 5.3, Figure 5.2, and Figure 5.3 we present more details for a purely spatial refinement, i.e. $h_t = \mathcal{O}(h_x^\beta)$ with $\beta \to 0$. A naive application of the pFMM algorithm for such a scheme leads to non optimal complexity due to the quadratic nearfield growth. The simple explanation for this behavior is that the spatial truncation is linked to the temporal discretization. Since in this case we have a fixed temporal discretization, the number of spatial interactions grows like $\mathcal{O}(N_x^2)$. The composite quadrature rule described in Section 4.6 resolves this problem by localizing spatial contributions (M is the dyadic splitting parameter), which in combination with the FGT leads to an optimal nearfield evaluation in this case as reported in Table 5.3, Figure 5.2, and Figure 5.3. One may wonder why the number of iterations in this case grows compared to the previously described optimal refinement scheme, where only a constant number of iterations was required. Presumably the simple explanation is that due to the dyadic splitting, the information contained in the block-diagonal preconditioner is reduced, which is why it does not work properly any more.

lev.	$N_x N_t$	L_x/L_t	M	rel. $L_2(\Gamma \times \Upsilon)$	iter.	time[sec]	memory[GB]
0	3,072	0/3	0	$1.47\ 10^{-1}$	8	$6.12\ 10^{1}$	$1.08\ 10^{-1}$
1	12,288	0/3	2	$1.02\ 10^{-1}$	11	$1.93\ 10^{2}$	$5.93\ 10^{-1}$
2	49,152	0/3	4	$8.81\ 10^{-1}$	14	$9.11\ 10^{2}$	$2.66\ 10^{0}$
3	196,608	0/3	6	$8.42\ 10^{-1}$	17	$4.41\ 10^{3}$	$1.29\ 10^{1}$

Table 5.3: Dirichlet IBVP with uniform space refinement – $h_t = const$.

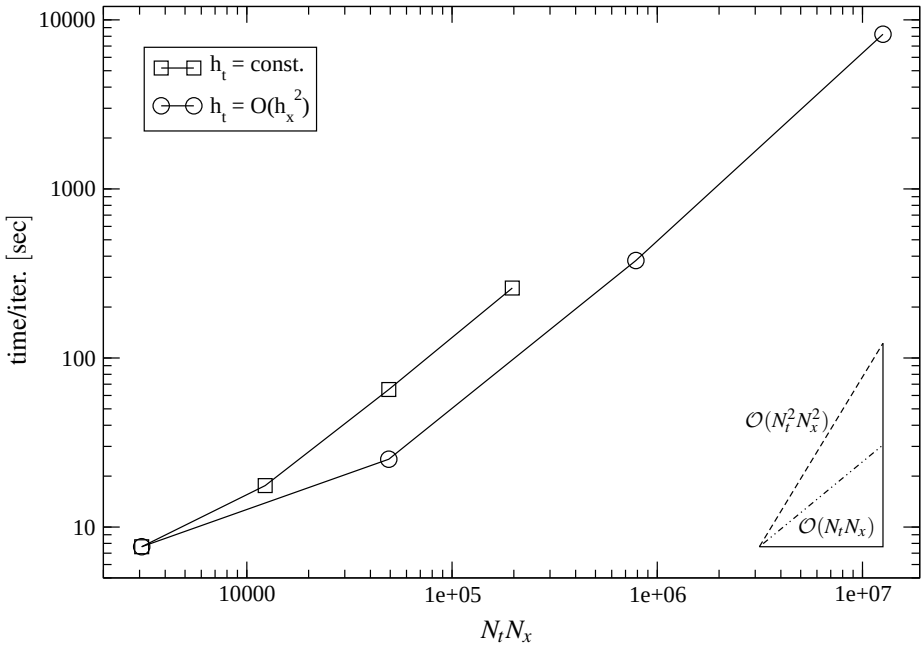

Figure 5.2: Dirichlet IBVP – computational complexity of the pFMM.

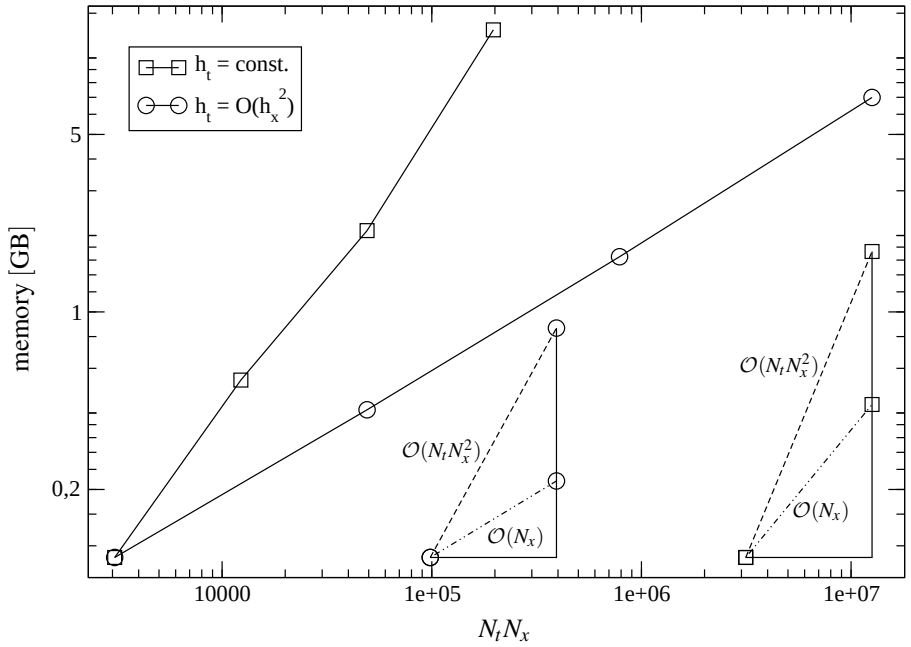

Figure 5.3: Dirichlet IBVP – memory consumption of the pFMM.

5.1.2 Initial Neumann BVP

Next we solve the pFMM approximated variational form related to the initial Neumann boundary value problem (3.20)

$$\langle \breve{\mathcal{D}} \bar{u}_h, w_h \rangle_{\Gamma\times\Upsilon} = \langle \left(\tfrac{\mathcal{I}}{2} - \breve{\mathcal{K}}'\right) \bar{g}_N, w_h \rangle_{\Gamma\times\Upsilon} \quad \forall w_h \in S^{c_1,d_0}_{h_x,h_t}(\Gamma\times\Upsilon)$$

for the approximate solution $\bar{u}_h \in S^{c_1,d_0}_{h_x,h_t}(\Gamma\times\Upsilon)$ with the perturbed right hand side $S^{d_0,d_0}_{h_x,h_t}(\Gamma\times\Upsilon) \ni \bar{g}_N = \mathcal{Q}_{h_t}\mathcal{Q}_{h_x} g_N$. Contrary to the previous example this problem is based on the second BIE, and hence the perfect benchmark problem to test the correct implementation of the adjoint double layer- and hyper-singular operator. In Table 5.4 and Figure 5.4 we report the relative $L_2(\Gamma\times\Upsilon)$ error for various space-time discretizations.

$N_x \backslash N_t$	8	32	128	512
194	$9.51\ 10^{-2}$	$2.76\ 10^{-2}$	$1.56\ 10^{-2}$	$1.33\ 10^{-2}$
776	$9.38\ 10^{-2}$	$2.22\ 10^{-2}$	$6.70\ 10^{-3}$	$3.31\ 10^{-3}$
3,104	$9.36\ 10^{-2}$	$2.18\ 10^{-2}$	$5.38\ 10^{-3}$	$1.83\ 10^{-3}$
12,416	$9.35\ 10^{-2}$	$2.17\ 10^{-2}$	$5.31\ 10^{-3}$	$1.36\ 10^{-3}$

Table 5.4: Relative Dirichlet $L_2(\Gamma\times\Upsilon)$ error.

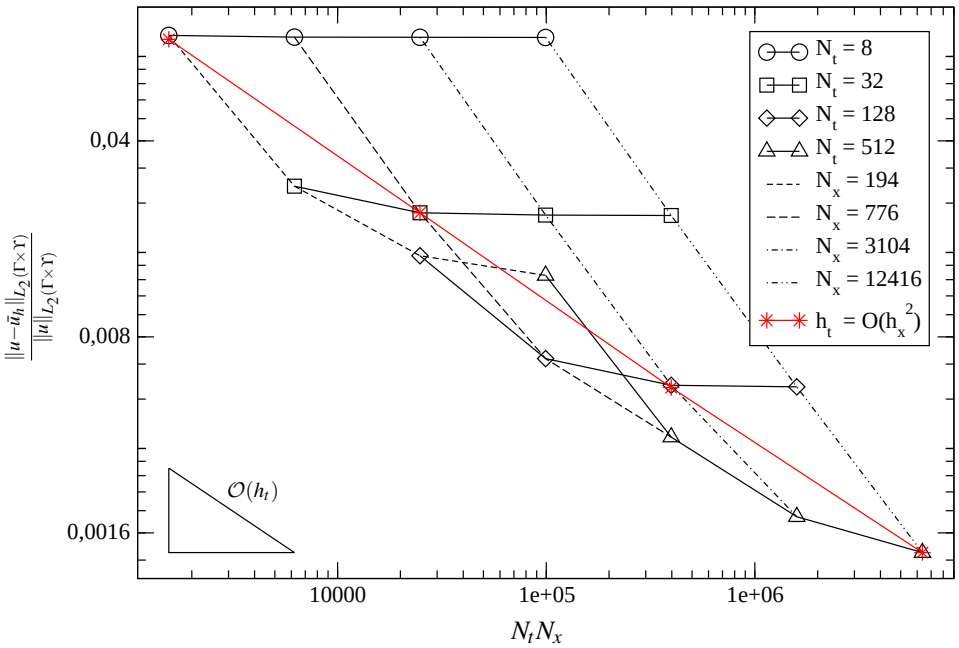

Figure 5.4: Relative Dirichlet $L_2(\Gamma\times\Upsilon)$ error for various space-time discretizations.

lev.	$N_x N_t$	L_x/L_t	rel. $L_2(\Gamma \times \Upsilon)$	iter.	time[sec]	memory[GB]
0	1,552	0/3	$9.51\ 10^{-2}$	6	$1.27\ 10^{2}$	$9.21\ 10^{-2}$
1	24,832	1/5	$2.22\ 10^{-2}$	6	$3.48\ 10^{2}$	$3.06\ 10^{-1}$
2	379,312	2/7	$5.38\ 10^{-3}$	6	$3.55\ 10^{3}$	$1.23\ 10^{0}$
3	6,356,992	3/9	$1.36\ 10^{-3}$	6	$6.27\ 10^{4}$	$5.18\ 10^{0}$

Table 5.5: Neumann IBVP with uniform space-time refinement – $h_t = \mathcal{O}(h_x^2)$.

lev.	$N_x N_t$	L_x/L_t	M	rel. $L_2(\Gamma \times \Upsilon)$	iter.	time[sec]	memory[GB]
0	1,552	0/3	0	$9.51\ 10^{-2}$	6	$1.27\ 10^{2}$	$9.21\ 10^{-2}$
1	6,208	0/3	2	$9.38\ 10^{-2}$	10	$3.67\ 10^{2}$	$4.14\ 10^{-1}$
2	24,832	0/3	4	$9.36\ 10^{-2}$	16	$1.46\ 10^{3}$	$2.11\ 10^{0}$
3	99,328	0/3	6	$9.35\ 10^{-2}$	22	$7.11\ 10^{3}$	$1.03\ 10^{1}$

Table 5.6: Neumann IBVP with uniform space refinement – $h_t = const$.

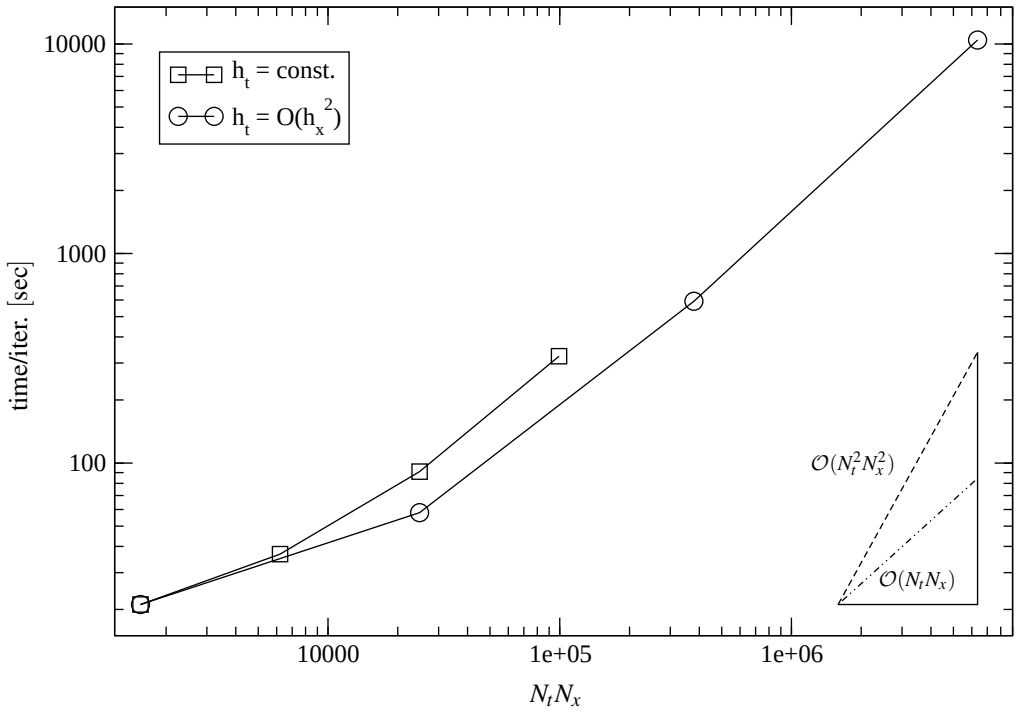

Figure 5.5: Neumann IBVP – computational complexity of the pFMM.

As stated in Lemma 3.2 we obtain the optimal convergence rate of $\mathcal{O}(h_t)$, see Table 5.4 and Figure 5.4. Moreover, in Figure 5.4 we observe that the refinement strategy of $h_t = \mathcal{O}(h_x^2)$ has the same slope as the envelope over all curves and, therefore, is optimal. In Table 5.5, Figure 5.5, and Figure 5.6 we present more results including computation

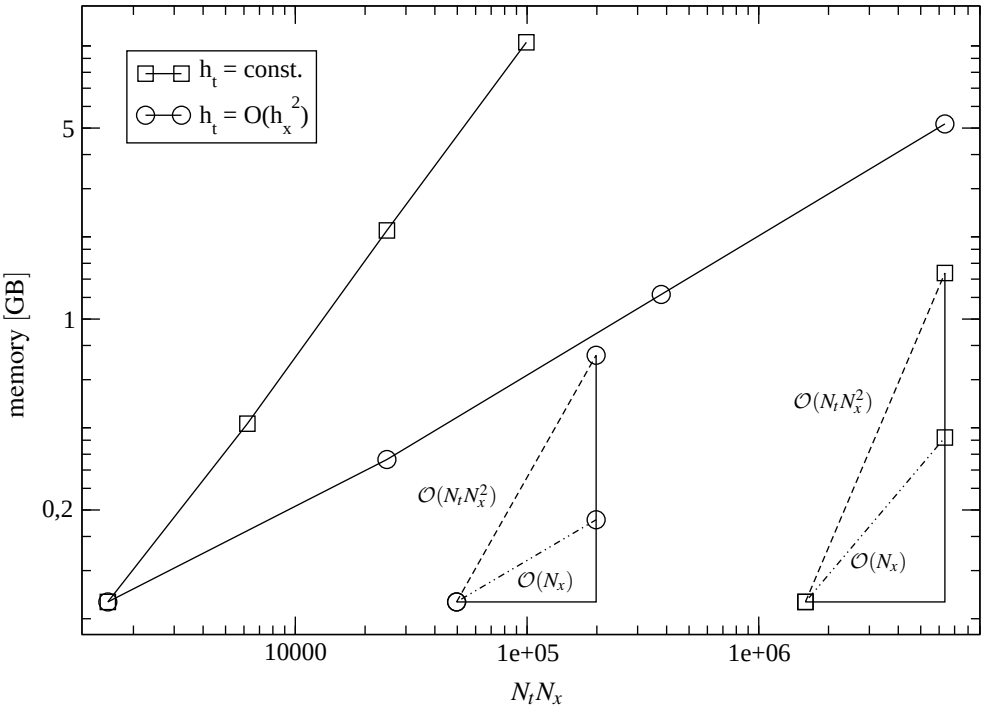

Figure 5.6: Neumann IBVP – memory consumption of the pFMM.

time and memory requirement for exactly this case. Additionally to the already mentioned $\mathcal{O}(h_t^2)$ behavior of the error in the L_2 norm we observe almost optimal behavior in terms of computation time and memory consumption. Again, in order to show that optimality in the number of unknowns is not only achieved for $h_t = \mathcal{O}(h_x^\beta)$ with $\beta = 2$ but also for $\beta < 2$, we present more details for $\beta \to 0$ in Table 5.6, Figure 5.5, and Figure 5.6. Observe that the number of CG iterations in this case increases for the same reason as in the previous example.

5.1.3 Initial Robin BVP

In our third example we solve the pFMM approximated variational form related to the initial Robin boundary value problem (3.25)

$$\langle (\breve{\breve{\mathcal{S}}} + \kappa)\bar{u}_h, v_h \rangle_{\Gamma\times\Upsilon} = \langle g_R, v_h \rangle_{\Gamma\times\Upsilon} \quad \forall v_h \in S^{c_1,d_0}_{h_x,h_t}(\Gamma\times\Upsilon)$$

for the approximate solution $\bar{u}_h \in S^{c_1,d_0}_{h_x,h_t}(\Gamma\times\Upsilon)$ with the perturbed right hand side $S^{d_0,d_0}_{h_x,h_t}(\Gamma\times\Upsilon) \ni \bar{g}_R = \mathcal{Q}_{h_t}\mathcal{Q}_{h_x} g_R$. While we have already tested all boundary integral operators with the previous two examples, this is the test case for the symmetric approximation of Steklov-Poincaré operator.

$N_x \backslash N_t$	8	32	128	512
194	$8.54\ 10^{-2}$	$2.19\ 10^{-2}$	$9.44\ 10^{-3}$	$7.76\ 10^{-3}$
776	$8.52\ 10^{-2}$	$2.11\ 10^{-2}$	$5.46\ 10^{-3}$	$5.55\ 10^{-3}$
3,104	$8.51\ 10^{-2}$	$2.10\ 10^{-2}$	$5.24\ 10^{-3}$	$1.39\ 10^{-3}$
12,416	$8.51\ 10^{-2}$	$2.09\ 10^{-2}$	$5.23\ 10^{-3}$	$1.33\ 10^{-3}$

Table 5.7: Relative Dirichlet $L_2(\Gamma \times \Upsilon)$ error.

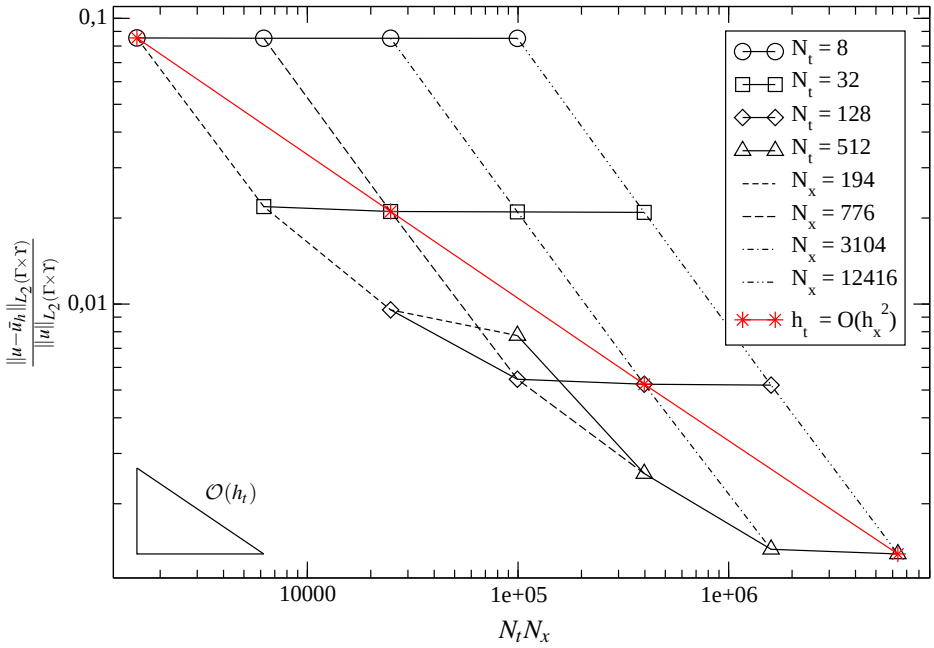

Figure 5.7: Relative Dirichlet $L_2(\Gamma \times \Upsilon)$ error for various space-time discretizations.

In Table 5.7 and Figure 5.7 we present the relative $L_2(\Gamma \times \Upsilon)$ for various space-time discretizations, which confirms the $\mathcal{O}(h_t)$ convergence provided by Lemma 3.4. Again, just like in the case of the initial Neumann boundary value problem, the slope of the envelope over all curves in Figure 5.7 suggests that with $h_t = \mathcal{O}(h_x^2)$ the optimal rate of convergence is obtained, indeed. In Table 5.8, Figure 5.8, and Figure 5.9 we present more details on exactly such a refinement scheme, which reveals the optimality in the number of unknowns with respect to computation time and memory requirement once again. After the previous two examples it seems needless to mention that the presented method remains optimal also for $h_t = \mathcal{O}(h_x^\beta)$ with $\beta < 0$, nonetheless, for completeness sake the confirmation can be found in by Table 5.9, Figure 5.8, and Figure 5.9.

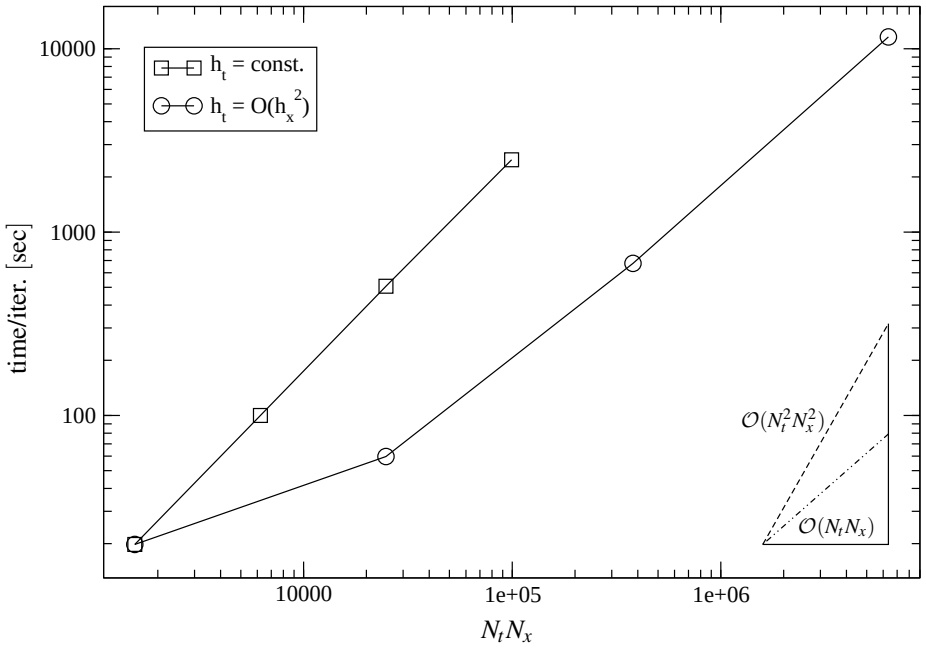

Figure 5.8: Robin IBVP – computational complexity of the pFMM.

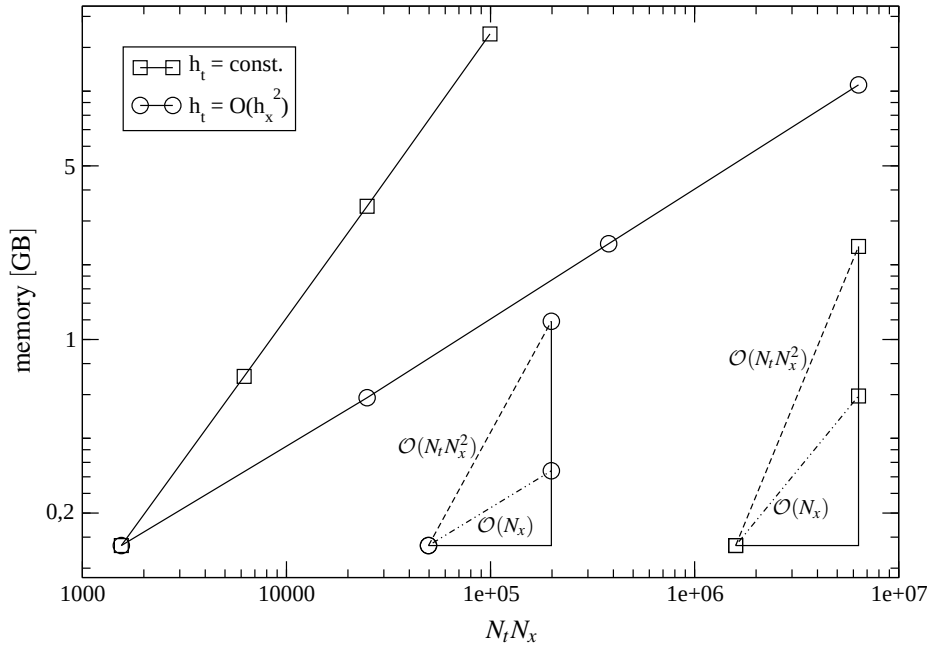

Figure 5.9: Robin IBVP – memory consumption of the pFMM.

lev.	N_xN_t	L_x/L_t	rel. $L_2(\Gamma\times\Upsilon)$	iter.	time[sec]	memory[GB]
0	1,552	0/3	$8.54\ 10^{-2}$	10	$1.98\ 10^{2}$	$1.47\ 10^{-1}$
1	24,832	1/5	$2.11\ 10^{-2}$	10	$5.97\ 10^{2}$	$5.83\ 10^{-1}$
2	379,312	2/7	$5.24\ 10^{-3}$	10	$6.75\ 10^{3}$	$2.43\ 10^{0}$
3	6,356,992	3/9	$1.33\ 10^{-3}$	10	$1.16\ 10^{5}$	$1.06\ 10^{0}$

Table 5.8: Robin IBVP with uniform space-time refinement – $h_t = \mathcal{O}(h_x^2)$.

lev.	N_xN_t	L_x/L_t	M	rel. $L_2(\Gamma\times\Upsilon)$	iter.	time[sec]	memory[GB]
0	1,552	0/3	0	$8.54\ 10^{-2}$	10	$1.98\ 10^{2}$	$1.47\ 10^{-1}$
1	6,208	1/5	2	$8.52\ 10^{-2}$	13	$1.30\ 10^{3}$	$7.10\ 10^{-1}$
2	24,832	2/7	4	$8.51\ 10^{-2}$	18	$9.12\ 10^{3}$	$3.44\ 10^{0}$
3	99,328	3/9	6	$8.51\ 10^{-2}$	23	$5.70\ 10^{4}$	$1.70\ 10^{1}$

Table 5.9: Robin IBVP with uniform space refinement – $h_t = const$.

5.1.4 Initial Dirichlet-Neumann-Robin BVP

Finally in our last benchmark problem we test the variational form of the mixed initial Dirichlet-Neumann-Robin boundary value problem (3.29)

$$\langle(\breve{\bar{\mathcal{S}}}+\kappa)\bar{\tilde{u}}_h, v_h\rangle_{\Gamma\times\Upsilon} = \langle \bar{g}_{NR} - (\breve{\bar{\mathcal{S}}}+\kappa)\bar{\tilde{g}}_D, v_h\rangle_{\Gamma\times\Upsilon} \quad v_h \in S^{c_1,d_0}_{h_x,h_t}(\Gamma_{NR}\times\Upsilon)\ .$$

With this example we check the correct extension of the given boundary data on the respective parts of the boundary, see Section 2.4.4.

$N_x\backslash N_t$	8	32	128	512
194	$8.51\ 10^{-2}$	$2.19\ 10^{-2}$	$8.28\ 10^{-3}$	$7.94\ 10^{-3}$
776	$8.49\ 10^{-2}$	$2.10\ 10^{-2}$	$5.45\ 10^{-3}$	$5.36\ 10^{-3}$
3,104	$8.49\ 10^{-2}$	$2.10\ 10^{-2}$	$5.24\ 10^{-3}$	$1.38\ 10^{-3}$
12,416	$8.49\ 10^{-2}$	$2.09\ 10^{-2}$	$5.19\ 10^{-3}$	$1.31\ 10^{-3}$

Table 5.10: Dirichlet *rel*. L_2 error for different $N_x\backslash N_t$.

Just like in the examples before we present the relative $L_2(\Gamma\times\Upsilon)$ error for various space-time discretizations in Table 5.10 and Figure 5.10 and observe the agreement with the theoretically derived error estimate for a $h_t = \mathcal{O}(h_x^2)$ refinement given in Lemma 3.5.

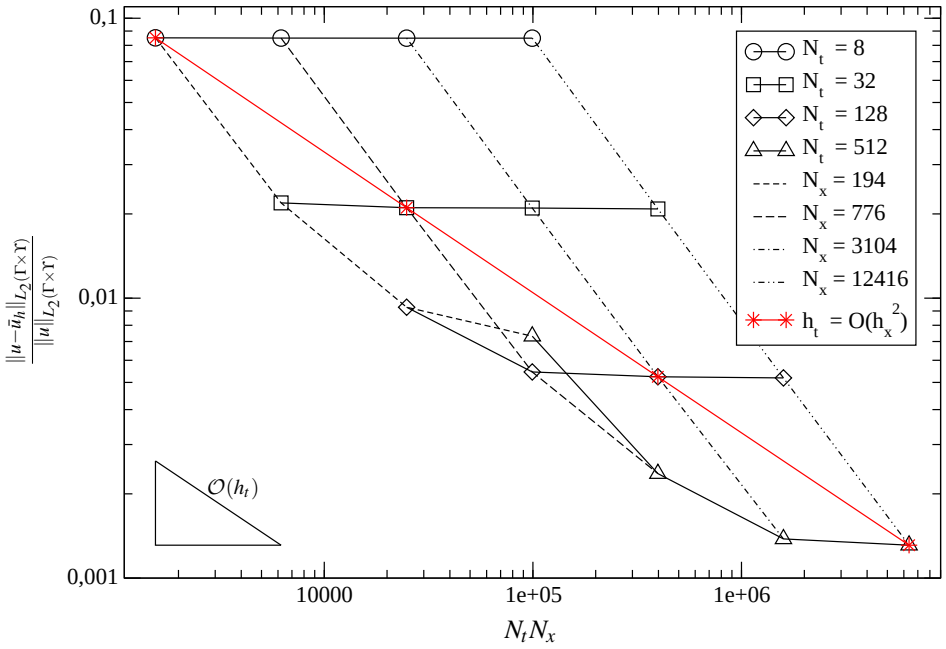

Figure 5.10: rel. Dirichlet $L_2(\Gamma\times\Upsilon)$ error for various space-time discretizations.

lev.	N_xN_t	L_x/L_t	rel. $L_2(\Gamma\times\Upsilon)$	iter.	time[sec]	memory[GB]
0	1,552	0/3	$8.51\ 10^{-2}$	14	$1.61\ 10^{2}$	$1.45\ 10^{-1}$
1	24,832	1/5	$2.10\ 10^{-2}$	14	$5.52\ 10^{2}$	$5.69\ 10^{-1}$
2	379,312	2/7	$5.24\ 10^{-3}$	14	$6.82\ 10^{3}$	$2.33\ 10^{0}$
3	6,356,992	3/9	$1.31\ 10^{-3}$	14	$1.26\ 10^{6}$	$1.05\ 10^{0}$

Table 5.11: Mixed IBVP with uniform space-time refinement – $h_t = \mathcal{O}(h_x^2)$.

lev.	N_xN_t	L_x/L_t	M	rel. $L_2(\Gamma\times\Upsilon)$	iter.	time[sec]	memory[GB]
0	1,552	0/3	0	$8.51\ 10^{-2}$	14	$1.61\ 10^{2}$	$1.45\ 10^{-1}$
1	6,208	1/5	2	$8.49\ 10^{-2}$	20	$1.37\ 10^{3}$	$6.83\ 10^{-1}$
2	24,832	2/7	4	$8.49\ 10^{-2}$	28	$1.39\ 10^{4}$	$3.32\ 10^{0}$
3	99,328	3/9	6	$8.49\ 10^{-2}$	40	$1.21\ 10^{5}$	$1.61\ 10^{1}$

Table 5.12: Mixed IBVP with uniform space refinement – $h_t = const$.

Finally, in Table 5.11, Table 5.12 and Figure 5.11, Figure 5.12 we find the confirmation that our method remains optimal in the number of unknowns for this initial boundary value problem regardless the refinement scheme, too.

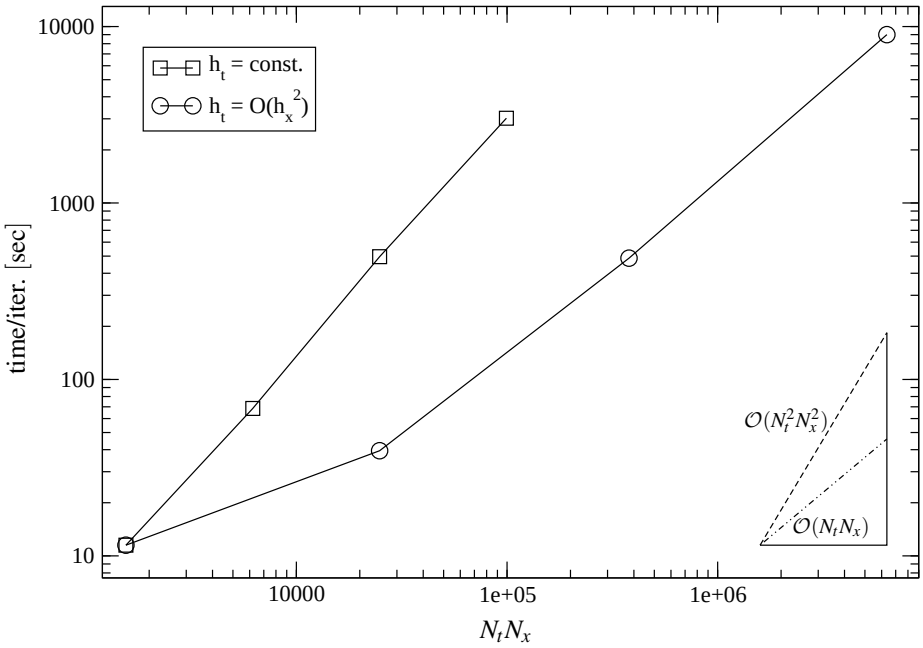

Figure 5.11: Mixed IBVP – computational complexity of the pFMM.

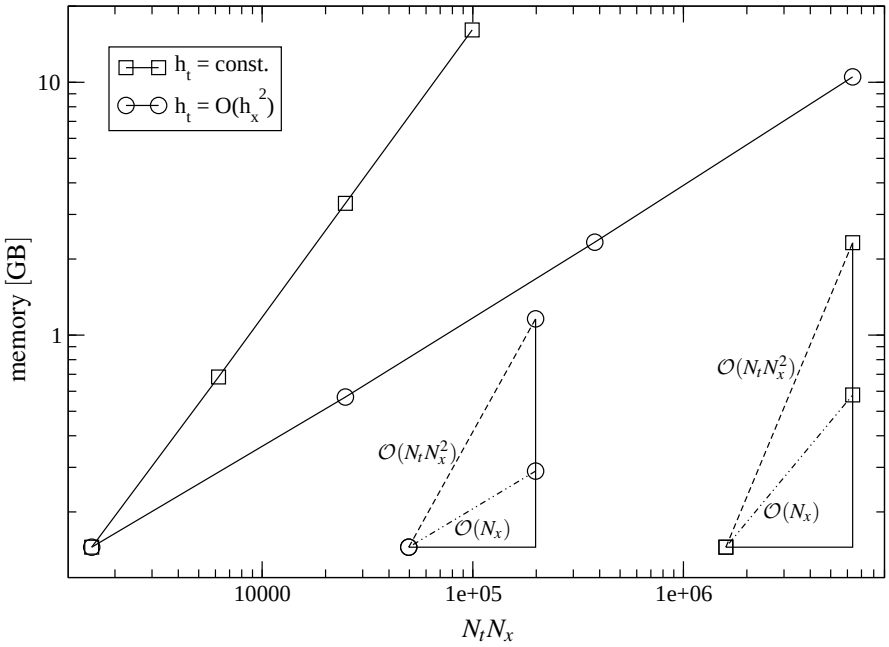

Figure 5.12: Mixed IBVP – memory consumption of the pFMM.

5.2 Industrial Applications

5.2.1 The Press Hardening Process

Process Description Press hardening (form hardening, hot forming) is a sheet metal forming process for the production of high-strength structural parts, mainly used in the automotive industry [47]. This process basically consists of the following steps shown in Figure 5.13: Waiting for the hot blank, closing of the binder and upper tool, fast forming, and rapid cooling of the blank in the closed and cooled tool.

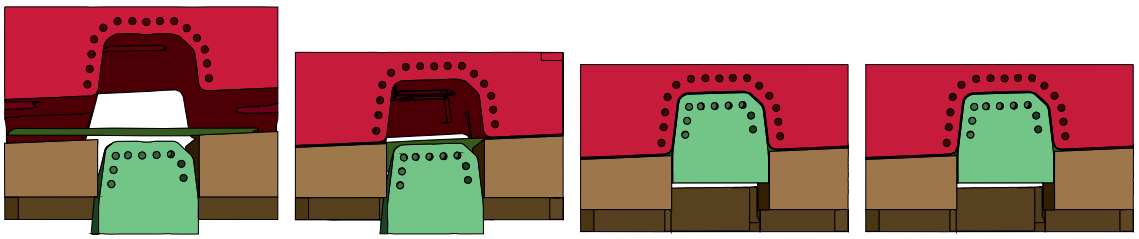

(a) Waiting. (b) Closing. (c) Forming. (d) Cooling.

Figure 5.13: Schematic press hardening process.

Press hardened components have two major advantages over cold formed ones. First, due to the fact that the hardening process takes place in the closed tool, the allotropic transformation of the micro-structure happens after the forming process, which reduces residual stresses and spring-back effects within the finished part. Second, the layout of the cooling channels allows to steer the local cooling rate of the tool and hence of the metal sheet. Since the mechanical properties of the formed components strongly depend on the cooling rate (e.g. a cooling rate of $27\,^{\circ\mathrm{C}}/_{\mathrm{sec}}$ is required to obtain a martensitic micro-structure for the widely used boron alloyed press hardening steel 22MnB5), it turns out that the press hardening process can be used to produce lightweight structural parts with distinct material properties in different regions.

Up until now it was common practice to neglect the hot forming tools within the overall simulation in the sense that they were only regarded as rigid bodies with constant temperature. Weiss [47] proposed to overcome this cruel approximation by an isolated simulation of the press hardening tools without considering the overall thermal-mechanically coupled process. His approach enables the design engineer to simulate and adapt the cooling performance of the tools within the design phase. As already mentioned earlier, the material properties of the final component depends on the cooling rate, which is linked to the temperature difference between the part and the tools. Hence, the design relevant thermal quantity is the surface temperature of the hot forming tools. This observation together with the fact that these tools and the cooling channel geometry can be almost arbitrarily com-

plicated suggests to use a direct Boundary Element Method for their thermal simulation.

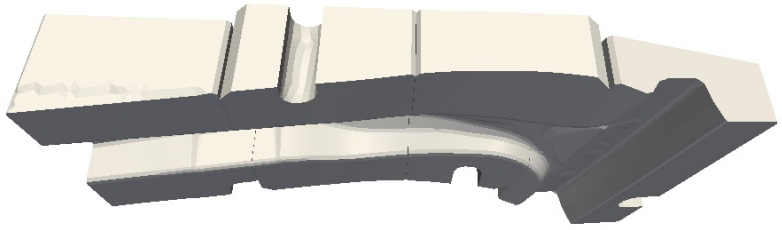

(a) Upper tool.

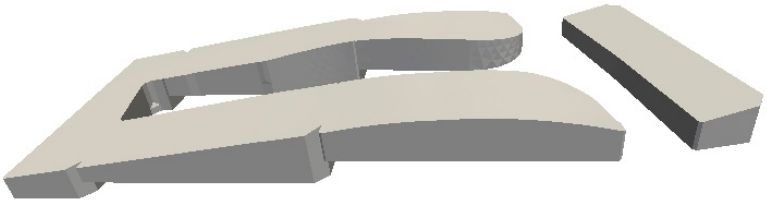

(b) Binder.

(c) Lower tool.

Figure 5.14: Arrangement of the press hardening tools for the simulated b-pillar.

Thermal Model The aim of Weiss' model [47] is to predict the quasi-static surface temperature distribution of press hardening tools based on an energy balance. Beside this information, it is important to know the closing surface temperature distribution of the tools, which is the temperature at the beginning of the forming step.

At the base of the tools, i.e. where they are connected to the hydraulic press, it is sufficient to assume a constant temperature, while for the mantle and cooling channels the heat

transfer coefficient (convective or Robin-type boundary condition) is easily determined [47]. However, for the active surface the situation is more involved. Assuming that the total energy $E_c[\mathrm{J}]$ to be withdrawn from the blank in one process cycle is absorbed by the tools, leads to the mean surface heat flux

$$q_m = \frac{E_c}{AT_c} ,$$

with the surface measure $A[\mathrm{m}^2]$ of the blank and the cycle duration $T_c[\mathrm{sec}]$. However, simply prescribing this averaged heat flux as a Neumann-type boundary condition is to rough of an approximation for the real process. With the argument that cooler areas of the tool withdraw more energy from the blank than hotter ones, Weiss [47] aims to use a Robin-type boundary condition

$$q(\mathbf{x},t) = \kappa(u(\mathbf{x},t) - u_\infty(\mathbf{x})) ,$$

which links the heat flux to the temperature difference rather than prescribing a constant surface heat flux. However, since the heat transfer coefficient $\kappa[\mathrm{W}/^\circ\mathrm{Cm}^2]$ is not known, a fictitious $\kappa_f[\mathrm{W}/^\circ\mathrm{Cm}^2]$ is introduced

$$q_m = \kappa_f(u_t - u_b)$$

with the mean temperature of the blank $u_b[^\circ\mathrm{C}]$ before the forming step, the mean quasi-static temperature of the tool $u_t[^\circ\mathrm{C}]$, and the mean surface heat flux $q_m[\mathrm{W}/\mathrm{m}^2]$ know from above. While the assumption for $u_\infty[^\circ\mathrm{C}]$ is an arbitrary choice, the assumption for $u_t[^\circ\mathrm{C}]$ needs to be verified after the real simulation and, if necessary, corrected (see [47, Chapter 6]). Finally, since the material properties of the tool do not vary significantly throughout the working temperature range, we assume a constant heat conduction coefficient $\lambda = 25\,\mathrm{W}/\mathrm{m}^\circ\mathrm{C}$, specific heat capacity $c_p = 450\,\mathrm{J}/\mathrm{kg}^\circ\mathrm{C}$, and density $\rho = 7647\,\mathrm{kg}/\mathrm{m}^3$.

Figure 5.14 depicts the general arrangement of the press hardening tools for a b-pillar, which consist of three parts, the upper tool, the lower tool and the binder. For the upper tool, the boundary conditions are given in Table 5.13, which are simply mirrored onto the lower tool, too. However, since the binder has neither a base area nor channels, these two types of boundary do not appear for this part of the assembly.

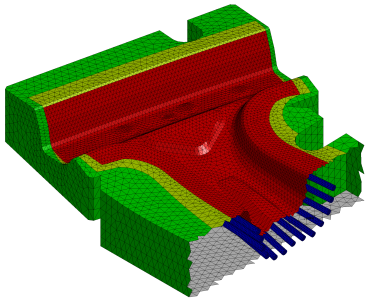

	$g_D^a/g_D^b\,[^\circ\mathrm{C}]$	$\kappa_f^a/\kappa_f^b[\mathrm{W}/^\circ\mathrm{Cm}^2]$	$u_\infty^a/u_\infty^b\,[^\circ\mathrm{C}]$
gray	23/23	-	-
green	-	10/10	23/23
blue	-	1100/1100	23/23
red	-	47/10	850/23

Table 5.13: BC's for heating (a) and cooling (b).

Thus, together with the boundary conditions for the heating (a) and cooling (b) process given in Table 5.13 and an initial temperature of $u_0 = 23\,^\circ\mathrm{C}$, the initial boundary value problem is given by

$$\begin{aligned}
\frac{\partial u(\tilde{\mathbf{x}},t)}{\partial t} &= \frac{\lambda}{\rho c_p}\Delta u(\tilde{\mathbf{x}},t) && (\tilde{\mathbf{x}},t) \in (\Omega \times \Upsilon)\,, \\
u(\tilde{\mathbf{x}},0) &= u_0 && \tilde{\mathbf{x}} \in \Omega\,, \\
u(\mathbf{x},t) &= \begin{cases} g_D^a & t \leq 15T_c \\ g_D^b & t > 15T_c \end{cases} && (\mathbf{x},t) \in (\Gamma_D \times \Upsilon)\,, \\
q(\mathbf{x},t) &= \begin{cases} \kappa_f^a(u(\mathbf{x},t) - u_\infty^a(\mathbf{x})) & t \leq 15T_c \\ \kappa_f^b(u(\mathbf{x},t) - u_\infty^b(\mathbf{x})) & t > 15T_c \end{cases} && (\mathbf{x},t) \in (\Gamma_R \times \Upsilon)\,.
\end{aligned}$$

Observe that the quasi-static working temperature of the tool will be reached after approximately 15 cycles of $T_c = 59.4\,\mathrm{sec}$ and the closing temperature after yet another $t_c = 43.8\,\mathrm{sec}$. Furthermore, it is important to note that the initial condition is constant throughout the whole domain. Therefore, this initial boundary value problem can trivially be transformed into a homogeneous one and the boundary integral formulation given in Subsection 2.4.4 is used as an equivalent description to find the surface temperature distribution $u(\mathbf{x},t)$ with $(\mathbf{x},t) \in (\Gamma \times \Upsilon)$ and $\Gamma = \Gamma_D \cup \Gamma_R$.

Due to the approximation of the Steklov-Poincaré operator (Lemma 3.3), the number of spatial unknowns in the system amounts to the combined number of all triangles plus the number of nodes on the Robin boundary. For the upper tool this yields $N_x = 142,754 + 64,112 = 206,866$, for the lower tool $N_x = 94,518 + 43,374 = 137,892$, and for the binder $N_x = 6,892 + 3,450 = 10,342$. The total time of $T = 15T_c + t_c = 891 + 43.8 = 943.8\,\mathrm{sec}$ is split into $N_t = 128$ time steps. Thus, for the total number of unknowns for the upper tool results in $N_x N_t = 26,478,848$ for the lower tool $N_x N_t = 17,650,176$ and for the binder $N_x N_t = 1,323,776$. Keeping in mind the initial temperature of $23\,^\circ\mathrm{C}$ in Figures 5.15 – 5.17 we present screen shots of the quasi-static working temperature after 15 cycles along with the closing temperature of the upper tool, the lower tool, and the binder, respectively. In these plots hotter regions are colored in red, while colder regions are colored in blue. Obviously the tools heat up throughout the production process as they withdraw the energy form the hot blanks. We observe that in regions, where the cooling channels are further away from the surface, the temperature is higher than in regions, where the channels are closer to the surface. Finally, the closing temperature is obtained by switching the boundary condition of the active surface after 15 cycles to the same parameters as for the mantle, i.e. a free surface in contact with the surrounding atmosphere, and letting the tools cool for $43.8\,\mathrm{sec}$.

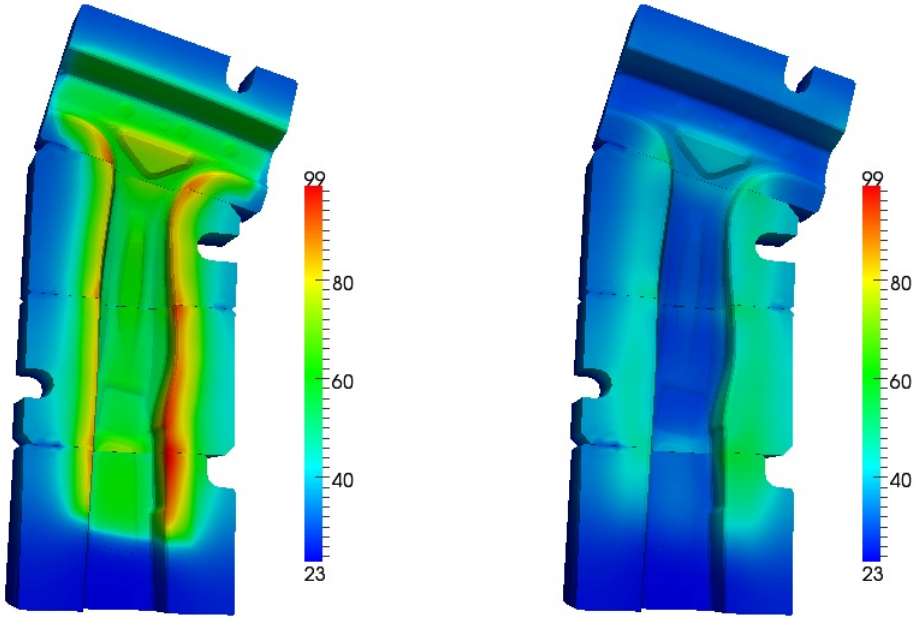

(a) Quasi-Static working temperature [°C]. (b) Closing temperature [°C].

Figure 5.15: Surface temperature of the upper tool.

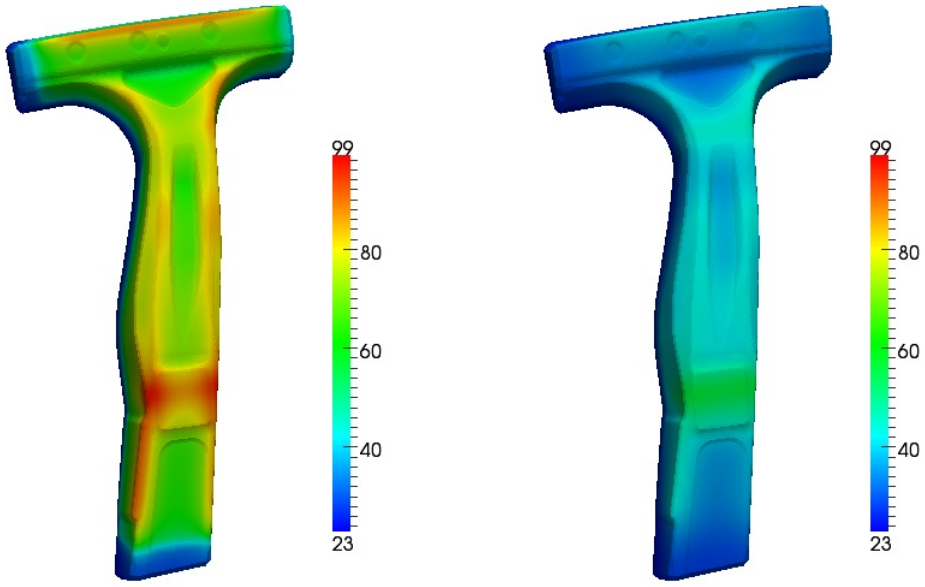

(a) Quasi-Static working temperature [°C]. (b) Closing temperature [°C].

Figure 5.16: Surface temperature of the lower tool.

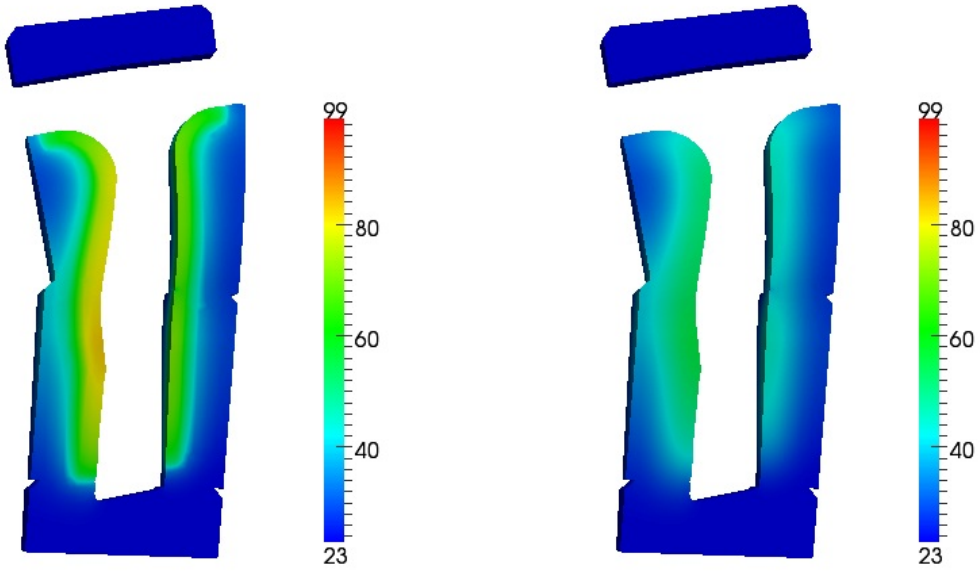

(a) Quasi-Static working temperature [°C]. (b) Closing temperature [°C].

Figure 5.17: Surface temperature of the binder.

At first sight the results visualized in Figures 5.15 – 5.17 seem plausible, however, we would like to have a more sound verification. In contrast to the benchmark problems of the previous section, there is no analytic solution to this problem though. Therefore, we resort to a comparison with in situ temperature measurements. In Figure 5.18 we show the location of three thermo-elements placed at significant positions within the upper tool. The thermo-element T1 and T3 are located close to the active surface inside the cooling channels, where we expect a rather strong temperature oscillation, while T2 is paced outside the cooling channels in a region, where we expect this effect to be less pronounced. Using the representation formula (2.8) we compute the temperature at these three points and compare the result with the measurement data in Figures 5.19 – 5.21. In all three plots we observe that not only the quasi-static temperature after 15 cycles matches quite accurately with the mean working temperature, but also the simulated closing temperature is within an acceptable range to the lowest temperature measured in a production cycle ($\pm 10\,°C$ accuracy is acceptable for the design engineers in this case). Additionally we observe that the region inside the cooling channels reacts much faster than the region behind the cooling channels, i.e. the quasi-static working temperature in the region inside the cooling channels (T1, T3) is reached much faster then outside (T2), this is what one would intuitively expect, too. Further, it is important to note that the misalignment of the cooling phase between simulation and real process is irrelevant. The choice of taking 15 cycles as the end of the start-up phase is motivated by experience and any other time in its neighborhood could be taken as start point for cooling phase.

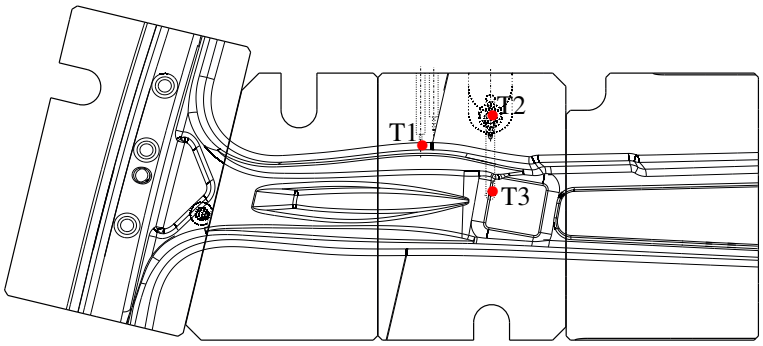

(a) Top view of the upper tool with the position of T1 – T3.

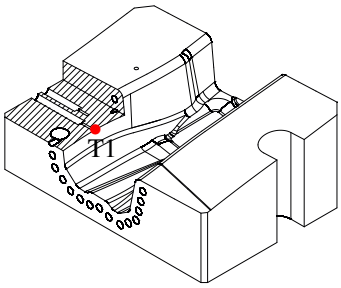

(b) Position of T1.

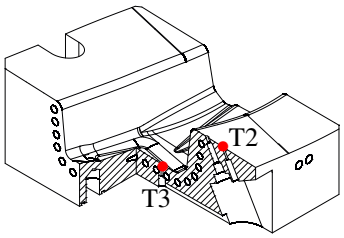

(c) Position of T2 and T3.

Figure 5.18: Position of all thermo-elements T1–T3 in the upper tool [47].

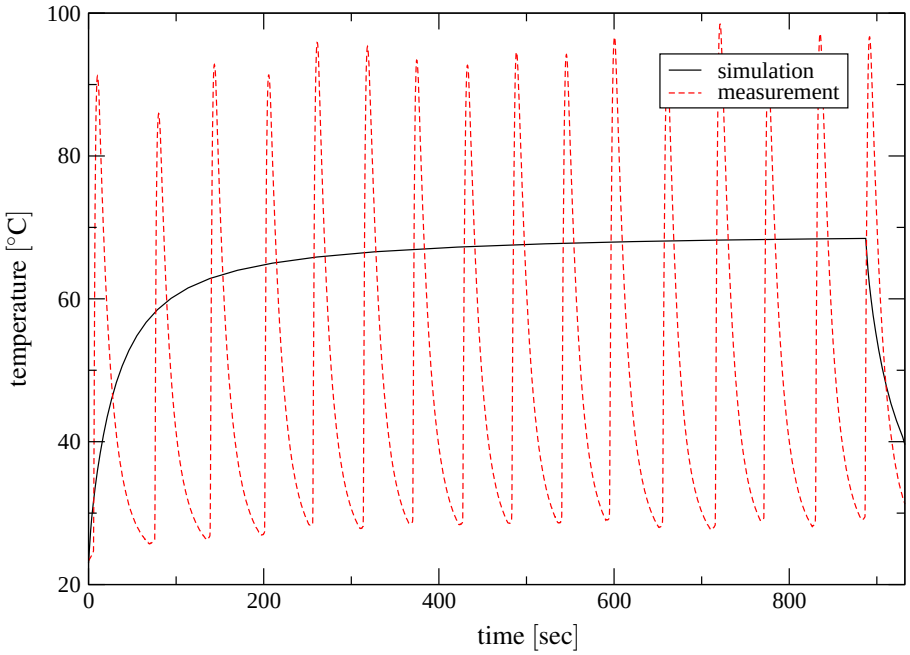

Figure 5.19: Surface temperature T1 – simulation vs. measurement [47].

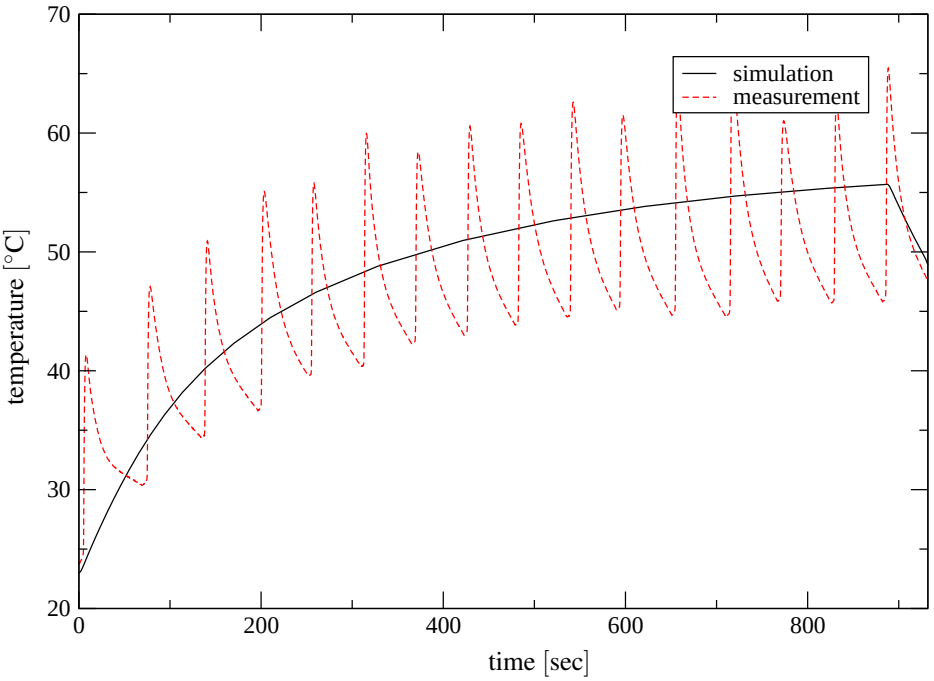

Figure 5.20: Surface temperature T2 – simulation vs. measurement [47].

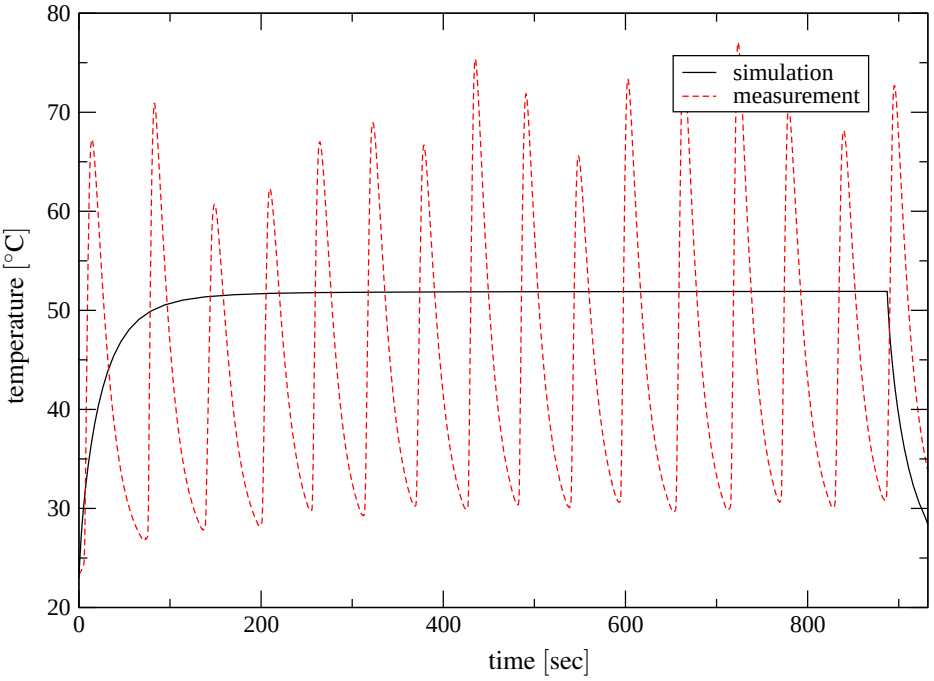

Figure 5.21: Surface temperature T3 – simulation vs. measurement [47].

6 CONCLUSION

With the intention to numerically simulate large scale heat conduction problems in Lipschitz domains we have presented a Galerkin Boundary Element Method for pure and mixed initial boundary value problems of the heat equation with homogeneous initial condition. Our motivation to work with a Boundary Element Method is given by the knowledge that an optimal formulation, i.e. optimal in the number of unknowns $N_x N_t = \mathcal{O}(h_x^{-2} h_t^{-1})$, will at some point always rule out other popular numerical methods (FEM, FDM, FVM), which are based on a volume discretization with the implication of $N_x N_t = \mathcal{O}(h_x^{-3} h_t^{-1})$.

Based on the framework of boundary integral operators of the heat equation, we have given a symmetric formulation for pure Dirichlet, Neumann, and Robin-type initial boundary value problems. Moreover, we have also given a symmetric formulation of a general mixed initial boundary value problem with a combination of all previously mentioned boundary conditions. Due to the ellipticity and boundedness of the single layer and hyper-singular operator in their energy norms and the boundedness of the double layer and adjoint double layer operator, these formulations are uniquely solvable and stable due to the lemma of Lax-Milgram. Furthermore, with Cea's Lemma we get uniqueness, stability and quasi-optimality of the approximate solution in the energy norm. Using conforming sub-spaces, e.g. piecewise polynomial tensor product spaces, we directly obtain error estimates in the energy norm through the approximation property of those finite dimensional spaces. For practical sake we use the well known regularity results of the thermal layer operators to derive estimates in the L_2 norm and confirm them in a series of benchmark problems. We do that not only for the case of $h_t = \mathcal{O}(h_x^a)$ with $a = 2$, but also for $a \to 0$ and $a \to \infty$.

Since standard Boundary Element Methods yield dense linear system of dimension $N_x N_t$ we end up with $\mathcal{O}(h_x^{-4} h_t^{-2})$ complexity for the solution and $\mathcal{O}(h_x^{-4} h_t^{-1})$ in terms of storage, which is due to the equidistant time discretization. To remedy this setback of the Boundary Element Method, we introduce the parabolic Fast Multipole Method to approximate the application of the linear system at a cost of almost $\mathcal{O}(h_x^{-2} h_t^{-1})$ and a memory requirement of $\mathcal{O}(h_x^{-2})$. These estimates hold for the parabolic farfield, however, not necessarily for the nearfield. We observe that the complexity of the nearfield amounts to $\mathcal{O}(h_x^{-2} h_t^{-1})$ for $h_t = \mathcal{O}(h_x^a)$ with $a \geq 2$. For $0 < a < 2$ the cost grows faster because the number of spatial unknowns grows faster than the spatial truncation decreases, especially for $a \to 0$ this leads to an explosion of the computational complexity and storage requirement. We resolved this inconvenience by a dyadic subdivision of the parabolic nearfield and application of a composite quadrature rule in time. We combined this quadrature rule with FGTs in space in those intervals, where the heat kernel is regular enough. With this strategy we link

the spatial truncation of the heat kernel to the temporal localization of the singularity and thus limit the direct evaluations to $\mathcal{O}(h_x^{-2}h_t^{-1})$ with $h_t = \mathcal{O}(h_x^a)$ and $0 < a < 2$. For the FGTs we simply extend the spatial cluster structure of the parabolic FMM to higher levels from where we choose the FGT level via the space-time scaling of the heat kernel once again. The confirmation that this algorithm is optimal indeed, is given in all benchmark problems by the investigation of a purely spatial refinement scheme, which corresponds to $h_t = \mathcal{O}(h_x^a)$ with $a \to 0$.

Finally, our method was used by Weiss [47] to perform the thermal simulation of press hardening tools, where its applicability to industrial problems of large scale is shown. We presented some results from an experimental setup as a part of Weiss' PhD thesis [47], where a kind of quasi-static start-up phase of the cyclic press hardening process with the cooling phase of one cycle at the end was simulated. These results, namely the quasi-static working temperature of the tools and the temperature at the end of the cooling phase, i.e. just before a new blank is formed, are the crucial results required by the engineers. After a satisfactory experimental validation of these results at some points inside the tools presented in [47] and summarized in Section 5.2, a real process at *WEBA GmbH* was simulated and validated with some further in-situ measurements. Unfortunately these results are confidential and can therefore not be presented in this work, however, they were pleasing enough for *WEBA GmbH* to use our algorithm for the simulation of further press hardening tools.

A ANISOTROPIC SOBOLEV SPACES

Here we recite some important properties of anisotropic Sobolev spaces [27, 28] as they play an important role in the whole numerical analysis framework [10, 35].

Definition A.1. *For real $r,s \geq 0$ the anisotropic Sobolev space*

$$H^{r,s}(\mathbb{R}^3 \times \mathbb{R}) := L_2\left(\mathbb{R}; H^r(\mathbb{R}^3)\right) \cap H^s\left(\mathbb{R}; L_2(\mathbb{R}^3)\right)$$

is associated with the norm

$$\|u\|^2_{H^{r,s}(\mathbb{R}^3\times\mathbb{R})} := \int\limits_{\mathbb{R}} \int\limits_{\mathbb{R}^3} \left[(1+|\xi|^2)^r + (1+|\tau|^2)^s\right] \mathcal{F}u(\xi,\tau) d\xi\, d\tau \,,$$

where $\mathcal{F}u(\xi,\tau)$ denotes the Fourier transform in space and time and for real $r,s<0$ we have by duality

$$H^{r,s}(\mathbb{R}^3 \times \mathbb{R}) := \left[H^{-r,-s}(\mathbb{R}^3 \times \mathbb{R})\right]' \,.$$

Definition A.2. *For an open domain Ω with Lipschitz boundary Γ and the time interval $\Upsilon := (0,T)$ with $\mathbb{R} \ni T > 0$ the space $H^{r,s}(\Gamma \times \Upsilon)$ with $\mathbb{R} \ni r,s \geq 0$ and $|r| \leq 1$ is obtained by restriction [10] and equipped with the quotient norm, while $H^{r,s}(\Gamma \times \Upsilon)$ for $\mathbb{R} \ni r,s < 0$ is defined by duality.*

Definition A.3. *Assume $\Gamma_i \subset \Gamma$ to be an open boundary part, then for $\mathbb{R} \ni r,s \geq 0$ we define the sub-space*

$$\widetilde{H}^{r,s}(\Gamma_i \times \Upsilon) := \left\{v = \tilde{v}_{|(\Gamma_i\times\Upsilon)} : \tilde{v} \in H^{r,s}(\Gamma \times \Upsilon),\ supp_{\mathbf{x}}(\tilde{v}) \subset \Gamma_i\right\} \subset H^{r,s}(\Gamma \times \Upsilon) \,, \quad |r| \leq 1 \,,$$

while for $\mathbb{R} \ni r,s < 0$ we need

$$H^{r,s}(\Gamma_i \times \Upsilon) := \left[\widetilde{H}^{-r,-s}(\Gamma_i \times \Upsilon)\right]' \,, \quad |r| \leq 1 \,.$$

Definition A.4. *Assume $\Gamma = \bigcup_{j=1}^J \overline{\Gamma}_j$ with Γ_j smooth, $\Gamma_i \cap \Gamma_j = \emptyset$ for $i \neq j$, and $r,s \geq 0$, then we define*

$$H^{r,s}_{pw}(\Gamma \times \Upsilon) := L_2(\Upsilon; H^r_{pw}(\Gamma)) \cap H^s(\Upsilon; L_2(\Gamma)) \,,$$

equipped with the norm

$$\|v\|_{H^{r,s}_{pw}(\Gamma\times\Upsilon)} := \sum_{j=1}^J \left(\|v_{|\Gamma_j}\|_{H^{r,s}(\Gamma_j\times\Upsilon)^2}\right)^{\frac{1}{2}} \,.$$

B ANALYTIC EXPRESSIONS OF FUNDAMENTAL SOLUTIONS

Analytic Expression cFMM

For the temporal nearfield of the cFMM in Section 4.3 we perform the time integration in (4.17) analytically. Since we used a piecewise constant time discretization we have

$$\mathsf{V}_{i-j} = \mathsf{V}_d = \begin{cases} h_t^2 \int_0^1 \int_0^t V((d+t-\tau)h_t)\mathrm{d}\tau\mathrm{d}t & d=0 \\ h_t^2 \int_0^1 \int_0^1 V((d+t-\tau)h_t)\mathrm{d}\tau\mathrm{d}t & d \geq 1\,, \end{cases}$$

which results in

$$\mathsf{V}_d = h_t^2 \left[V^{(-2)}((d+1)h_t) - 2V^{(-2)}(dh_t) + V^{(-2)}((d-1)h_t) \right]\,,$$

with

$$V^{(-2)}(\delta) = \begin{cases} 0 & \delta \leq 0 \\ \frac{4\sqrt{\delta}}{3\pi}\left[\delta - (\delta+1)\exp\left(-\frac{1}{\delta}\right) + \left(\sqrt{\frac{\pi}{\delta}} + \frac{3\sqrt{\pi\delta}}{2}\right)\operatorname{erfc}\left(\frac{1}{\sqrt{\delta}}\right)\right] & \delta > 0\,. \end{cases}$$

Analytic Expressions pFMM

Within the acceleration of the temporal nearfield in Section 4.6 we perform the time integration for $V_{1,M}^{\pm}(\mathbf{r})$, $K_{1,M}^{\pm}(\mathbf{r})$, $K'^{\pm}_{1,M}(\mathbf{r})$, $D_{1,M}^{\pm}(\mathbf{r})$ analytically. Since we used a piecewise constant time discretization we have

$$V_{1,M}^{-}(\mathbf{r}) = \frac{1}{8\pi}\left[\sqrt{\frac{4h_t\mu^M}{\pi}}\exp\left(-\frac{|\mathbf{r}|^2}{4h_t\mu^M}\right) - \operatorname{erfc}\left(\frac{|\mathbf{r}|}{\sqrt{4h_t\mu^M}}\right)|\mathbf{r}|\right]$$

$$V_{1,M}^{+}(\mathbf{r}) = \frac{-1}{8\pi}\left[\sqrt{\frac{4h_t\mu^M}{\pi}}\exp\left(-\frac{|\mathbf{r}|^2}{4h_t\mu^M}\right) - \operatorname{erfc}\left(\frac{|\mathbf{r}|}{\sqrt{4h_t\mu^M}}\right)\left(\frac{2h_t}{|\mathbf{r}|} + |\mathbf{r}|\right)\right]$$

$$K_{1,M}^{-}(\mathbf{r}) = -\frac{\mathbf{r}^\top \mathbf{n}_\mathbf{y}}{8\pi}\left[\operatorname{erfc}\left(\frac{|\mathbf{r}|}{\sqrt{4h_t\mu^M}}\right)\right]$$

$$K_{1,M}^{+}(\mathbf{r}) = -\frac{\mathbf{r}^\top \mathbf{n}_\mathbf{y}}{8\pi}\left[\operatorname{erfc}\left(\frac{|\mathbf{r}|}{\sqrt{4h_t\mu^M}}\right)\left(\frac{2h_t}{|\mathbf{r}|^2} - 1\right) + \frac{4h_t}{|\mathbf{r}|}\sqrt{\frac{1}{4\pi h_t\mu^M}}\exp\left(-\frac{|\mathbf{r}|^2}{4h_t\mu^M}\right)\right]$$

$$K'^{-}_{1,M}(\mathbf{r}) = \frac{\mathbf{r}^{\top}\mathbf{n}_{\mathbf{x}}}{8\pi}\left[\operatorname{erfc}\left(\frac{|\mathbf{r}|}{\sqrt{4h_t\mu^M}}\right)\right]$$

$$K'^{+}_{1,M}(\mathbf{r}) = \frac{\mathbf{r}^{\top}\mathbf{n}_{\mathbf{x}}}{8\pi}\left[\operatorname{erfc}\left(\frac{|\mathbf{r}|}{\sqrt{4h_t\mu^M}}\right)\left(\frac{2h_t}{|\mathbf{r}|^2}-1\right)+\frac{4h_t}{|\mathbf{r}|}\sqrt{\frac{1}{4\pi h_t\mu^M}}\exp\left(-\frac{|\mathbf{r}|^2}{4h_t\mu^M}\right)\right]$$

$$D^{-}_{1,M}(\mathbf{r}) = \frac{\mathbf{n}_{\mathbf{x}}{}^{\top}\mathbf{n}_{\mathbf{y}}}{4\pi}\left[\sqrt{\frac{1}{4\pi h_t\mu^M}}\exp\left(-\frac{|\mathbf{r}|^2}{4h_t\mu^M}\right)-\frac{1}{r}\operatorname{erfc}\left(\frac{|\mathbf{r}|}{\sqrt{4h_t\mu^M}}\right)\right]$$

$$D^{+}_{1,M}(\mathbf{r}) = \frac{\mathbf{n}_{\mathbf{x}}{}^{\top}\mathbf{n}_{\mathbf{y}}}{4\pi r}\left[\operatorname{erfc}\left(\frac{|\mathbf{r}|}{\sqrt{4h_t\mu^M}}\right)+\frac{1-\mu^M}{\mu^M}\sqrt{\frac{1}{4\pi h_t\mu^M}}\exp\left(-\frac{|\mathbf{r}|^2}{4h_t\mu^M}\right)\right]$$

REFERENCES

[1] M. Abramowitz and I. A. Segun, editors. *Handbook of Mathematical Functions*. U.S. Govt. Print. Off., 1964.

[2] R. A. Adams and J. F. Fournier. *Sobolev Spaces*, volume 140. Elsevier, 2003.

[3] D. Arnold and P. J. Noon. Coercivity of the Single Layer Heat Potential. *J. Comput. Math.*, 7:100–104, 1989.

[4] H. D. Baehr and K. Stephan. *Heat and Mass Transfer*. Springer, 2006.

[5] K. J. Bathe. *Finite Element Procedures*. Prentice-Hall, 1996.

[6] S. C. Brenner and L. R. Scott. *The Mathematical Theory of Finite Element Methods*. Springer, 2008.

[7] R. M. Brown. The Method of Layer Potentials for the Heat Equation in Lipschitz Cylinders. *Amer. J. Math.*, 111(2):339–379, 1989.

[8] M. M. Chawla and M. K. Jain. Error Estimates for Gauss Quadrature Formulas for Analytic Functions. *Math. Comp.*, 11(101):82–90, 1968.

[9] H. Cheng, L. Greengard, and V. Rokhlin. A Fast Adaptive Multipole Algorithm in Three Dimensions. *J. Comput. Phys.*, 155:468–498, 1999.

[10] M. Costabel. Boundary Integral Operators for the Heat Equation. *Integral Equations Operator Theory*, 13:498–552, 1990.

[11] M. Costabel. *Encyclopedia of Computational Mechanics*, chapter Time-Dependent Problems with the Boundary Integral Equation Method. John Wiley & Sons, 2004.

[12] J. Crank and P. Nicolson. A Practical Method for Numerical Evaluation of Solutions of Partial Differential Equations of the Heat-Conduction Type. *Proc. Camb. Phil. Soc.*, 43, 1947.

[13] P. J. Davis. *Interpolation and Approximation*. Blaisdell, 1963.

[14] S. Erichsen and S. A. Sauter. Efficient Automatic Quadrature in 3-d Galerkin BEM. *Comput. Methods Appl. Mech. Eng.*, 157:215–224, 1998.

[15] N. R. Eyres, D. R. Hartree, J. Ingham, R. Jackson, R. J. Sarjant, and J. B. J. B. Wagstaff. The Calculation of Variable Heat Flow in Solids. In *Mathematical and Physical Sciences*, Philosophical Transactions of the Royal Society of London. Series A. Philosophical Transactions of the Royal Society of London, 1946.

[16] L. Greengard and P. Lin. Spectral Approximation of the Free-Space Heat Kernel. *Appl. Comput. Harmon. Anal.*, 9:83–97, 1999.

[17] L. Greengard and V. Rokhlin. A Fast Algorithm for Particle Simulations. *J. Comput. Phys.*, 73:325–348, 1987.

[18] L. Greengard and V. Rokhlin. A new Version of the Fast Multipole Method for the Laplace Equation in Three Dimensions. *Acta Mech.*, 6:229–269, 0 1997.

[19] L. Greengard and J. Strain. A Fast Algorithm for the Evaluation of Heat Potentials. *Comm. Pure Appl. Math.*, 43:949–963, 1990.

[20] L. Greengard and J. Strain. The Fast Gauss Transfrom. *SIAM J. Sci. Comput.*, pages 79–94, 1991.

[21] K. Griebermann. Multilevel Approximation of Boundary Integral Operators. *Computing*, 67:183–207, 2001.

[22] W. Hackbusch and Z. P. Nowak. On the Fast Matrix Multiplication in the Boundary Element Method by Panel Clustering. *Numer. Math.*, 54:463–491, 1989.

[23] F. P. Incropera and D. P. DeWitt. *Fundamentals of Heat and Mass Transfer*. John Wiley & Sons, 2002.

[24] O. D. Kellog. *Foundations of Potential Theory*. Springer, 1929.

[25] L. Kielhorn. *A Time-Domain Symmetric Galerkin BEM for Viscoelastodynamics*, volume 5 of *Computation in Engineering and Science*. Verlag der Technischen Universtiät Graz, 2009.

[26] J. R. Li and L. Greengard. High Order Accurate Methods for the Evaluation of Layer Heat Potentials. *SIAM J. Sci. Comput.*, 31:3847–3860, 2009.

[27] J. L. Lions and E. Magnes. *Non-Homogeneous Boundary Value Problems and Applications*, volume 1. Springer, Berlin, 1972.

[28] J. L. Lions and E. Magnes. *Non-Homogeneous Boundary Value Problems and Applications*, volume 2. Springer, Berlin, 1972.

[29] Y. J. Liu and N. Nishimura. The Fast Multipole Boundary Element Method for Potential Problems: A Tutorial. *Eng. Anal. Bound. Elem.*, 30:371–381, 2006.

[30] Ch. Lubich and R. Schneider. Time Discretization of Parabolic Boundary Integral Equations. *Numer. Math.*, 63:455–481, 1992.

[31] M. Messner, J. Tausch, and M. Schanz. Fast Galerkin Method for Parabolic Space-Time Boundary Integral Equations. *J. Comput. Phys.*, 2012. submitted.

[32] Ma. Messner, Mi. Messner, F. Rammerstorfer, P. Urthaler, Th. Traub, and B. Kager. Hyperbolic and Elliptic Numerical Analysis C++ BEM Library. http://www.mech.tugraz.at/HyENA, 2013.

[33] T. N. Narasimhan. Fourier's Heat Conduction Equation: History, Influence, and Connections. *Rev. Geophys.*, 1999.

[34] N. Nishimura, K. Yoshida, and S. Kobayashi. A Fast Multipole Boundary Integral Equation Method for Crack Problems in 3D. *Eng. Anal. Bound. Elem.*, 23:97–105, 1999.

[35] P. J. Noon. *The Single Layer Heat Potential and Galerkin Boundary Element Methods for the Heat Equation*. PhD thesis, University of Maryland, 1988.

[36] G. Of, O. Steinbach, and W. L. Wendland. Applications of a Fast Multipole Galerkin Boundary Element Method in Linear Elastostatics. *Comp. Vis. Science*, 8:201–209, 2005.

[37] W. Pogorzelski, A. Kacner, J. Schorr-Con, and Z. S. Olesiak. *Integral Equations and their Applications*, volume 1. Pergamon Press Oxford, 1966.

[38] F. J. Rizzo and D. J. Shippy. A Method of Solution for Certain Problems of Transient Heat Conduction. *AIAA J.*, 8(11):2004–2009, 1970.

[39] S. Sauter and C. Schwab. *Randelementmethoden: Analyse, Numerik und Implementierung Schneller Algorithmen*. Teubner, 2004.

[40] O. Steinbach. *Numerical Approximation Methods for Elliptic Boundary Value Problems*. Springer, 2008.

[41] J. Strain. Fast Adaptive Methods for the Free-Space Heat Equation. *SIAM J. Sci. Comput.*, 15:185–206, 1994.

[42] G. Strang and G. J. Fix. *An Analysis of the Finite Element Method*. Prentice-Hall, 1973.

[43] J. Tausch. A fast method for solving the heat equation by layer potentials. *J. Comput. Phys.*, 224:956–969, 2007.

[44] J. Tausch. Nyström Discretization of Parabolic Boundary Integral Equations. *Appl. Numer. Math.*, 59(11):2843–2856, 2009.

[45] J. Tausch. Fast Nyström Methods for Parabolic Boundary Integral Equations. In U. Langer, M. Schanz, O. Steinbach, and W. L. Wendland, editors, *Fast Boundary Element Methods in Engineering and Industrial Applications*, volume 63 of *Lecture Notes in Applied and Computational Mechanics*, pages 185–219. Springer, 2011.

[46] J. Tausch and A. Weckiewicz. Multidimensional Fast Gauss Transforms by Chebyshev Expansions. *SIAM J. Sci. Comput.*, 31:3547–3565, 2009.

[47] W. Weiss. *Thermische Auslegung von Werkzeugen für Presshärteprozesse*. PhD thesis, Graz University of Technology, 2013.

[48] E. L. Wilson and R. E. Nickell. Application of the Finite Element Method to Heat Conduction Analysis. *Nucl. Eng. Des.*, 4(3):276–286, 1966.